COLLISIONAL RELAXATION AND TRANSFER OF LASER-INDUCED MULTIPOLE MOMENTS IN THE EXCITED STATE OF NEON ATOMS

by

Takeshi MANABE

December 1979

Kyoto University

Kyoto, Japan

COLLISIONAL RELAXATION AND TRANSFER OF LASER-INDUCED MULTIPOLE MOMENTS IN THE EXCITED STATE OF NEON ATOMS

by

Takeshi MANABE

December 1979

Kyoto University

Kyoto, Japan

ACKNOWLEDGEMENT

The author would like to express his sincere appreciation to Professor Toru Ogawa for his continuous guidance, many stimulating suggestions and discussions throughout the present work. The author is deeply grateful to Dr. Tsutomu Yabuzaki for many helpful discussions and encouragements in all phases of this work, and for his critical reading of the manuscript.

The author also wishes to express his deep appreciation to Professors Susumu Kato and Iwane Kimura for their valuable comments and constructive suggestions.

The author wishes to express his gratitude to Dr. Shigeru Nakayama for valuable advices in the early stages. Some of the experiments were performed with the help of Messrs. Toshiaki Suzuki and Shinya Tsuda. He is also indebted to Dr. Taisuke Endo for his suggestion of the use of the Faraday filter.

It is a pleasure to acknowledge the help and the encouragements of Mr. Masao Kitano and other staffs of Ionosphere Research Laboratory and Professor Kimura's group.

Numerical calculations in this work were performed at the Data Processing Center of Kyoto University.

ABSTRACT

This thesis deals with a theoretical and experimental study on the collisional relaxation and transfer of multipole moments induced by laser light in the excited state of atoms.

There has been increasing interest in collisional mixing of atoms among Zeeman substates associated with the development of experimental techniques such as the optical pumping. We refer to this type of collisions as depolarizing collisions, because the mixing results in the destruction of the macroscopic polarization which is created in a Zeeman multiplet, for instance, by polarized light in an optical-pumping experiment. Early experimental studies of depolarizing collisions have been made by using a spectral lamp as a light source whose spectral width is generally broader than that of the atomic absorption spectrum. Recently, the development of tunable lasers has enabled us to study on this subject for the excited state which cannot be excited by using conventional light sources. Moreover, the experiment using a laser makes a striking contrast to that using a spectral lamp by the fact that the laser excites atoms velocity-selectively due to the axial mode structure, so that the collisions of atoms excited by a laser are no longer isotropic. Nevertheless, almost all theories heretofore have assumed isotropic collisions.

The first half of this thesis is devoted to the study of

the effects of anisotropic collisions on atoms excited by a single-mode laser light. From the argument of symmetry, it is found that the most remarkable feature of anisotropic collisions is the appearance of the transfer between different multipole components within a Zeeman multiplet, which is absent for the case of isotropic collisions. Theoretical calculations of the transfer rates as well as the relaxation rate of each multipole component are made for resonant and nonresonant collisions. Furthermore, for nonresonant collisions, numerical calculations are made for atoms in the state with J=1. As the result, it is shown that the effects of anisotropy are unnegligible for the case of single-mode excitation even when the laser is tuned around the center of the absorption line. It is suggested that our calculations are easily applicable to general cases of excitations with arbitrary spectral profile.

In order to verify the theoretical predictions, we experimentally investigated the magnetic depolarization in the $2p_4$ state of neon excited by a single-mode dye laser. The effects of anisotropic collisions with neon atoms in their ground state are observed as the modification of the width of the Hanle signal and as the transfer from alignment (electric quadrupole momemt) to orientation (magnetic dipole moment) and that from orientation to alignment. Although the theoretical calculations have been made for the excited state with J=1, we find rather a good agreement between the theoretical results and the experimental ones for the $2p_4$ state (J=2).

In the latter part of this thesis, the effects of isotropic collisions on the alignment in the excited state of neon are studied by means of the double resonance in a multi-mode He-Ne laser operating at 632.8 nm. In this experiment, the resonance signal observed in the laser output can be attributed to the magnetic resonance of alignment in the $2p_4$ state. We have measured the alignment destroying cross sections for the $2p_4$ state of neon colliding with the ground-state rare gas atoms: He^3, He^4, Ne, Ar, and Kr. These experimental cross sections are compared with those predicted by the theory in which the van der Waals interaction is assumed. As the result, we find the anomalous fact that the cross section for He^3 is larger than that for He^4 and both of them are larger than that for neon, which is inconsistent with the theory. Importance of the short-range repulsive interaction for collisions with helium is emphasized, rather than the long-range van der Waals interaction.

CONTENTS

CHAPTER I

GENERAL INTRODUCTION

I.1 Introduction

This thesis is concerned with the collisional relaxation among Zeeman substates in the excited state of neon. Ever since the inventions of experimental techniques such as "optical pumping" or "double resonance", relaxation among Zeeman substates in the excited states or in the ground states has been one of the most interesting subjects and has been extensively studied theoretically and experimentally. Furthermore, recent development of lasers has made it possible to study more precisely this subject in the excited states which are not optically connected with the ground state. In many of these experiments, lasers have been used as convenient light sources in place of conventional spectral lamp. Nevertheless, besides some nonlinear effects originating in the high spectral brightness of lasers, the spectral feature can produce characteristic phenomena which cannot be found in experiments with conventional light sources. Since the laser light has an axial-mode structure, the velocity distribution of atoms interacting with the laser light becomes anisotropic, so that the averaged collisional effect on these atoms is anisotropic.

One of the purposes of this thesis is to study theoretically

and experimentally the effect of anisotropic collisions on the relaxation among Zeeman substates. Another purpose is to measure the cross sections for collisions between the excited state neon atoms and various rare-gas atoms. The measurements of cross sections of free atoms provide some important informations about interatomic interactions and allow us to check the validity of the theory of atomic collisions.

As an introduction of this thesis, we first present a brief survey on the theory of atomic collisions of our interest and, in particular, on studies about collisional depolarizations in the excited states. We also present a short review of experimental and theoretical studies concerning with various types of anisotropic relaxations. We finally present the outline of the present work.

I.2 Depolarizing Collisions

Since the earliest treatment by Lorentz in 1906[1], it has become possible to investigate collisions between atoms or molecules from a spectroscopical point of view. Lorentz used the classical oscillator model for the radiating atom which has a definite collision cross section, and assumed that each collision changes the phase of the oscillator or interrupts the oscillation. The Fourier integral of the radiation from this oscillator yields the spectral profile which is the well-known Lorentzian profile subjected to the pressure broadening caused by collisions.

Weisskopf[2] extended the classical model of Lorentz by taking account of the temporal change in the frequency of the radiating oscillator as the source of the phase shift, and defined the collision radius as the impact parameter of the collion which produces the phase shift equal to unity. As the result, the collision cross section is related to the interaction potential.

The development of the quantum mechanics has allowed more rigorous treatment of collisions and radiation. Foley[3] developed the phase shift theory for the two-level system and employed the quantum theory of radiation in estimating the spectral intensity. He showed that there is a shift in line position as well as the line broadening, both being proportional to the pressure, and that the ratio of the shift to the broadening depends only on the type of the interatomic interaction, which is in good agreement with experimental data in the optical region.

The theories presented so far have mainly treated the spectra in the optical region, therefore it has been assumed that no transition is caused by collisions (the adiabatic approximation). It is clear that these theories are inapplicable to the spectra in the infra-red, microwave, and radiofrequency regions, because the transitions among corresponding states can be caused by collisions (the energy separations for these spectral regions are smaller than the thermal energy kT). Collisional perturbation on a Zeeman multiplet, which we shall deal with in the present work, corresponds to the problem in this region. Anderson[4] extended the theory applicable to the spectra in the infra-red

and microwave regions by taking account of the multiplet structures of the states. The inclusion of the multiplet structure makes the problem much complicated because the interaction Hamiltonian does not commute with itself at different time. Anderson proposed two approximate methods, one of which was the perturbation method with a cutoff procedure for close collisions, and the other was to ignore the noncommutativity. This theory has been generalized to the cases of pressure broadening of complex molecular spectra, in which both of the colliding particles have multiplet structures[5].

In optical-pumping experiments such as the Hanle effect[6),7)] and the double resonance[8),9)], collisional relaxation among Zeeman substates in the excited- or ground-state multiplet becomes important. By the term "optical pumping"[10)], we mean the creation of large population imbalance in some multiplet by the absorption of light with definite polarization. Thus created population imbalance is closely related to the macroscopic polarization in the state, namely the magnetic dipole moment so-called "orientation" and the electric quadrupole moment so-called "alignment" etc. If the pumping light is suddenly switched off, the population imbalance relaxes to the thermal equilibrium in which there is generally no population imbalance in a weak magnetic field. This relaxation is caused by interatomic collisions, collisions with the container wall[11),12)], radiation trapping[13),14)], and spatial diffusion[15)]. In particular, this type of interatomic collisions is referred to as "depolar-

izing collisions".

In the earliest work, by extending the theory of Anderson to the case of depolarizing collisions, Byron and Foley[16] treated the pressure broadening of optical-rf double-resonance line, and derived the expression for the cross section for the depolarizing collisions. More recently, many authors investigated the depolarizing collisions by using the density-matrix formalism on the basis of irreducible representation [17)-24)]. Omont calculated cross sections for orientation and alignment of the excited state with J=1 by using the Anderson's approximation[19]. In spite of the approximation, the results explained well experimental cross sections for collisions between mercury atoms[20]. However,in the case of collisions between atoms of different species (nonresonant collisions) where close collisions become important, the Anderson's approximation becomes less valid. In order to study about nonesonant collisions without this approximation, Berman and Lamb[22] made numerical calculations by taking account of the noncommutativity of the interaction Hamiltonian, and found good agreements with experimental results for some of nonresonant collisions as well as for resonant collisions, while it has been pointed out that their theory might be invalid for the collisions with light atoms such as helium.

In cases of collisions between alkali atoms and rare-gas atoms, there have been many experimental observations of depolarizing cross sections for collisions with helium anomalously larger than those expected from the theory assuming the van der

Waals interaction[25)-32)]. On the other hand, Faroux and Brossel[33)] observed an anomalous temperature dependence of depolarizing cross section for Hg-He collisions: the experimental cross section is nearly independent of the temperature, while the theory using the van der Waals interaction predicts the dependence $T^{-1/5}$. As the result, they showed that the hard-sphere model is better than the van der Waals interaction for Hg-He collisions. Recently, similar anomalous temperature dependence of cross section has been observed for collisions between neon and helium by Carrington et al.[23),34),35)].

Another anomaly in the case of collisions between neon and helium has been found in the pressure-induced g_J-shift of the excited-state neon[36),37),38)] which cannot be explained by the above theory. The pressure-induced g_J-shift of the $2p_4$ state of neon perturbed by collisions with helium has been firstly observed by Yabuzaki et al. as the pressure shift of magnetic resonance line in the double resonance of the He-Ne laser[36)], while such shift has not been observed in the case of collisions with neon within the relative experimental error. Recently, Hermann et al.[37),38)] have observed similar shift of the $2p_4$ state by measuring the mode-crossing signal[39),40)] of the He-Ne laser in axial magnetic field, while no pressure shift has been observed in the experiments concerning the $2s_2$ state of neon. Rare-gas-induced g_J-shifts, which are much smaller than the g_J-shift of neon, have been found in some alkali atoms in their ground states, and they have been explained by means of semi-

empirical calculations by Herman[41]. However, this explanation cannot be used to explain such a large g_J-shift of neon in the excited state.

It should be pointed out that the short-range repulsive interaction becomes important in place of the van der Waals interaction in cases of collisions with light atoms such as helium. Some authors have pointed out that the deviation from the straight-line trajectory caused by the short-range interaction becomes important for alkali-rare-gas collisions[42),43),44)]. The origin of the short-range repulsive interaction is thought to be the exchange force induced by the overlap of electron clouds of colliding atoms.

I.3 Anisotropic Relaxation of the Excited State

In almost all theories heretofore, it has been assumed that all directions of relative trajectories for collisions are equally probable, that is, collisions occur isotropically. As has been discussed by many authors[17),19),22)], this isotropic situation simplifies the expressions for collisional depolarizations in the Zeeman multiplet such that each multipole components in the multiplet relaxes independently without coupling with each other. In optical-pumping experiments, multipole moments are created by polarized light: the orientation and the alignment are created by the absorptions of circularly and linearly polarized light, respectively. If collisions are isotropic, the

fluorescence from atoms excited by linearly polarized light has no circularly polarized component, because there is no transfer from alignment to orientation . In general optical-pumping experiments using a spectral lamp as a pumping light source, the condition of isotropic collisions is generally satisfied.

On the other hand, in experiments using a laser, this condition of the isotropic collisions is not always satisfied. In order to elucidate the anisotropic situation, let us consider the simplest case that atoms are excited by a single-mode laser tuned around the transition frequency ν_0 from the ground state to an excited state. The velocity distribution of the ground-state atoms is given by an isotropic Maxwellian distribution as is shown by a Gaussian function in Fig. 1.1. When the ground-state atoms are irradiated by a single-mode laser light with the frequency ν propagated along the z direction, only the atoms moving with velocities, which compensate the detuning $(\nu-\nu_0)$ by the Doppler effect [$v_z = c(\nu-\nu_0)/\nu_0$], are effectively excited. As the result of the velocity-selective excitation, the velocity distribution of the excited atoms is no longer isotropic as seen in Fig. 1.1, so that the average effect of collisions with the ground-state atoms (perturbers), whose velocity distribution is isotropic, becomes anisotropic.

The most remarkable feature of anisotropic collisions is that these collisions cause the transfer between different multipole components, which is absent in the isotropic case. Especially, the transfer from alignment to orientation should

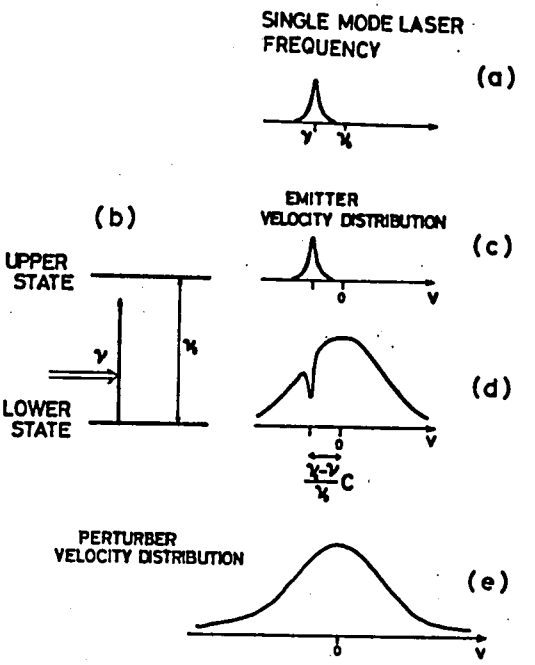

Fig. 1.1 The velocity distribution of emitters (c), and that of perturbers (e). The emitters are excited from the lower state (d) by a single-mode laser light with a frequency ν (a) detuned from the center frequency ν_0 of the absorption line (b).

be manifested in the circularly polarized fluorescence from atoms excited by linearly polarized light. Conversely, the reverse transfer should be manifested in the linearly polarized fluorescence from atoms excited by circularly polarized light.

In spite of the importance of anisotropic collisions in experiments using a single-mode laser, there have been a few number of studies of anisotropic relaxations and none of them are applicable directly to the case of single-mode excitation.

The earliest experiment on anisotropic collisions is that made by Nedelec et al.[45]. They attributed the anomalous magnetic-resonance signal of mercury vapour to anisotropic collisions due to the convection of aligned mercury atoms in the cell which had a temperature gradient. However, Lombardi has pointed out the invalidity of their explanation of the experimental resuls[46]. Rebane has made the theoretical calculations of the effect of anisotropic collisions for the simple case that the rest atoms are perturbed by atoms moving along a particular direction, and has estimated the efficiency of conversion of incident linearly polarized light to circularly polarized fluorescence[47]. Recently Carré et al. have observed the transfer from alignment to orientation in the $4\,^1D$ state of helium, excited by an accelerated Na^+ beam, under the influence of anisotropic collisions with the ground-state helium atoms[48),49),50].

Recently, some authors[51),52)] have investigated the effect of anisotropic collisions on the correlation between Doppler and collisional broadening of optical spectral line profile. As is

well known, the translational motions of radiating atoms produce frequency shift due to the Doppler effect. As the result, the over-all spectral line profile is generally given by a convolution integral of homogeneously broadened line and the Doppler profile given by a Gaussian function. In this context, each Doppler-shifted component of the spectral line is homogeneously broadened by anisotropic collisions. They have derived the deviation of the line profile from the well-knowen Voigt profile.

On the other hand, Gough[53] has pointed out that, in the experiment of the sensitized fluorescence concerning the coherence transfer[54),55)], the anisotropy should be taken into account in averaging over all collisions unless multiple scattering is negligible. For instance, the case of the Hg-Cd collisions of the second kind which are exothermic, only the sensitized fluorescence arising from collisions along the direction of observation is effectively observed, since it undergoes less multiple scattering because of the high recoil velocity after the collision. As the result, the observed collisions cannot be treated isotropically.

Now, it may be suggestive to review some studies of depolarizations in different types of anisotropic situations other than the anisotropic collisions. Lombardi has observed the transfer from alignment to orientation in the excited state of helium which is initially aligned by rf capacitive discharge[46]. In his experiment, the situation has only axial and plane-reflection symmetries because of the presence of the oscillating rf electric

field of the capacitive discharge. On the other hand, Gay has shown theoretically that, when the static magnetic field applied to atoms is so strong that the Larmor precession cannot be neglected during each collisional interaction, the decay rates of multipole moments become dependent on the strength of the magnetic field[56)-59)]. This is the result of the axial symmetry of the system, which appears even when collisions are isotropic. This axial symmetry gives rise to the transfer between alignment and population.

Another mechanism of transfer between different components has been studied by Rebane and Rebane[60)]. They have shown that, in the presence of hyperfine structures, the transfer between orientation and alignment becomes possible under the influence of a weak magnetic field even when collisions are isotropic. If atoms are initially aligned, this alignment is transferred to the alignment of hyperfine coherence by isotropic collisions, then this alignment of hyperfine coherence is transferred to the orientation of this coherence by a weak magnetic field, and this orientation is transferred to the orientation within a Zeeman multiplet by isotropic collisions.

Recently, in the field of astrophysics, a great interest has been aroused by interstellar maser emissions (see, for instance, the review articles Refs. 61-63). The most remarkable feature of hydroxyl maser emissions with the wavelength 18cm from certain regions of ionized hydrogen ("HII regions") is a great predominance of circular polarization over linear one. Although many authors

have already attempted to account for the predominance of circular polarization by supposing various types of pumping mechanisms[64] or by taking account of some nonlinear phenomena[65),66),67)] or Zeeman effects[68)], there has been no satisfactory explanation so far. It has been believed that most of sources of circularly polarized maser emissions are associated with regions of star formation. In such regions, the presence of anisotropic radiation, shock-fronts from protostars, and weak magnetic field are reasonable, so that the maser sources seem to be under considerably anisotropic circumstances. Therefore, it will be rather rational to consider the intermolecular collisions in such regions to be anisotropic. We suspect that the above-mentioned transfer from alignment to orientation caused by anisotropic collisions may give some explanation about the predominance of circular polarization of interstellar masers.

It may be worthwhile to note that the collisional depolarization is one of the most important processes which determine the polarization of a gaseous laser with no anisotropic elements such as Brewster-angled windows. Fork et al.[69)] and de Lang and Bouwhuis[70)] have reported stable circularly polarized oscillation of a single-mode He-Ne laser operating at the $2s_2(J=1)-2p_1(J=0)$ transition in a weak magnetic field. It has been suggested [71),72)] that this predominance of circular polarization in a weak magnetic field is related to the fact that depolarizing collisions are more effective in the decay of orientation than of alignment. According to this suggestion, Wang et al.[73)]

have measured the cross sections for destructions of alignment and orientation by measuring the critical magnetic field for the transition from circular polarization to linear one. In their analysis, they have assumed isotropic collisions. However, in such experiments, the anisotropy of collisions seems to become important because of the single-mode operation of the laser as is mentioned before. Perhaps, the transfer between alignment and orientation must more or less play some important role to determine the polarization property of the laser without anisotropic elements.

I.4 Outline of the Present Work

In this thesis, we study the depolarizations in the excited state of neon atoms under the influence of collisions with atoms in their ground state. In the first place, particular attention is paid on the anisotropy of averaged collisional effects on atoms excited by a single-mode laser (Chapter II and III). Secondly, we study the effects of anisotropic collisions on the magnetic-depolarization signals in optical-pumping experiments using a single-mode laser (Chapter IV). On the other hand, we study the effects of isotropic collisions on the magnetic-resonance signals by means of the optical-rf double resonance in a multi-mode He-Ne laser, and we report the results of the measurements of alignment destroying cross sections (Chapter V).

We here describe in more detail on the study discussed in each chapter.

Chapter II is devoted to present some mathematical formalisms which will be found to be useful in treating optical-pumping signals and anisotropic collisions in the following chapters. At first, we review the density matrix formalism and its representation on the basis of irreducible tensorial sets. In almost all cases of usual experimental conditions, the situations are more or less related with some symmetry, so that it is rational to simplify the expressions by using the irreducible representation rather than the conventional magnetic quantum number representation. Next, we present the equation of motion for the density matrix on the irreducible basis. This master equation is the generalization of the well-known Bloch equation for the spin-1/2 state, and is applicable either to the magnetic depolarization or to the double resonance for the state with arbitrary total angular momentum. In addition, the irreducible representation generally provides by far the simplest and the most physical expressions for the relaxation terms in this master equation because of the high symmetry of the relaxation process. We study various symmetry properties of the relaxation matrix for multipole moments regardless of particular origins of relaxations. Particular attentions are paid on axial and plane-reflection symmetries, which will be encountered in the following chapters.

In chapter III, we investigate theoretically the effects

of anisotropic collisions on multipole moments in the excited state of atoms excited by a single-mode laser[74]. Calculations are carried out along the line of the work of Berman and Lamb[22], in whch the electrostatic dipole-dipole interaction is assumed. In these calculations, their assumption of isotropic collision is removed. Apart from isotropic collisions, the velocity distribution of excited atoms along the laser beam is assumed to be given by a delta function as seen in Fig 1.1, while the transverse velocity distribution is given by a two-dimensional Maxwellian. Before considering the single-mode laser excitation, we first investigate the effects of anisotropic collisions on atoms moving in a fixed direction, which will be relevant to the collisions in atomic-beam experiments. In the next place, after averaging over the velocity distribution of the excited atoms, we consider the case of single-mode laser excitation. We calculate the transfer rate between orientation and alignment as well as the relaxation rates of multipole moments for the excited state with J=1 perturbed by nonresonant collisions. These rates are obtained as functions of the detuning of the laser frequency from the center of the absorption line. The results can easily be extended to the case of the excitation by light with arbitrary spectral profile.

In chapter IV, we propose some experimental methods which allow us to observe the effects of anisotropic collisions[74]. By taking account of the anisotropic relaxations discussed in chapter III, we analyse the magnetic-depolarization signals for

each excitation by linearly- or circularly-polarized laser beam. The experiments are carried out with respect to neon atoms in the $2p_4$ state (J=1) excited by a single-mode dye laser[75]. The effects of anisotropic collisions are manifested in the change in the width of the Hanle signal when the degree of anisotropy is changed by changing the detuning of the laser. However, the observed change in the width has been so small , as has been expected from the theory, that we could not obtain reliable informations about anisotropic collisions.

On the other hand, the transfer between alignment and orientation is a more clear manifestation of anisotropic collisions, since it is completely absent in the case of isotropic collisions. We observed the transfer from alignment to orientation in circularly polarized fluorescence emitted by atoms excited by linearly polarized laser beam. The experimental results are compared with the theoretical calculations where the existence of two isotopes in natural neon is taken into account, and a relatively good agreement is found. We also observed the reverse process, i.e. the transfer from orientation to alignment, by observing the linearly polarized fluorescence emitted by atoms excited by circularly polarized laser beam.

In chapter V, we study the effect of alignment destroying collisions on the double-resonance signal observed in the output of the multi-mode He-Ne laser operating at 632.8 nm. In this experiment, the observed resonance is due to the magnetic resonance in the $2p_4$ state of neon. In order to investigate the

collisions of neon atoms with various rare-gas perturbers, we used a He-Ne laser tube, adulterated with argon or krypton in some cases. The alignment destroying cross sections of neon in the $2p_4$ state for collisions with He^3, He^4, Ne, Ar, and Kr were measured from the pressure broadenings of the double-resonance signals[76]. These experimental results are compared with the cross sections estimated from the isotropic-collision theory in which the van der Waals interaction is assumed. Particular attention is paid on the difference between the measured cross section for collisions with He^3 and that for He^4. A relatively large discrepancy is found between the measured cross sections for collisions with He^3 and He^4 and the theory assuming the van der Waals interactions. As a cause of this discrepancy, we emphasize the importance of the short-range repulsive interaction rather than the van der Waals interaction for collisions with light perturbers such as helium atoms.

CHAPTER II

IRREDUCIBLE REPRESENTATION OF DENSITY MATRIX AND THE MASTER EQUATION

II. 1 Introduction

Symmetry property is of a great importance in atomic and nuclear physics. In particular, rotational symmetry allows some convenient frame works for many problems concerning with the angular momentum. It is worthwhile noting that optical pumping is a technique to create some anisotropy in the internal states of atoms by anisotropic irradiation of polarized light. Although the optical-pumping process is not fully isotropic, there remain some lower symmetries such as axial symmetry and plane-reflection symmetry. On the other hand, most of the relaxation processes are isotropic or highly symmetric. The main purpose of the present work is to study the anisotropic relaxations which retain axial and plane-reflection symmetries.

Since all physical systems which we are going to deal with have some rotational symmetry (i.e. axial symmetry), the formalism based on the irreducible tensorial sets[77),78)] allows very convenient expressions for optical pumping and relaxation. In this context, the internal states of atoms are expanded in terms of multipole moments which are irreducible with respect

to rotation. This multipole representation makes much simpler the relation between the atomic internal states and the polarization of light, which is absorbed or emitted, than the magnetic quantum number representation.

In this chapter. we review the density matrix formalism for the optical pumping and relaxation processes on the basis of irreducible representation. We at first present the way of expanding the density matrix of the system in terms of irreducible components. It should be noted that the irreducible representation simplifies the transformation properties of the system with respect to the rotation of coordinates, compared with the ordinary representation. We give the master equation for the density matrix in the irreducible representation for the optical pumping in the excited state.

The latter half of this chapter is devoted to discuss about the general properties of the relaxation matrix for the density matrix, which come from different types of symmetries. It should be emphasized that the symmetry properties of the relaxation matrix hold good, irrespective of the origin of the relaxation process. Almost all of the conventional theories have assumed isotropic relaxations (i.e. spherical symmetry). However , since we are interested in anisotropic collisions for atoms excited by a single-mode laser, axial and plane-reflection symmetries become important.

II . 2 Irreducible Representation of the Density Matrix

The density matrix is now a very well-known concept[79]. The use of the density matrix to describe the internal state of atoms or molecules allows an illuminating way in interpreting the optical signals from the ensemble of atoms, and almost inevitable in the study of relaxation processes.

When one deals with the relaxation of the ensemble of atoms (a large system), not an individual atom, it is convenient to introduce the density matrix. The use of the density matrix simplifies the expression for the mean value of some atomic observable A as

$$< A > = \mathrm{Tr}[\ \rho A\ ], \tag{2.1}$$

where the density matrix ρ is defined by

$$\rho = \frac{1}{N}\sum_{i=1}^{N} |\psi_i><\psi_i|, \tag{2.2}$$

where $|\psi_i>$ is the wave function of the i-th atom and N is the number of atoms in the ensemble.

If one represents the density matrix using the standard basis of angular momentum $|\alpha JM>$ where J and M are the total angular momentum and its projection on the quantization axis, and α labels a set of the other quantum numbers to specify the state, this matrix can be written as

$$\rho = \sum_{\substack{\alpha JM \\ \alpha'J'M'}} \rho_{\alpha JM,\alpha'J'M'} |\alpha JM\rangle\langle\alpha'J'M'|, \tag{2.3}$$

where

$$\rho_{\alpha JM,\alpha'J'M'} = \langle\alpha JM|\rho|\alpha'J'M'\rangle. \tag{2.4}$$

In this representation, the diagonal component $\rho_{\alpha JM,\alpha JM}$ is the probability of finding the atoms in the Zeeman substate specified by $\{\alpha JM\}$. On the other hand, the off-diagonal component means the quantity so called atomic coherence. In particular, $\rho_{\alpha JM,\alpha JM'}$ is called Zeeman coherence, and $\rho_{\alpha JM,\alpha'J'M'}$ is called optical coherence between the states $\{\alpha JM\}$ and $\{\alpha'J'M'\}$ connected by an optical transition.

Many physical systems, some of which we shall deal with in the following chapters, usually have some simple symmetry property such as spherical or axial symmetry. Accordingly, the irreducible tensorial technique provides a very convenient framework for the present work[77),78)]. Although the basis $|\alpha JM\rangle$ is irreducible with respect to rotation, the dyadic product basis $|\alpha JM\rangle\langle\alpha'J'M'|$ seen in Eq.(2.3) becomes reducible, and the transformation of this dyadic basis under rotation is the same as that of the product of two angular momentum eigenvectors $(-1)^{J'-M'}|\alpha JM\rangle|\alpha'J'-M'\rangle$. Using the vector coupling technique of two angular momenta[80)], we can transform this reducible basis to irreducible tensorial basis $T^k_q(\alpha J,\alpha'J')$:

$$T^k_q(\alpha J,\alpha'J') = \sum_{MM'}(-1)^{J'-M'}\langle JJ'M-M'|kq\rangle|\alpha JM\rangle\langle\alpha'J'M'|, \tag{2.5}$$

where $< J\ J'\ M\ M' |\ k\ q >$ is the Clebsch-Gordan coefficient[80] which is related to the 3-j symbol $\begin{pmatrix} J & J' & k \\ M & M' & -q \end{pmatrix}$ by the relation

$$\begin{pmatrix} J & J' & k \\ M & M' & -q \end{pmatrix} = \frac{(-1)^{J-J'+q}}{\sqrt{2k+1}} < J\ J'\ M\ M' |\ k\ q >. \qquad (2.6)$$

These T^k_q's form an orthonormal basis system in the sense that they satisfy the condition

$$\mathrm{Tr}[\ T^k_q(\alpha J_1,\alpha' J_1')T^{k'}_{q'}(\beta J_2,\beta' J_2')^\dagger] = \delta_{\alpha\beta}\delta_{\alpha'\beta'}\delta_{J_1J_2}\delta_{J_1'J_2'} \times \delta_{kk'}\delta_{qq'}\ , \qquad (2.7)$$

and the Hermitian conjugate of T^k_q is

$$T^k_q(\alpha J,\alpha' J')^\dagger = (-1)^{J-J'+q}\ T^k_{-q}(\alpha' J',\alpha J). \qquad (2.8)$$

It should be noted that our definition of T^k_q is widely used by many authors but some Russian authors such as D'yakonov and Perel'[17] use a different definition of T^K_q which is different in its normalization.

Using this irreducible basis, we can expand the density matrix as follows:

$$\rho = \sum_{\substack{\alpha\alpha' JJ' \\ kq}} \rho^k_q(\alpha J,\alpha' J')T^k_q(\alpha J,\alpha' J'). \qquad (2.9)$$

Irreducibility of this representation makes the rotational transformation of the density matrix in a rather simple form given by

$$[\mathcal{D}\rho\,\mathcal{D}^{-1}]^k_q = \sum_{q'} \mathcal{D}^k_{qq'}\,\rho^k_{q'}(\alpha J,\alpha' J'), \tag{2.10}$$

where $\mathcal{D}^k_{qq'}$ is the rotation matrix[80].

The Hermiticity of the density matrix is expressed as

$$\rho^k_q(\alpha J,\alpha' J') = (-1)^{J-J'+q}\rho^k_{-q}(\alpha' J',\alpha J)^*. \tag{2.11}$$

From Eqs. (2.3) and (2.9), the relation between $\rho_{\alpha JM,\alpha' J' M'}$ and $\rho^k_q(\alpha J,\alpha' J')$ is

$$\rho^k_q(\alpha J,\alpha' J') = \sum_{MM'} (-1)^{J'-M'} \langle JJ'\,M\,-M'|\,kq\rangle \rho_{\alpha JM,\alpha' J' M'} \tag{2.12a}$$

or

$$\rho_{\alpha JM,\alpha' J' M'} = \sum_{kq} (-1)^{J'-M'} \langle J\,J'\,M\,-M'|\,kq\rangle \rho^k_q(\alpha J,\alpha' J'). \tag{2.12b}$$

For the most part of the present work, the discussion is confined within a particular Zeeman multiplet, so that we use ρ^k_q instead of $\rho^k_q(\alpha J,\alpha J)$ for the sake of simplicity. We note again that the density matrix f^k_q defined by D'yakonov and Perel' is related to our ρ^k_q by the equation

$$\rho^k_q = \sqrt{(2k+1)/(2J+1)}\; f^k_{-q}\,. \tag{2.13}$$

The relations between ρ^k_q and $\rho_{MM'}$ for Zeeman multiplets with J=1 and J=2 are tabulated in Table 1.1.

The physical meaning of ρ^k_q is rather clear than that of

Table 1.1 The Relations Between ρ_q^k and $\rho_{mm'}$

We can obtain ρ_q^k for $q<0$, using the relation Eq. (2.11).

J=1

$$\rho_0^0 = \sqrt{1/3}(\rho_{11} + \rho_{00} + \rho_{-1-1})$$
$$\rho_0^1 = \sqrt{1/2}(\rho_{11} - \rho_{-1-1}) \qquad \rho_1^1 = -\sqrt{1/2}(\rho_{10} + \rho_{0-1})$$
$$\rho_0^2 = \sqrt{1/6}(\rho_{11} - 2\rho_{00} + \rho_{-1-1})$$
$$\rho_1^2 = -\sqrt{1/2}(\rho_{10} - \rho_{0-1}) \qquad \rho_2^2 = \rho_{1-1}$$

J=2

$$\rho_0^0 = \sqrt{1/5}(\rho_{22} + \rho_{11} + \rho_{00} + \rho_{-1-1} + \rho_{-2-2})$$
$$\rho_0^1 = -\sqrt{1/10}(2\rho_{22} + \rho_{11} - \rho_{-1-1} - 2\rho_{-2-2})$$
$$\rho_1^1 = \sqrt{1/10}(\sqrt{2}\rho_{21} + \sqrt{3}\rho_{10} + \sqrt{3}\rho_{0-1} + \sqrt{2}\rho_{-1-2})$$
$$\rho_0^2 = \sqrt{1/14}(2\rho_{22} - \rho_{11} - 2\rho_{00} - \rho_{-1-1} + 2\rho_{-2-2})$$
$$\rho_1^2 = -\sqrt{1/14}(\sqrt{6}\rho_{21} + \rho_{10} - \rho_{0-1} - \sqrt{6}\rho_{-1-2})$$
$$\rho_2^2 = \sqrt{1/7}(\sqrt{2}\rho_{20} + \sqrt{3}\rho_{1-1} + \sqrt{2}\rho_{0-2})$$
$$\rho_0^3 = \sqrt{1/10}(\rho_{22} - 2\rho_{11} + 2\rho_{-1-1} - \rho_{-2-2})$$
$$\rho_1^3 = -\sqrt{1/10}(\sqrt{3}\rho_{21} - \sqrt{2}\rho_{10} - \sqrt{2}\rho_{0-1} + \sqrt{3}\rho_{-1-2})$$
$$\rho_2^3 = \sqrt{1/2}(\rho_{20} - \rho_{0-2})$$
$$\rho_3^3 = -\sqrt{1/2}(\rho_{2-1} + \rho_{1-2})$$
$$\rho_0^4 = \sqrt{1/10}(\rho_{22} - 4\rho_{11} + 6\rho_{00} - 4\rho_{-1-1} + \rho_{-2-2})$$
$$\rho_1^4 = -\sqrt{1/14}(\rho_{21} - \sqrt{6}\rho_{10} + \sqrt{6}\rho_{0-1} - \rho_{-1-2}$$
$$\rho_2^4 = \sqrt{1/14}(\sqrt{3}\rho_{20} - 2\sqrt{2}\rho_{1-1} + \sqrt{3}\rho_{0-2})$$
$$\rho_3^4 = -\sqrt{1/2}(\rho_{2-1} - \rho_{1-2})$$
$$\rho_4^4 = \rho_{2-2}$$

$\rho_{MM'}$. The component with k=0 is called "population" since the sum of populations over the Zeeman substates $\sum_M \rho_{MM}$ is expressed only by ρ_0^0. The components with k=1 are called "orientation" since they are related to the three standard components of the expectation value $< \vec{J} >$ which is proportional to the magnetic dipole moment of the state. Thus we obtain the three components as[81)]

$$\rho_0^1 = \sqrt{3/J(J+1)(2J+1)} < J_z > ,$$

$$\rho_{\pm 1}^1 = \mp\sqrt{3/2J(J+1)(2J+1)} < J_\mp > , \qquad (2.14)$$

where $J_\mp = J_x \pm iJ_y$, and the z direction is taken to the quantization axis. The components with k=2 are called "alignment" and their five components are related to the five standard components of the electric quadrupole moment. These five components are expressed as[81)]

$$\rho_0^2 = \sqrt{5/J(J+1)(2J-1)(2J+1)(2J+3)} < 3J_z^2 - J(J+1) >,$$

$$\rho_{\pm 1}^2 = \mp\sqrt{15/2J(J+1)(2J-1)(2J+1)(2J+3)} < J_z J_\mp + J_\mp J_z > ,$$

$$\rho_{\pm 2}^2 = \sqrt{15/2J(J+1)(2J-1)(2J+1)(2J+3)} < J_\mp^2 > . \qquad (2.15)$$

The component with k>2 are called 2^k-pole moment, i.e. "octupole moment" for k=3, "hexadecapole moment" for k=4, etc.

As the components ρ_0^k are related to the projections of observables on the z axis, they are called "longitudinal components". As is seen in Table 1.1, ρ_0^k can be expressed with the populations of Zeeman sublevels. On the other hand, the components ρ_q^k with $q \neq 0$ are called "transverse components" and can be expressed with off-diagonal components of the density matrix (Zeeman coherence $\rho_{MM'}$, where $M-M'=q$).

II.3 Master Equation for the Density Matrix

It is well known that the optical pumping of the state with $J=1/2$ of an ensemble of atoms can be characterized by a magnetization (i.e. orientation). The time evolution of the macroscopic magnetization can be described by the Bloch equation[82] which was formulated to describe the motions of nuclear magnetic moments in the presence of external magnetic fields. In more general cases ($J \geq 1$) where the internal state cannot be characterized only by a magnetization, we must introduce multipole moments that can be expressed in terms of the density matrix. The time evolution of the density matrix is governed by an equation of motion:

$$\frac{d\rho}{dt} = -\frac{i}{\hbar}\left[\mathcal{H}_0 + \mathcal{H}_F\ ,\ \rho\right] + \left(\frac{d\rho}{dt}\right)_{rel} + \left(\frac{d\rho}{dt}\right)_{pump} . \qquad (2.16)$$

This equation is considered to be a quantum mechanical generalization of the Liouville equation.

In Eq. (2.16), $\mathcal{H}_0$ is the Hamiltonian of an isolated atom, $\mathcal{H}_F$ is the Hamiltonian of interaction of atoms with an external magnetic field $\vec{H}$. The explicite form of $\mathcal{H}_F$ is given by $\mathcal{H}_F = \hbar g \mu_B \vec{J} \cdot \vec{H}$ where g is the g-factor of the Zeeman multiplet and μ_B is the Bohr magneton. For the most part of this work, our discussions are confined within a particular Zeeman multiplet. Hence, the term $(-i/\hbar)[\mathcal{H}_0, \rho]$ on the right-hand side of Eq. (2.16) can be eliminated by means of the use of the interaction representation. In spite of the use of the interaction representation, as far as this equation is projected onto a single Zeeman multiplet, Eq. (2.16) is subjected no change except for the elimination of the term $(-i/\hbar)[\mathcal{H}_0, \rho]$. This is because of the fact that all Zeeman substates in a multiplet have the same secular frequency $\langle \alpha JM | \mathcal{H}_0 | \alpha JM \rangle / \hbar$ which is independent of the magnetic quantum number M. Thus the first term of Eq. (2.16) is reduced to that of the interaction with the external magnetic field $(-i/\hbar)[\mathcal{H}_F, \rho]$. This term can be expressed with the irreducible representation through Eqs. (2.12) :

$$(-i/\hbar)[\mathcal{H}_F, \rho]^k_q = ig\mu_B \{ \sqrt{(k-q)(k+q+1)/2}\, H_1 \rho^k_{q+1} - qH_0 \rho^k_q - \sqrt{(k+q)(k-q+1)/2}\, H_{-1} \rho^k_{q-1} \}, \quad (2.17)$$

where the standerd components of $\vec{H}$ are defined as

$$H_1 = -\sqrt{1/2}(H_x + iH_y), \quad H_0 = H_z, \quad H_{-1} = \sqrt{1/2}(H_x - iH_y). \quad (2.18)$$

The second term on the right-hand side of Eq. (2.16) represents the effect of relaxation due to randomly fluctuating perturbations such as interatomic collisions which are discussed in chapter III, collisions with walls of the container[11),12)], trapping of resonance radiation[13)], spontaneous emission, etc. These effects cannot be expressed by a simple Hamiltonian. This term is expressed by using the Liouville operator which is represented by the relaxation matrix Γ :

$$\left(\frac{d\rho_{mm'}}{dt}\right)_{rel} = -\sum_{nn'} \Gamma^{nn'}_{mm'} \rho_{nn'} \qquad (2.19a)$$

where m, m', n, and n' are the magnetic quantum numbers. The minus sign in the right-hand side is chosen for the convenience in order to obtain positive decay rate when Γ can be diagonalized. In the irreducible representation, Eq. (2.19a) becomes

$$\left(\frac{d\rho^k_q}{dt}\right)_{rel} = -\sum_{k'q'} \Gamma^{kk'}_{qq'} \rho^{k'}_{q'} \ . \qquad (2.19b)$$

The symmetry properties will be discussed in the next section.

The last term of Eq. (2.16) describes the optical pumping by the resonant light field. Optical pumping effects in the excited state and the ground state have been extensively studied quantum-mechanically by Barrat and Cohen-Tannoudji[83),84)]. When the excited state with J=j is pumped from the ground state with $J=j_g$ by the resonance light, the optical pumping term is given by

$$\left(\frac{d\rho_{mm'}}{dt}\right)_{pump} = F_0 \sum_{\mu\mu'} \langle jm|\vec{e}\cdot\vec{d}|j_g\mu\rangle \rho_{\mu\mu'} \langle j_g\mu'|\vec{e}^*\cdot\vec{d}|jm'\rangle, \quad (2.20)$$

where $\vec{e}$ is the polarization vector of the light, $\vec{d}$ is the electric dipole operator of the atom, $\rho_{\mu\mu'}$ is the ground-state density matrix, and F_0 is defined as follows :

$$F_0 = \frac{1}{\pi\hbar^2} \int \frac{\gamma_{eg}}{(\omega-\omega_{eg}+\vec{k}\cdot\vec{v})^2 + \gamma_{eg}^2} u(\omega) f(v) dv d\omega. \quad (2.21)$$

In Eq. (2.21), ω and $\vec{k}$ are the angular frequency and the wave vector of the light, $u(\omega)$ is the energy spectrum of the light, $f(v)$ is the velocity distribution of the ground-state atoms, ω_{eg} is the energy seperation of the optical transition in angular frequency units, and γ_{eg} is the decay rate of the optical coherece. If we assume that the ground state is not polarized, $\rho_{\mu\mu'}$ is diagonal so that

$$\left(\frac{d\rho_{mm'}}{dt}\right)_{pump} = F_0' \sum_{\mu} \langle jm|\vec{e}\cdot\vec{d}|j_g\mu\rangle\langle j_g\mu|\vec{e}^*\cdot\vec{d}|jm'\rangle. \quad (2.22)$$

After the transformation to the irreducible representation, Eq. (2.22) becomes

$$\left(\frac{d\rho_q^k}{dt}\right)_{pump} = F_q^k , \quad (2.23a)$$

and

$$F_q^k = (-1)^{j+j_g}\sqrt{2k+1}\,|\langle j \| d \| j_g\rangle|^2 \begin{Bmatrix} 1 & 1 & k \\ j & j & j_g \end{Bmatrix} F_0' \Phi_q^k(\vec{e}), \quad (2.23b)$$

where $< j \| d \| j_g >$ is the reduced matrix element of $\vec{d}$ and the curly bracket is the 6-j symbol[80], and $\Phi_q^k(\vec{e})$ is defined as

$$\Phi_q^k(\vec{e}) = \sum_{q_1 q_2} (-1)^{q_2} e_{q_1} (e_{q_2})^* \begin{Bmatrix} 1 & 1 & k \\ q_1 & -q_2 & -q \end{Bmatrix}, \qquad (2.24)$$

where e_q is the standard compoment of $\vec{e}$ defined in the similar manner as in Eq. (2.18). From the property of the 3-j symbol, k should have the values, 0, 1, and 2 in order to have non-vanishing Φ_q^k. In other words, only population, orientation, and alignment can be created by a single photon process .

It should be noted that in Eq. (2.20) the Zeeman splittings of the excited and ground states have been assumed to be much smaller than the spectral width of the exciting light, and that Eq. (2.20) has been derived by the perturbation method up to the second order with respect to the light field, so that the higher-order effects have been neglected. If we consider the higher-order effects, the multipole moments with k>2 must be created in the states with $J \geq 2$. Recently, the hexadecapole moment (k=4) in the $2p_4$ state of neon has been observed[85], but we neglect these higher-order effects .

II. 4 Symmetry Properties of Relaxation

Before dealing with the collisional relaxation process in detail, this section is intended to show a number of general properties of relaxation matrix which always hold good, irrespec-

tive of the origin of relaxation. Most of the relaxation processes occur in a highly symmetric system: isotropic (spherically symmetric) or axially symmetric. The formalism based on the irreducible representation provides by far the simplest expressions for the relaxation term in Eq. (2.16) because of the symmetry properties, and it makes the physical interpretations of the relaxation matrix clear.

II.4.1 Rotational Transformation of the Relaxation Matrix

Whatever symmetry exists, the Hermiticity of the density matrix imposes a constraint on the relaxation matrix. If we combine Eq. (2.19a) and the Hermiticity relation $\rho^{*}_{mm'} = \rho_{m'm}$, we find

$$\Gamma^{nn'*}_{mm'} = \Gamma^{n'n}_{m'm} . \qquad (2.25a)$$

Irreducible equivalent for Eq. (2.25a) can be obtained from Eq. (2.19b) combined with Eq. (2.11) :

$$\Gamma^{kk'}_{qq'} = (-1)^{q-q'} \Gamma^{k\ k'\ *}_{-q-q'} . \qquad (2.25b)$$

Equation (2.25a) also implies that the population transfer rates Γ^{nn}_{mm} between Zeeman sublevels are always real. It follows that $\Gamma^{kk'}_{00}$ must be real.

In order to find other general properties of the relaxation

matrix ascribed to rotational symmetries, it is necessary to obtain the transformation of the relaxation matrix under an arbitrary rotation of the system. The relaxation matrix $\Gamma^{nn'}_{mm'}$ are transformed in a complicated way under the rotation, while the irreducible representation yields more simple relation. If the density matrix is transformed to $\bar{\rho}$ by a rotation, it is easily shown from Eq. (2.10) that Eq. (2.19b) can be transformed as

$$\left(\frac{d\bar{\rho}^{k}_{q}}{dt}\right)_{rel} = -\sum_{k'q'} \bar{\Gamma}^{kk'}_{qq'} \bar{\rho}^{k'}_{q'} , \tag{2.26}$$

where

$$\bar{\rho}^{k}_{q} = \sum_{q'} \mathcal{D}^{k}_{qq'} \rho^{k}_{q'}, \tag{2.27}$$

and

$$\bar{\Gamma}^{kk'}_{qq'} = \sum_{q_1 q_1'} \mathcal{D}^{k}_{qq_1} \Gamma^{k\,k'}_{q_1 q_1'} \mathcal{D}^{\dagger k'}_{q_1' q'} . \tag{2.28}$$

The coupling of two rotation matrix can be expanded in the form of the Clepsch-Gordan series[86], thus we obtain

$$\bar{\Gamma}^{kk'}_{qq'} = \sum_{Kq_1q_1'} (-1)^{q'-q_1'} \langle k\,k'\,q-q' | K\,q-q' \rangle \langle k\,k'\,q_1-q_1' | K\,q_1-q_1' \rangle \times \mathcal{D}^{K}_{q-q'\,q_1-q_1'} \Gamma^{k\,k'}_{q_1 q_1'} . \tag{2.29}$$

This is the transformation of the relaxation matrix under an arbitrary rotation. If the system has a symmetry under a certain rotation, $\bar{\Gamma}^{kk'}_{qq'}$ must be invariant under this rotation.

II.4.2 Axial Symmetry

We now consider the case that the system has an axial symetry. In this case, it is convenient to take the quantization axis (the z axis) in the direction of the axis of symmetry. If the rotation angle about the z axis is α, the rotation matrix $\mathcal{D}^{K}_{q-q'\,q_1-q_1'}$ in Eq. (2.29) equals to $\exp\{-i(q-q')\alpha\}$. From the invariance of $\bar{\Gamma}^{kk'}_{qq'}$ of Eq. (2.29) under an arbitrary rotation about the z axis, it can be shown that the relaxation matrix must be diagonal with respect to q:

$$\Gamma^{kk'}_{qq'} = \delta_{qq'}\Gamma^{kk'}_{qq} . \tag{2.30}$$

This equation, combined with Eqs. (2.3) and (2.19), gives the relation as

$$\Gamma^{kk'}_{qq} = \sum_{mm'} (-1)^{m+m'} \langle j\ j\ m\ q-m \mid kq \rangle \langle j\ j\ m'\ q-m' \mid kq \rangle \Gamma^{m'\ m'-q}_{m\ \ m-q} , \tag{2.31}$$

where j and m are the total angular momentum and its projection on the z axis.

As the relation given by Eq. (2.30) gives only the conservation of q, there generally exists the coupling between the multipole moments with different values of k. The coupling between orientation (k=1) and alignment (k=2) will be studied in more detail for the atoms excited by a single-mode laser, subjected to anisotropic collisions with the ground-state atoms.

II.4.3 Spherical Symmetry

Spherical symmetry is the highest one among all rotational symmetries, and the system having such symmetry is mentioned to be isotropic. In fact, this brings about further constraint on the relaxation matrix in addition to that given by Eq. (2.30). Since $\bar{\Gamma}^{kk'}_{qq'}$ in Eq. (2.29) should be invariant under any rotations specified by arbitrary Euler angles because of the spherical symmetry, the rotation matrix in the right-hand side of Eq. (2.29) should be independent of the Euler angles. Consequently, only the terms with $K=q-q'=q_1-q_1'=0$ contribute to the sum of the right-hand side of Eq. (2.29). Then we obtain

$$\bar{\Gamma}^{kk'}_{qq'} = \delta_{qq'}\delta_{kk'}\sum_{q_1}(-1)^{q-q_1}\langle k\,k\;q\;-q|00\rangle\langle k\,k\;q_1\;-q_1|00\rangle\Gamma^{kk}_{q_1q_1}$$

$$= \delta_{qq'}\delta_{kk'}\sum_{q_1}\frac{1}{2k+1}\Gamma^{k\,k}_{q_1q_1} \quad . \tag{2.32}$$

From the rotational invariance, $\bar{\Gamma}^{kk}_{qq}$ should be equal to Γ^{kk}_{qq}. then it is easily found that

$$\Gamma^{kk'}_{qq'} = \delta_{qq'}\delta_{kk'}\Gamma^{kk}_{qq} \quad , \tag{2.33}$$

and that the relaxation matrix Γ^{kk}_{qq} is independent of the value of q. From Eqs. (2.31) and (2.33), we obtain the relation between Γ^{kk}_{qq} and $\Gamma^{nn'}_{mm'}$:

$$\Gamma^{kk}_{qq} = \sum_{mm'}(-1)^{m+m'}\langle j\;j\;m\;q-m\;|\,k\,q\rangle\langle j\;j\;m'\;q-m'|\,k\,q\rangle\Gamma^{m'm'-q}_{m\;m-q} \tag{2.34}$$

Equation (2.33) shows that each multipole component decays independently and does not couple with any other components. Moreover, all multipole components with the same order k decay with equal decay rates.

II.4.4 Symmetry with Respect to Plane Reflections

Axial symmetry is often accompanied with the symmetry under reflections with respect to planes containing the axis of symmetry. The reflection with respect to a plane is considered as the product of inversion and the rotation with angle π about the axis perpendicular to the plane. Since ρ^k_q is invariant under inversion as is the general case of the angular momentum, the relaxation matrix should be invariant under rotations with angle π about all axes perpendicular to the axis of symmetry (the z axis). Then we introduce the rotation matrix $\mathcal{D}^k_{qq'}(\alpha,\pi,-\alpha)$ where α is an arbitrary azimuthal angle of the axis of the rotation. Substituting this rotation matrix into Eq. (2.28) and using Eq.(2.30), the arbitrarity of α yields

$$\Gamma^{kk'}_{qq} = (-1)^{k+k'}\Gamma^{k\ k'}_{-q-q} \quad . \tag{2.35}$$

Equation (2.35) implies that $\Gamma^{kk'}_{qq}=0$ for odd k+k'. This relation, combined with the Hermiticity relation (2.25b), leads to the relation given by

$$\Gamma^{kk'}_{qq'} = (-1)^{k+k'}\Gamma^{kk'*}_{qq} \quad . \tag{2.36}$$

From this relation, we find that $\Gamma_{qq}^{kk'}$ is real for even k+k', and pure imaginary for odd k+k'. Therefore the diagonal components Γ_{qq}^{kk} of the relaxation matrix are always real.

II.5 Concluding Remarks

In this chapter, we have introduced the irreducible tensor by which the density matrix can be expanded. On this irreducible basis, we derived the master equation for the density matrix of the atomic internal state excited by polarized light.

Furthermore, we have studied on the symmetry properties of the relaxation matrix, which are applicable to any types of relaxations irrespective of their origin: interatomic collisions, collisions with the walls of the container, spontaneous emission, trapping by multiple scattering of resonance radiation, etc. If the situation is isotropic, each multipole components decays without coupling with each other, and the relaxation rates are the same for all components of a multipole moment. On the other hand, if the situation is anisotropic, the coupling between different multipole components appears, and the relaxation rate depends not only on the order k but also on the component q of the multipole. In the following chapters, particular attentions may be given to the transfer between orientation and alignment of atoms excited by a single-mode laser.

In this case of single-mode laser excitation, the situation is no more isotropic, but has only axial and plane-reflection symmetries.

CHAPTER III

DEPOLARIZATION OF THE EXCITED STATE BY ANISOTROPIC COLLISIONS

III.1 Introduction

Collisional relaxation among Zeeman substates of the excited states has been extensively studied theoretically and experimentally in past two decades. In most of these experiments, the atoms were excited by the light from a spectral lamp or by collisions with electrons in a weak rf discharge, so that the velocity distribution of the excited atoms can generally be described by an isotropic Maxwellian function when self-absorption of the incident light can be neglected. As a result, the collisions of the excited atoms (emitter atoms) with the ground-state atoms (perturber atoms) are considered to be isotropic, i.e., all collision directions are equally probable. It is obvious from the argument of symmetry given in Sec. II.4.3 that isotropic collisions cause the independent relaxation of each multipole component of the excited Zeeman multiplet without coupling with each other such that

$$\frac{d\rho_q^k}{dt} = -\Gamma^k \rho_q^k \,. \qquad (3.1)$$

This equation also implies that each relaxation rate Γ^k is independent of the value of q which characterizes the component of each multipole. In recent years, gas lasers have been used to study the relaxations of orientation and alignment of the laser levels[87)-93)], and now tunable lasers such as Dye lasers are considered to be powerful light sources because they remove the limitations on the levels to be studied.

When atoms are excited by laser light, the velocity distribution of excited atoms along the axis of the laser propagation is generally different from the Maxwellian distribution whose width is determined by the gas temperature, because of the axial-mode structure of the spectrum of the laser light. Therefore, the averaged collisional effect on the excited atoms is no longer isotropic

In this chapter, we would like to present the theoretical treatment of the collisional relaxation of atoms excited by a single-mode laser light. Since the spectral width of the single-mode output of a laser is generally much narrower than the Doppler width of the absorption spectrum, the velocity distribution of excited emitters along the light axis generally becomes narrower than the distribution perpendicular to the light axis which are given by a two-dimensional Maxwellian function. Consequently, the collisions with perturber atoms become anisotropic, and the degree of anisotropy can be changed by changing the detuning of the laser frequency from the absorption line center. In case of anisotropic collisions, the relaxation of ρ_q^k is no longer

given by Eq. (3.1), and can generally be expressed as

$$\frac{d\rho_q^k}{dt} = -\sum_{k'q'} \Gamma_{qq'}^{kk'} \rho_{q'}^{k'} , \qquad (3.2)$$

which shows that the transfer among multipole components with different orders becomes possible as has been mentioned in the previous chapter.

The purpose of the present chapter is to calculate the relaxation matrix $\Gamma_{qq'}^{kk'}$ for atoms excited by a single-mode laser. the calculations are made mainly along the line of the work of Berman and Lamb[22], by removing their assumption of isotropic collisions. The next section is devoted to present the assumptions which we have made in the present calculations and to discuss about their validities. In Sec. III.3, before considering the average collisional effect, we derive the time-evolution matrix for the wave function for a single completed collision. The calculations have not been only for the excited state with J=1 but also for the excited state with J=2. The latter results will actually be applied to the alignment destroying cross sections of neon in the $2p_4$ state perturbed by rare gases, which have been measured in the present work. We calculate the averaged relaxation matrix for emitters moving with a definite velocity, which is obtained by averaging over the perturber velocity distribution. These results may be applicable to the atomic collisions in atomic beam experiments. Finally, we obtain the relaxation matrix for emitters with J=1 excited by a single-mode laser,

after averaging over the emitter velocity distribution.

Although we have analyzed the case of the single-mode excitation, the results obtained here are easily applicable to the more general case that atoms are excited by the light with arbitrary spectrum.

III.2 Assumptions and Approximations

We intend to obtain the explicit equation of motion for the density matrix of atoms in an excited state which are perturbed by collisions with other atoms. The collisions which we are interested in are those between an excited atom and another atom in its ground state, because most of atoms are in their ground state at any time. The atoms in the excited state are called "emitters", and the ground-state atoms which perturbe the emitters are called "perturbers". The mechanism of atomic collision is too complicated to treat completely, so that a number of assumptions and approximations must be made.

III.2.1 The Impact Approximation

We make use of the "impact approximation", in which collisions with perturbers experienced by a single emitter are assumed to be well separated to each other. As the result, each collision is assumed to be independent from the others. This implies that the collision time τ_c, which is defined as the average duration of a collisional interaction, is much shorter than the

the mean time between collisions, so that only the binary collisions are important. Many authors, for example Anderson[4], Omont[19] and Berman and Lamb[22], made clear the conditions under which this impact approximation is valid. In our experiments discussed in the latter part of the present work, the effective interatomic distance for a collisional interaction is about 10^{-7}cm, which leads to $\tau_c \sim 10^{-12}$sec for the temperature T~400K. While, the mean time between collisions which is defied as $(n_p \bar{v}_R \sigma)^{-1}$, where n_p is the perturber density, $\bar{v}_R$ is the mean relative velocity, and σ is the cross section, is of the order of 10^{-7}sec for the pressure (~1 Torr). This implies that the validity of the impact approximation is justified for our purpose. Due to this approximation, the collisional process is determined by the form of the interaction.

III.2.2 The Classical-Linear-Path Approximation

The relative motion of the two colliding atoms is assumed to follow a classical trajectory, while the internal state of atom is treated quantum-mechanically. This semi-classical treatment was widely accepted by many authors. It is generally simpler than the fully quantum-mechanical theories[94),95)] in which the atomic motion is also treated quantum-mechanically. The latter is necessary particularly when the close or slow collisions are important. However, in the present case, collisions occur in the gas temperature of about 400K at most, so that the semi-

classical theory seems to be valid. In the semi-classical theory we can think of the motion of atoms only in terms of packets of translational wave functions.

In addition to this, we assume that the relative motion of colliding atoms is not affected by the collisions, namely the relative trajectory of the perturber with respect to the emitter is a linear path. This "classical-linear-path approximation" holds good for collisions with the effective cross section larger than the kinetic cross section. On the other hand, it is necessary to consider the modification of the relative trajectory from the linear path when the repulsive interaction due to the overlap of electron clouds of two colliding atoms are dominant. The modifications are very complicated because of the fact that they are dependent on the internal states of atoms. In fact, the relative trajectories are modified in different manners for colliding atoms in different magnetic substates because of the anisotropic nature of the interaction between two colliding atoms. Here, we use the classical-linear-path approximation for the sake of simplicity.

III.2.3 The Electrostatic Dipole-Dipole Approximation

The collisional interaction is assumed to be electrostatic for the low-energy collisions which we are interested in. This interaction can be expanded by the multipole expression[96]. Since we consider collisions between neutral atoms, the leading

term, which is the lowest order with respect to the inverse power of the interatomic separation R, is the electrostatic dipole-dipole interaction which is given by

$$V(\vec{R}(t)) = \frac{1}{R(t)^3}\{\vec{d}_e \cdot \vec{d}_p - 3(\vec{d}_e \cdot \vec{u})(\vec{d}_p \cdot \vec{u})\}, \tag{3.3}$$

where R(t) is the interatomic separation at time t, $\vec{u}$ is the unit vector along the interatomic axis directed to the perturber, and $\vec{d}_e$ and $\vec{d}_p$ are the electric dipole operators of the emitter and the perturber, respectively. This interaction Hamiltonian is transformed under rotation in the same manner as the second-order irreducible tensor, so that Eq. (3.3) can be expressed in terms of the spherical harmonics $Y^2_q(\theta,\phi)$, as

$$V(\vec{R}(t)) = \frac{1}{R(t)^3}\left(\frac{24\pi}{5}\right)^{1/2} \sum_q (-1)^q \; V^2_q \; Y^2_{-q}(\theta,\phi) \; , \tag{3.4}$$

where θ and ϕ are the polar angles of $\vec{R}$, and V^2_q is the second-order irreducible tensorial product of $\vec{d}_e$ and $\vec{d}_p$ defined as

$$V^2_q = \sum_{q_1 q_2} < 1 \; 1 \; q_1 \; q_2 | \; 2 \; q > d_{eq} d_{pq}. \tag{3.5}$$

In Eq. (3.5), d_{eq} and d_{pq} are the standard components of $\vec{d}_e$ and $\vec{d}_p$, respectively. This shows the anisotropy of the interaction of a single collision, which is the cause of the complicated relaxations of multipole moments of the excited states. This approximation becomes invalid for close collisions.

Collisions between emitters and perturbers are classified into two types. The first type is the "resonant collision" which cause the excitation transfer from the emitter to the perturber and occurs only between the same kind of atoms. In this type of collisions, the dipole-dipole interaction contributes to the relaxation in the first order. Furthermore, this type must be considered only when the emitter is in the resonant state connected to the ground state by the allowed dipole transition, which collides with the same kind atom in the ground state. The second type is the "nonresonant collision" which is sometimes called "foreign gas collision", because this type of collision is important when the emitter and the perturber are different atoms. However, this type of collision occurs even for the same kind atoms when the emitter is in the excited state other than the resonant state. In this type , the lowest-order contribution of the dipole-dipole interaction is in its second order, which gives rise to the van der Waals interaction ($\sim R^{-6}$) (the induced dipole-induced dipole interaction). The R^{-6} dependence of this interaction leads to the relatively short effective range of interaction that occasionally becomes comparable to that of repulsive interaction. In such cases, the dipole-dipole approximation becomes invalid.

III.2.4 The Sudden Approximation

Finally, we make use of the "sudden approximation", in

which the life time for the spontaneous decay is assumed to be much longer than τ_c, and the external magnetic field is assumed to be weak such that the Larmor precession of the excited state can be neglected during a single collision. The former condition is satisfied in the case of our interest, because the radiative lifetime is about 10^{-8} sec, while $\tau_c \sim 10^{-12}$ sec. The latter condition is equivalent to the assumption that the Zeeman splitting of the excited state is much smaller than τ_c^{-1}, which enables us to treat a collision as a nonadiabatic process with respect to collisional transitions among Zeeman substates. Gay et al. have shown that this assumption becomes invalid in the presence of a strong magnetic field stronger than several kilogauss[56)-59)]. In the present experiments discussed in Chap. IV and V, the external magnetic field ($\lesssim$ 0.1 kG) is so weak that the latter condition is satisfied.

III.3 Collisional Depolarizations of Emitters Moving with a Definite Velocity

In this section, before investigating the anisotropic collisions between emitters excited by a single-mode laser and perturbers, we consider simpler anisotropic collisions between emitters moving with a definite velocity and perturbers whose velocity distribution is given by an isotropic Maxwellian distribution. The situation has an axial symmetry with respect to the axis along the direction of the emitter velocity. Such a situation may

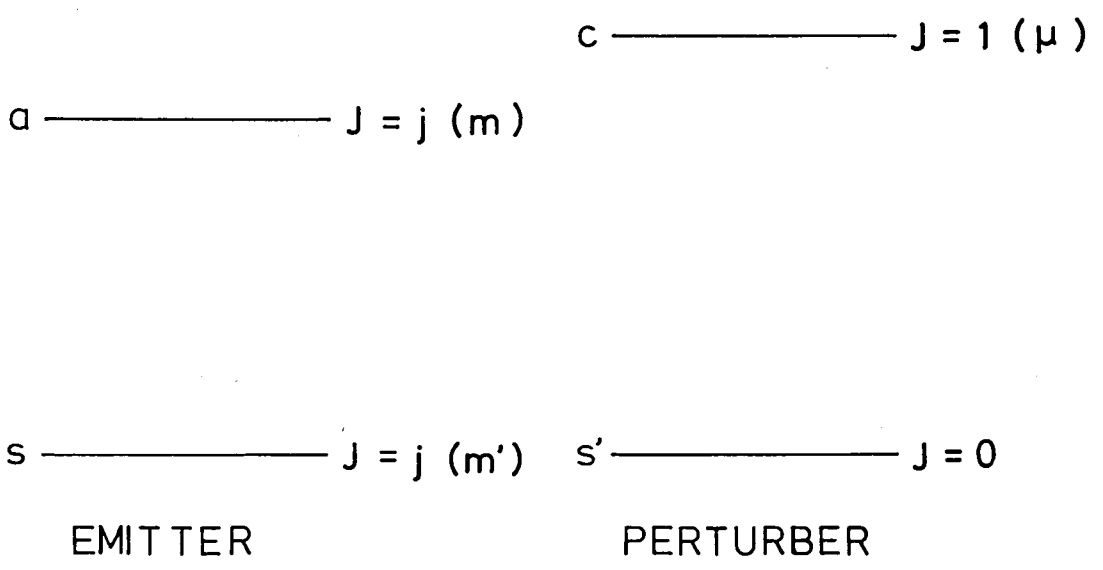

Fig. 3.1 Schematic diagrams of energy levels of the emitter and the perturber to be considered.

be approximately realized in the atomic-beam experiments in which a well-collimated beam is optically excited to the excited state and passes through gaseous atoms.

We consider mainly nonresonant collisions. Our procedure of theoretical calculations follows closely the work of Berman and Lamb[22] who have treated the isotropic collisions. In our case, we have to average the collisinal effects over the perturber velocity distribution, in stead of averaging them over the isotropic relative-velocity distribution of colliding atomic pairs.

III.3.1 The effects of a single collision

The model of energy schemes of the emitter and perturber is shown in Fig. 3.1. Between the upper and lower states of the emitter and perturber, the electric dipole transitions are assumed to be allowed. Consider the case that the emitter is initially in the excited state a with the total angular momentum J=j, while the perturber is in the ground state s' with J=0. During a single collision, the emitter and perturber undergo virtual transitions to intermediate states s with J=j' and c with J=1, respectively. The intermediate state s of the emitter is, of course, not necessary to be the ground state. After the single collision, both of the two atoms return to the initial states a and s', but the final state of the emitter within the Zeeman multiplet a may differ from the initial state.

A part of the wave function of our interest can be expanded as follows :

$$
\begin{aligned}
|\psi(t)> = & \sum_{m} a_{m}(t)\,|ajm;s'00>\exp(-iE_{ms'}t/\hbar) \\
& + \sum_{m'\mu} c_{m'\mu}(t)\,|sj'm';cl\mu>\exp(-iE_{m'\mu}t/\hbar) \\
& + \sum_{m\mu} d_{m\mu}(t)\,|ajm;cl\mu>\exp(-iE_{m\mu}t/\hbar) \\
& + \sum_{m'} e_{m'}(t)\,|sj'm';s'00>\exp(-iE_{m's'}t/\hbar), \qquad (3.6)
\end{aligned}
$$

where $|\alpha JM;\beta J'M'>$ is the product of the kets for the eigen states of the emitter $|\alpha JM>$ and the perturber $|\beta J'M'>$, and the total energy $E_{MM'}$ is defined as

$$
\begin{aligned}
E_{MM'} &= <\alpha JM|\,\mathcal{H}_e\,|\alpha JM> + <\beta J'M'|\,\mathcal{H}_p\,|\beta J'M'>, \\
&= E_{\alpha JM} + E_{\beta J'M'}, \qquad (3.7)
\end{aligned}
$$

where $\mathcal{H}_e$ and $\mathcal{H}_p$ are the Hamiltonians of isolated emitter and perturber, respectively.

The time evolution of this wave function is governed by the Schrödinger equation :

$$
i\hbar\frac{d}{dt}|\psi(t)> = [\,\mathcal{H}_e + \mathcal{H}_p + V(t)\,]\,|\psi(t)>, \qquad (3.8)
$$

where V(t) is the interaction Hamiltonian of the colliding atoms given by Eq. (3.3).

It is obvious from the selection rules of dipole transitions

that the interaction Hamiltonian V(t) can be represented in a matrix form :

$$V(t) = \begin{array}{c} \\ aj*;s'00 \\ sj'*;cl* \\ aj*cl* \\ sj'*;s'00 \end{array} \begin{array}{c} \begin{array}{cccc} aj*;s'00 & sj'*;cl* & aj*;cl* & sj'*;s'00 \end{array} \\ \begin{pmatrix} 0 & Z(t) & 0 & 0 \\ Z(t)^{\dagger} & 0 & 0 & 0 \\ 0 & 0 & 0 & G(t) \\ 0 & 0 & G(t)^{\dagger} & 0 \end{pmatrix} \end{array}, \tag{3.9}$$

where the asterisks represent sets of magnetic quantum numbers of the associated states, and hence Z(t) is a $(2j+1)\times 3(2j'+1)$ submatrix and G(t) is a $3(2j'+1)\times(2j+1)$ submatrix. As we consider the case that the atomic system is initially in the state $|aj*;s'00\rangle$, we are interested only in the submatrices Z and $Z^{\dagger}$. We will consider a collision in the reference frame Ω_0 chosen as seen in Fig. 3.2, in which the emitter is fixed at the origin while the perturber moves with relative velocity $\vec{v}_R$ in the $-x_c$ direction and with the impact parameter $\vec{b}$ in the z_c direction. It is the same as Berman's collision frame which is different from the frame used by Carrington et al.[24] and Cooper and Stacey[52]. [To transfer from our frame to that of Cooper and Stacey, a rotation given by the Euler angles $(\pi,\pi/2,\pi)$ is required.] If we choose t=0 as the time for the closest approach of two atoms, we find that

$$\vec{R} = \vec{b} + \vec{v}_R t, \tag{3.10}$$

and

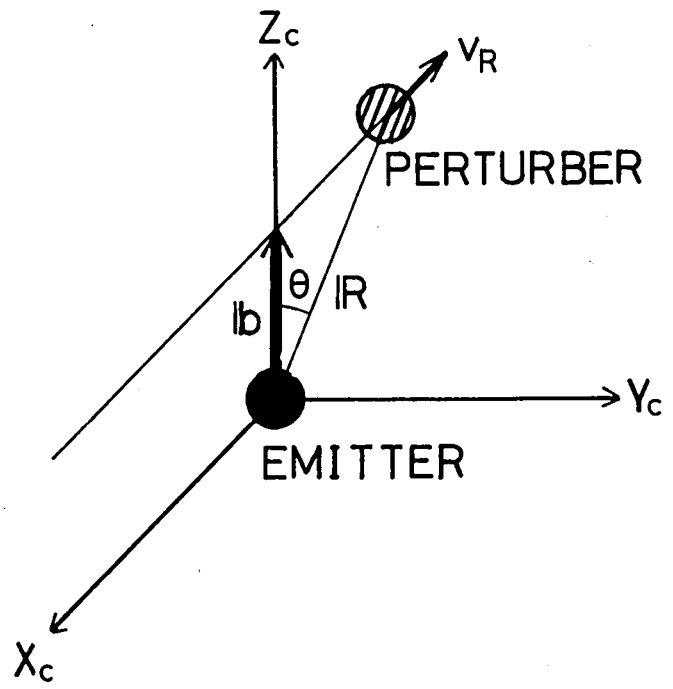

Fig. 3.2 Reference frame Ω_0 in which the emitter is fixed at the origin and the perturber moves with relative velocity $\vec{v}_R$ in the x_c direction. The z_c axis is chosen along the direction of the impact parameter $\vec{b}$.

$$\sin\theta = \frac{v_R t}{R(t)}, \quad \cos\theta = \frac{b}{R(t)}. \tag{3.11}$$

where θ is the polar angle of the vector $\vec{R}$.

In the case that j=1 and j'=0, we can represent the interaction matrix Z in our reference frame, using Eqs. (3.3)–(3.5), as

$$\langle a1*;s'00|Z|s00;c1*\rangle = -\frac{1}{6R(t)^3}\langle a1\|d_e\|s0\rangle\langle s'0|d_p|c1\rangle \begin{pmatrix} A & -3\sqrt{2}B & 3C \\ -3\sqrt{2}B & 2A & 3\sqrt{2}B \\ 3C & 3\sqrt{2}B & A \end{pmatrix}, \tag{3.12}$$

where $\langle \alpha J\|d\|\beta J'\rangle$ is the reduced matrix element of the electric dipole operator, the rows and columns are arranged in decreasing order of magnetic quantum numbers, and

$$A = 2 - 3\sin^2\theta, \quad B = \sin\theta\cos\theta, \quad C = \sin^2\theta. \tag{3.13}$$

In the cases those j=2 and j'=1, and j=2 and j'=2,

$$\langle a2*;s'00|Z|s1*;c1*\rangle = -\frac{\sqrt{5}}{60R(t)^3}\langle a2\|d_e\|s1\rangle\langle s'0\|d_p\|c1\rangle\tilde{D}, \tag{3.14}$$

$$\langle a2*;s'00|Z|s2*;c1*\rangle = -\frac{\sqrt{5}}{60R(t)^3}\langle a2\|d_e\|s2\rangle\langle s'0\|d_p\|c1\rangle\tilde{E}, \tag{3.15}$$

where the explicit forms of matrices $\tilde{D}$ and $\tilde{E}$ are shown in Tables 3.1.

The probability amplitudes a_m and $c_{m'\mu}$ in Eq. (3.6) can be considered as the components of column vectors $\vec{a}$ and $\vec{c}$, which are expressed as

Table 3.1(a) The Matrix Elements $\langle a2m;s'00|\tilde{D}|slm';cl\mu\rangle$

The factors A, B, and C are defined by Eqs.(3.13).

$\tilde{D}$		m';μ								
		1;1	1;0	1;-1	0;1	0;0	0;-1	-1;1	-1;0	-1;-1
m	2	$2\sqrt{3}A$	$-6\sqrt{6}B$	$6\sqrt{3}C$	0	0	0	0	0	0
	1	$-6\sqrt{3}B$	$-2\sqrt{6}A$	$6\sqrt{3}B$	$\sqrt{6}A$	$-6\sqrt{3}B$	$3\sqrt{6}C$	0	0	0
	0	$3\sqrt{2}C$	$-6B$	$\sqrt{2}A$	$-12B$	$-4\sqrt{2}A$	$-12B$	$\sqrt{2}A$	$-6B$	$3\sqrt{2}C$
	-1	0	0	0	$3\sqrt{6}C$	$6\sqrt{3}B$	$\sqrt{6}A$	$-6\sqrt{3}B$	$-2\sqrt{6}A$	$6\sqrt{3}B$
	-2	0	0	0	0	0	0	$6\sqrt{3}C$	$6\sqrt{6}B$	$2\sqrt{3}A$

Table 3.1(b) The matrix Elements $\langle a2m;s'00|\tilde{E}|s2m';c1\mu\rangle$

The factors A, B, and C are defined by Eqs.(3.13).

$\tilde{E}$	m' ; μ														
m	2;1	2;0	2;-1	1;1	1;0	1;-1	0;1	0;0	0;-1	-1;1	-1;0	-1;-1	-2;1	-2;0	-2;-1
2	-12B	$-4\sqrt{2}$A	12B	-2A	$6\sqrt{2}$B	-6C	0	0	0	0	0	0	0	0	0
1	6C	$6\sqrt{2}$B	2A	-6B	$-2\sqrt{2}$A	6B	$-\sqrt{6}$A	$6\sqrt{3}$B	$-3\sqrt{6}$C	0	0	0	0	0	0
0	0	0	0	$3\sqrt{6}$C	$6\sqrt{3}$B	$\sqrt{6}$A	0	0	0	$-\sqrt{6}$A	$6\sqrt{3}$B	$-3\sqrt{6}$C	0	0	0
-1	0	0	0	0	0	0	$3\sqrt{6}$C	$6\sqrt{3}$B	$\sqrt{6}$A	6B	$2\sqrt{2}$A	-6B	-2A	$6\sqrt{2}$B	-6C
-2	0	0	0	0	0	0	0	0	0	6C	$6\sqrt{2}$B	2A	12B	$4\sqrt{2}$A	-12B

$$\vec{a} = \begin{pmatrix} a_j(t) \\ a_{j-1}(t) \\ \vdots \\ a_{-j}(t) \end{pmatrix}, \quad \vec{c} = \begin{pmatrix} c_{j',1}(t) \\ c_{j'-1,1}(t) \\ \vdots \\ c_{-j',1}(t) \end{pmatrix}. \tag{3.16}$$

The time evolution of $\vec{a}$ and $\vec{c}$ are governed by the time-dependent Schrödinger equation in the interaction representation given by

$$i\hbar\dot{\vec{a}} = \tilde{Z}(t)\vec{c}\,, \quad i\hbar\dot{\vec{c}} = \tilde{Z}(t)^{\dagger}\vec{a}\,, \tag{3.17}$$

where the matrix $\tilde{Z}(t)$ is given by

$$\tilde{Z}(t) = \exp\{i(\mathcal{H}_e + \mathcal{H}_p)t/\hbar\}Z(t)\exp\{-i(\mathcal{H}_e + \mathcal{H}_p)t/\hbar\}. \tag{3.18}$$

Since the emitter is in the excited state a before the collision ($t=-\infty$), the initial conditions for Eq. (3.17) are given by

$$\vec{a}(-\infty) = \vec{a}_0\,,$$
$$\vec{c}(-\infty) = 0\,. \tag{3.19}$$

The formal integration of Eq. (3.17) gives the integral equation for the wave vector $\vec{a}$:

$$\vec{a}(t) = \vec{a}_0 + (i\hbar)^{-2}\int_{-\infty}^{t}dt'\tilde{Z}(t')\int_{-\infty}^{t'}dt''\tilde{Z}(t'')^{\dagger}\vec{a}(t''). \tag{3.20}$$

Substituting Eq.(3.18) into Eq.(3.20), we obtain

$$\vec{a}(t) = \vec{a}_0$$

$$+(i\hbar)^{-2}\int_{-\infty}^{t}dt'Z(t')\int_{-\infty}^{t'}dt''Z(t'')^{\dagger}\exp\{-i\Delta\omega(t'-t'')\}\vec{a}(t''), \tag{3.21}$$

where $\Delta\omega$ is the energy separation between the initial and intermediate states of the emitter-perturber system :

$$\Delta\omega = (E_{cs} - E_{as'})/\hbar. \tag{3.22}$$

Here we have assumed that the Zeeman splittings are so small that the Larmor precessions are negligible during the single collision (the "sudden approximation"). Namely, the differences in the phase factor $\exp\{-i(\mathcal{H}_e + \mathcal{H}_p)t/\hbar\}$ in Eq.(3.18) for the Zeeman substates are negligibly small, hence $\Delta\omega$ has been assumed to be independent of magnetic quantum numbers.

In the case of nonresonant collision, the energy separation $\Delta\omega$ is always much larger than τ_c^{-1}. In our typical case to be considered in Chap. V, $|\Delta\omega| \sim 10^{16}$ rad/sec while $\tau_c \sim 10^{-12}$ sec, then the inequality $|\Delta\omega| \gg \tau_c^{-1}$ is satisfied. Accordingly, both $Z(t'')^{\dagger}$ and $\vec{a}(t'')$ are slowly varying functions of time, compared with $\exp(-i\Delta\omega t'')$. Then the integrand in the integral with respect to t'' in Eq.(3.21) contributes only when t''=t'. Hence, the double integral is reduced to a single integral :

$$\vec{a}(t) = \vec{a}_0 - (i\hbar^2\Delta\omega)^{-1}\int_{-\infty}^{t}dt'Z(t')Z(t')^{\dagger}\ \vec{a}(t'). \tag{3.23}$$

If we introduce a time evolution matrix M defined as

$$\vec{a}(t) = M(t)\vec{a}_0 \ , \quad M(-\infty) = 1 \ , \tag{3.24}$$

we can rewrite Eq.(3.23) in the form of a differential equation

$$\frac{dM(t)}{dt} = iY(t)M(t), \tag{3.25}$$

where

$$Y(t) = \frac{1}{\hbar^2\Delta\omega} Z(t)Z(t)^{\dagger} \ . \tag{3.26}$$

Using the transformation from t to θ given by Eqs.(3.11), Eq.(3.25) can be rewritten as

$$\frac{dM(t)}{dt} = i\tilde{Y}(\theta)M(\theta), \tag{3.27}$$

where

$$\tilde{Y}(\theta) = \frac{b}{v_R\cos^2\theta} Y(t), \tag{3.28}$$

with the initial condition $M(\theta=-\pi/2)=1$. For some typical values of j and j', the matrix $\tilde{Y}(\theta)$ is expressed as follows :

(a) j=1, j'=0 ;

$$\tilde{Y}(\theta) = \frac{2B}{b^5 v_R}\cos^4\theta \begin{pmatrix} 2+3\sin^2\theta & 3\sqrt{2}\sin\theta\cos\theta & -3\sin^2\theta \\ 3\sqrt{2}\sin\theta\cos\theta & 2(4-3\sin^2\theta) & -3\sqrt{2}\sin\theta\cos\theta \\ -3\sin^2\theta & -3\sqrt{2}\sin\theta\cos\theta & 2+3\sin^2\theta \end{pmatrix}, \tag{3.29}$$

where the rows and columns are arranged in decreasing order of magnetic quantum numbers, and

$$B = \frac{1}{36\hbar^2\Delta\omega}|\langle a1\|d_e\|s0\rangle\langle s'0\|d_p\|c1\rangle|^2. \qquad (3.30)$$

(b) j=2, j'=1 ;

$$\tilde{Y}_D(\theta) = \frac{12B_D}{b^5 v_R}\cos^4\theta\tilde{D}\cdot\tilde{D}^\dagger , \qquad (3.31)$$

$$B_D = \frac{1}{720\hbar^2\Delta\omega_D}|\langle a2\|d_e\|s1\rangle\langle s'0\|d_p\|c1\rangle|^2. \qquad (3.32)$$

(c) j=2, j'=2 ;

$$\tilde{Y}_E(\theta) = \frac{12B_E}{b^5 v_R}\cos^4\theta\tilde{E}\cdot\tilde{E}^\dagger , \qquad (3.33)$$

$$B_E = \frac{1}{720\hbar^2\Delta\omega_E}|\langle a2\|d_e\|s2\rangle\langle s'0\|d_p\|c1\rangle|^2. \qquad (3.34)$$

The explicit form of the matrices $\tilde{D}\cdot\tilde{D}^\dagger$ and $\tilde{E}\cdot\tilde{E}^\dagger$ are shown in Table 3.2.

Here, we introduce the density matrix of the emitter-perturber system. However, as the perturber has been assumed to be in the nondegenerate ground state before and after the collision, the density matrix of the emitter-perturber system is deduced to the density matrix of the excited state of emitter, which is defined as $\rho_{mm'}=a_m a_{m'}^*$. The change in the density matrix caused by a single completed collision in the reference frame Ω_0 is given by

$$\delta\rho_{mm'}(b,v_R,\Omega_0,h)=[M(t=\infty)\,\rho(-\infty,h)M(t=\infty)^\dagger]_{mm'}-\rho_{mm'}(-\infty,h), \qquad (3.35)$$

Table 3.2

(a) The Matrix Element $\langle a2m;s'00|\tilde{D}\cdot\tilde{D}^{\dagger}|a2m';s'00\rangle$

The factors B and C are defined by Eqs.(3.13).

$\tilde{D}\cdot\tilde{D}^{\dagger}$		m'				
		2	1	0	-1	-2
m	2	2(2+3C)	6B	$-\sqrt{6}$C	0	0
	1	6B	10-3C	$\sqrt{6}$B	-3C	0
	0	$-\sqrt{6}$C	$\sqrt{6}$B	6(2-C)	$-\sqrt{6}$B	$-\sqrt{6}$C
	-1	0	-3C	$-\sqrt{6}$B	10-3C	-6B
	-2	0	0	$-\sqrt{6}$C	-6B	2(2+3C)

(b) The Matrix Element $\langle a2m;s'00|\tilde{E}\cdot\tilde{E}^{\dagger}|a2m';s'00\rangle$

The factors B and C are defined by Eqs.(3.13).

$\tilde{E}\cdot\tilde{E}^{\dagger}$		m'				
		2	1	0	-1	-2
m	2	6(2-C)	-6B	$\sqrt{6}$C	0	0
	1	-6B	3(2+C)	$-\sqrt{6}$B	3C	0
	0	$\sqrt{6}$C	$-\sqrt{6}$B	2(2+3C)	$\sqrt{6}$B	$\sqrt{6}$C
	-1	0	3C	$\sqrt{6}$B	3(2+C)	6B
	-2	0	0	$\sqrt{6}$C	6B	6(2-C)

where the density matrix just before the collision is given by $\rho(-\infty,h)$ which depends generally on the past collision history h experienced by the emitter. We can rewrite Eq.(3.35) as

$$\delta\rho_{mm'}(b,v_R,\Omega_0,h) = \sum_{nn'} M^{nn'}_{mm'}(b,v_R,\Omega_0)\rho_{nn'}(-\infty,h), \qquad (3.36)$$

where

$$M^{nn'}_{mm'}(b,v_R,\Omega_0) = M_{mn}(\infty)M_{m'n'}(\infty)^* - \delta_{mn}\delta_{m'n'}, \qquad (3.37)$$

and m,m',n, and n' are the magnetic quantum numbers of the excited state a.

III.3.2 Average Collisional Effects on Emitters Moving with a Definite Velocity

In this subsection, we intend to derive the macroscopic rate equation for emitters moving with a definite velocity fixed in the velocity space, under the influence of collisions with gaseous perturbers. For this purpose, we must average Eq.(3.36) over all possible impact parameters, perturber velocities, and collision histories.

In the proceeding of these calculations, the use of our reference frame makes the calculations rather complicated, so that we will introduce a new reference frame Ω_0', in which the perturber moves in the z_c direction with the impact parameter directed in the x_c direction (see Fig. 3.3). This frame is the

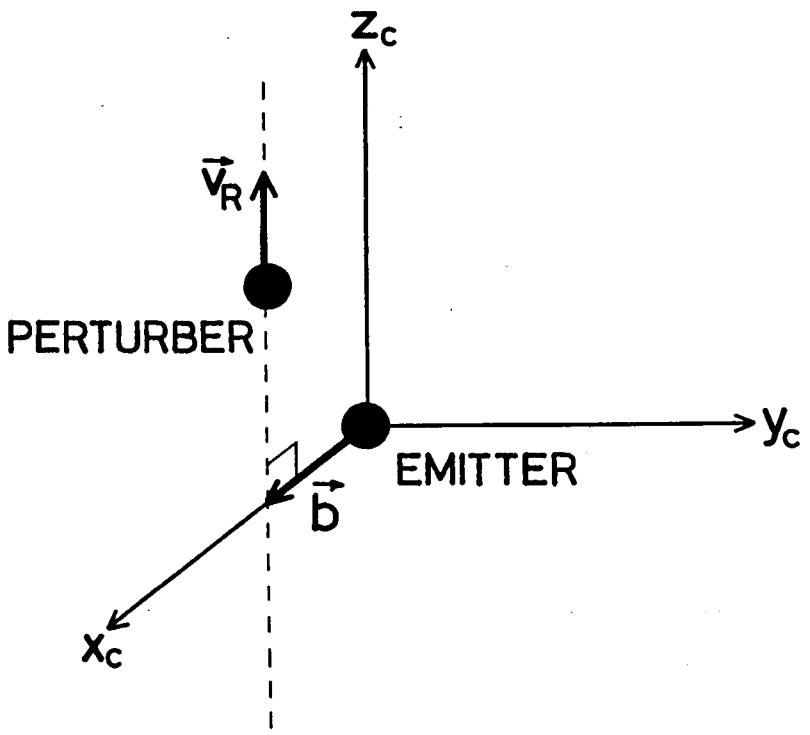

Fig. 3.3 Reference frame Ω_0' in which the perturber moves along the z_c direction with the impact parameter directed in the x_c direction.

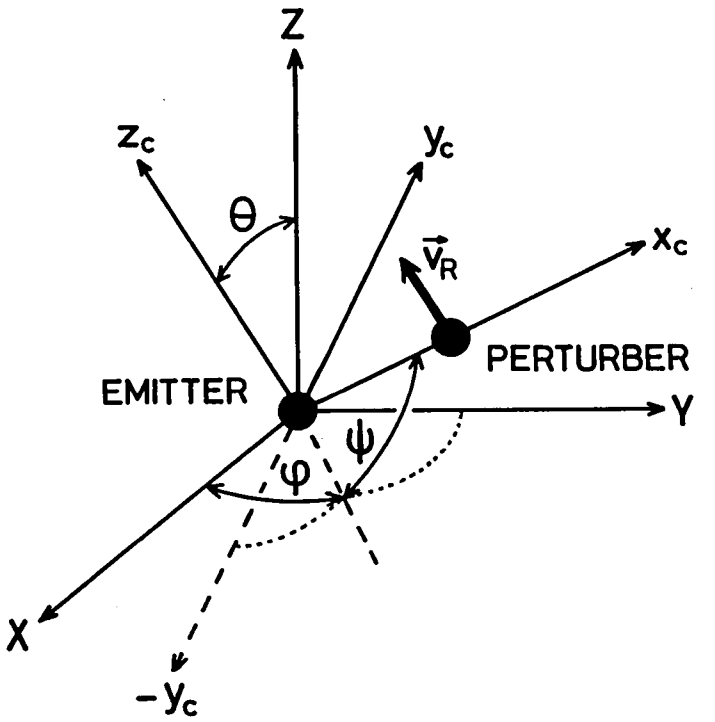

Fig. 3.4 Relationship between the reference frame Ω_0' (x_c, y_c, z_c) and the frame (X,Y,Z) in which the emitter velocity $\vec{v}_e$ is fixed in the Z direction.

same as Cooper's (x',y',z') frame[52]. The transfer from the reference frame Ω_0 to the new reference frame Ω_0' can be made by a rotation given by the Euler angles $\Omega_1=(\pi,\pi/2,\pi)$. The density matrix is transformed by this rotation as

$$\rho(\Omega_0') = \mathcal{D}(\Omega_1)\rho(\Omega_0)\mathcal{D}(\Omega_1)^{-1}. \tag{3.38}$$

Then we obtain the change in the density matrix by a single collision in the new frame Ω_0' :

$$\delta\rho_{mm'}(b,v_R,\Omega_0',h) = \sum_{nn'} M^{nn'}_{mm'}(b,v_R,\Omega_0')\rho_{nn'}(-\infty,h), \tag{3.39}$$

where

$$M^{nn'}_{mm'}(b,v_R,\Omega_0') = \sum_{\substack{\mu\mu' \\ \nu\nu'}} \mathcal{D}^{j*}_{n\nu}(\Omega_1)\mathcal{D}^{j*}_{m'\mu'}(\Omega_1)\mathcal{D}^{j}_{m\mu}(\Omega_1)\mathcal{D}^{j}_{n'\nu'}(\Omega_1) \times M^{\nu\nu'}_{\mu\mu'}(b,v_R,\Omega_0). \tag{3.40}$$

Now, we will start from Eq.(3.39), which must be averaged over the perturber velocity distribution. Here, we assume that emitters have a definite velocity $\vec{v}_e$ in a particular direction while perturbers have an isotropic Maxwellian velocity distribution. We introduce a new frame (X,Y,Z) which moves with the velocity $\vec{v}_e$ along the Z direction such that the emitter is fixed at the origin. The relationship between this frame and the frame Ω_0' is shown in Fig.3.4 for a certain direction of the relative velocity $\vec{v}_R$. It may be found that we can transform

(x_c,y_c,z_c) to (X,Y,Z) by a rotation given by the Euler angles $\Omega_2=(-\frac{\pi}{2}-\phi,\ \theta,-\frac{\pi}{2}-\psi)$, where θ is the angle between the directions of $\vec{v}_e$ and $\vec{v}_R$. The distribution of perturber velocity $\vec{v}_p$ is assumed to be isotropic Maxwellian given by

$$f_p(\vec{v}_p) = (\alpha_p/\pi)^{3/2}\exp(-\alpha_p v_p^2) \ , \tag{3.41}$$

where $\alpha_p=m_p/2kT$, m_p is the mass of the perturber, k is the Boltzmann constant, and T is the absolute gas temperature. Since the perturber velocity is given by $\vec{v}_p=\vec{v}_e+\vec{v}_R$, the distribution of the relative velocity $\vec{v}_R$ becomes a shifted Maxwellian, which can be expressed as

$$f_p(\vec{v}_e+\vec{v}_R) = (\alpha_p/\pi)^{3/2}\exp\{-\alpha_p(v_e^2+v_R^2+2v_e v_R\cos\theta)\}. \tag{3.42}$$

We consider the average change $\delta\rho_{mm'}$ for all possible collisions occurring in a time interval δt which is chosen to be small enough to contain at most one collision but much larger than τ_c :

$$\delta\rho_{mm'}=<\sum_{nn'}\int_0^\infty db\int d^3v_R P(b,v_R,\Omega_2)M_{mm'}^{nn'}(b,v_R,\Omega_2)\rho_{nn'}(-\infty,h)>_h \ , \tag{3.43}$$

where

$$M_{mm'}^{nn'}(b,v_R,\Omega_2)=\sum_{\substack{\mu\mu'\\ \nu\nu'}} \mathcal{D}_{n\nu}^{j*}(\Omega_2)\,\mathcal{D}_{m'\mu'}^{j*}(\Omega_2)\,\mathcal{D}_{m\mu}^{j}(\Omega_2)\,\mathcal{D}_{n'\nu'}^{j}(\Omega_2) \times M_{\mu\mu'}^{\nu\nu'}(b,v_R,\Omega_1') \ , \tag{3.44}$$

and $<\ >_h$ indicates an average over all possible cillision histories.

The probability density $P(b,v_R,\Omega_2)$ of occurrence of a collision specified by b, v_R, and Ω_2 in δt is given by

$$P(b,v_R,\Omega_2) = n_p b v_R f(\vec{v}_e+\vec{v}_R)\delta t, \tag{3.45}$$

where n_p is the density of perturber. Since P and $M^{nn'}_{mm'}$ are independent of h, $<\ >_h$ acts only on $\rho_{nn'}(-\infty,h)$. If we rewrite $<\rho_{nn'}(-\infty,h)>_h$ as $\rho_{nn'}$, we can transform Eq.(3.43) to a differential form :

$$\frac{d\rho_{mm'}}{dt} = -\sum_{nn'} \tilde{\Gamma}^{nn'}_{mm'}(v_e)\rho_{nn'} , \tag{3.46}$$

where the relaxation matrix $\tilde{\Gamma}^{nn'}_{mm'}(v_e)$ is given by

$$\tilde{\Gamma}^{nn'}_{mm'}(v_e) = -n_p \sum_{\substack{\mu\mu' \\ \nu\nu'}} \int_0^\infty db \int d^3v_R b v_R f_p(\vec{v}_e+\vec{v}_R) M^{\nu\nu'}_{\mu\mu'}(b,v_R,\Omega_1') \times \mathfrak{D}^{j*}_{n\nu}(\Omega_2)\mathfrak{D}^{j*}_{m'\mu'}(\Omega_2)\mathfrak{D}^{j}_{m\mu}(\Omega_2)\mathfrak{D}^{j}_{n'\nu'}(\Omega_2) . \tag{3.47}$$

The product of four rotation matrices can be reduced to a sum of rotation matrices by using the Clebsch-Gordan series [see, e.g., Eq.(4.25) in Ref. 86]. Thus we obtain

$$\tilde{\Gamma}^{nn'}_{mm'}(v_e) = -\sum (-1)^{n-\nu+m'-\mu'} <jjn-n'|JM><jj\nu-\nu'|JN><jjm-m'|J'M'> \times <jj\mu-\mu'|J'N'><JJ'-MM'|KQ><JJ'-NN'|KQ'> \times \int_0^\infty db \int d^3v_R n_p v_R f_p(\vec{v}_e+\vec{v}_R)\mathfrak{D}^{K}_{QQ'}(\Omega_2) M^{\nu\nu'}_{\mu\mu'}(b,v_R,\Omega_1') , \tag{3.48}$$

where the summation is taken over μ, μ', ν, ν', M, M', N, N', J, J', K, Q, and Q'.

Since our system has an axial symmetry with respect to the Z axis, it is convenient to represent the density matrix on the irreducible basis as has been discussed in Chap. II. From the axial symmetry discussed in Sec. II.4.2, the average collisional relaxation of the density matrix can be written as

$$\frac{d\rho_q^k}{dt} = -\sum_{k'} \tilde{\Gamma}_{qq}^{kk'}(v_e)\rho_q^{k'}. \tag{3.49}$$

The relaxation matrix elements $\tilde{\Gamma}_{qq'}^{kk'}(v_e)$ with $q \neq q'$ always vanish. Substituting Eq.(3.48) into Eq.(2.31), we obtain

$$\tilde{\Gamma}_{qq}^{kk'}(v_e) = -\sum (-1)^{K-q+\nu-\mu'} \langle jj\mu-\mu' | kN \rangle \langle jj\nu-\nu' | k'N' \rangle$$
$$\times \langle kk'q-q | K0 \rangle \langle kk'N-N' | KQ' \rangle$$
$$\times \int_0^\infty db \int d^3v_R n_p b v_R f_p(\vec{v}_e+\vec{v}_R) \Omega_{0Q'}^K(\Omega_2) M_{\mu\mu'}^{\nu\nu'}(b, v_R, \Omega_1'). \tag{3.50}$$

The averaging over $\vec{v}_R$ in Eq.(3.50) is performed by using the transformation

$$\int d^3v_R \longrightarrow \int_0^\infty v_R^2 dv_R \int_0^\pi \sin\theta d\theta \int_0^{2\pi} d\phi \int_0^{2\pi} d\psi.$$

Since the perturber velocity distribution $f_p(\vec{v}_e+\vec{v}_R)$ is symmetric with respect to thr Z axis, $f_p(\vec{v}_e+\vec{v}_R)$ is independent of ϕ and ψ. The angular integration over ϕ and ψ is readily performed by using the relation

$$\int_0^{2\pi}d\phi\int_0^{2\pi}d\psi\,\mathcal{D}^{K}_{QQ'}(\Omega_2) = 4\pi^2\delta_{Q0}\delta_{Q'0}P_K(\cos\theta), \qquad (3.51)$$

where P_K is the Legendre's polynomial. From now on, we will denote $\tilde{\Gamma}^{kk'}_{qq}$ as $\tilde{\Gamma}^{kk'}_{q}$ for the sake of simplicity. After integrating over ϕ and ψ, we obtain

$$\tilde{\Gamma}^{kk'}_{q}(v_e) = -\sum_{\substack{KN\\ \mu\mu'\\ \nu\nu'}} (-1)^{K-q+\nu-\mu'} \langle jj\mu-\mu'|k\,N\rangle\langle jj\nu-\nu'|k'N\rangle \times \langle kk'N-N|K0\rangle\langle kk'q-q|K0\rangle \tilde{m}^{\nu\nu'}_{\mu\mu',K}(v_e), \qquad (3.52a)$$

where

$$\tilde{m}^{\nu\nu'}_{\mu\mu',K}(v_e) = 4\pi^2 n_p \int_0^\infty db \int_0^\infty v_R dv_R \int_0^\infty \sin\theta d\theta b V_R f_p(\vec{v}_e+\vec{v}_R) P_K(\cos\theta) \times M^{\nu\nu'}_{\mu\mu'}(b,v_R,\Omega_1'). \qquad (3.52b)$$

Substituting Eq.(3.42) into Eq.(3.52b), we obtain

$$\tilde{m}^{\nu\nu'}_{\mu\mu',K}(v_e) = 4\pi(\alpha_p/\pi)^{3/2}\exp(-\alpha_p v_e^2) \times \int_0^\infty v_R^2 dv_R \exp(-\alpha_p v_R^2) F_K(2\alpha_p v_e v_R) \tilde{M}^{\nu\nu'}_{\mu\mu'}(v_R), \qquad (3.53)$$

where

$$F_K(x) = \frac{1}{2}\int_0^\pi \sin\theta d\theta e^{-x\cos\theta} P_K(\cos\theta) = (-2)^K \sum_{m=0}^{\infty} \frac{(m+K)!}{(2m+2K+1)!\,m!} x^{2m+K}, \qquad (3.54)$$

and

$$\tilde{M}^{\nu\nu'}_{\mu\mu'}(v_R) = 2\pi n_p \int_0^\infty b db v_R M^{\nu\nu'}_{\mu\mu'}(b, v_R, \Omega_1') \ . \tag{3.55}$$

For nonresonant collisions, from Eqs.(3.25)–(3.37), we find that the dependence of $M^{\nu\nu'}_{\mu\mu'}(\xi,\Omega_1') \equiv M^{\nu\nu'}_{\mu\mu'}(b, v_R, \Omega_1')$ on b and v_R can be expressed in terms of a parameter $\xi[\equiv B/(b^5 v_R)]$ as $M^{\nu\nu'}_{\mu\mu'}(\xi,\Omega_1') \equiv M^{\nu\nu'}_{\mu\mu'}(b, v_R, \Omega_1')$. If we replace the integral over b with that over ξ, Eq.(3.55) becomes

$$\tilde{M}^{\nu\nu'}_{\mu\mu'}(v_R) = \frac{\sqrt{\pi}}{2\Gamma(9/5)} (\alpha_p v_R)^{3/10} M^{\nu\nu'}_{\mu\mu'} \ , \tag{3.56}$$

with

$$M^{\nu\nu'}_{\mu\mu'} \equiv \frac{2\pi}{5} n_p B^{2/5} \langle v_p^{3/5} \rangle \int_0^\infty M^{\nu\nu'}_{\mu\mu'}(\xi,\Omega_1') \, \xi^{-7/5} d\xi \ , \tag{3.57}$$

where $\Gamma(x)$ is the gamma function, and $\langle v_p^{3/5} \rangle$ is the average value of the 3/5-th power of the perturber velocity defined as

$$\langle v_p^{3/5} \rangle = \int_0^\infty 4\pi v_p^2 dv_p f_p(v_p) v_p^{3/5} = \frac{2}{\sqrt{\pi}} (2kT/m_p)^{3/10} \Gamma(9/5) . \tag{3.58}$$

Substituting Eq.(3.56) into Eq.(3.53), we can reduce Eq.(3.53) to a simple infinite series :

$$\tilde{\mathcal{M}}^{\nu\nu'}_{\mu\mu',K}(v_e) = (-2)^K M^{\nu\nu'}_{\mu\mu'} \exp(\alpha_p v_e^2) \sum_{m=0}^{\infty} \frac{(m+K)!\,\Gamma(m+\frac{K}{2}+\frac{9}{5})}{(2m+2K+1)!\,m!\,\Gamma(9/5)} (4\alpha_p v_e^2)^{m+\frac{K}{2}} . \tag{3.59}$$

For resonant collisions, Berman and Lamb[22] have shown that $M^{\nu\nu'}_{\mu\mu'}(\eta,\Omega_1') \equiv M^{\nu\nu'}_{\mu\mu'}(b, v_R, \Omega_1')$ where $\eta \equiv A/(b^2 v_R)$ and $A \equiv \frac{1}{6\hbar} |\langle aj \| d \| sj' \rangle|^2$. From Eq.(3.55), we find that $\tilde{M}^{\nu\nu'}_{\mu\mu'}(v_R)$ is independent of the relative velocity v_R :

$$\tilde{M}^{\nu\nu'}_{\mu\mu'}(v_R) = n_p \pi A \int_0^{\pi} M^{\nu\nu'}_{\mu\mu'}(\eta, \Omega_1) \eta^{-2} d\eta$$

$$\equiv M^{\nu\nu'}_{\mu\mu'} \quad . \tag{3.60}$$

Then, for resonant collisions, we obtain

$$\tilde{\mathcal{M}}^{\nu\nu'}_{\mu\mu',K}(v_e) = (-2)^K M^{\nu\nu'}_{\mu\mu'} \exp(\alpha_p v_e^2) \sum_{m=0}^{\infty} \frac{(m+K)!\,\Gamma(m+\frac{K}{2}+\frac{3}{2})}{(2m+2K+1)!\,m!\,\Gamma(3/2)} . \tag{3.61}$$

It is readily verified that $\tilde{\Gamma}^{kk'}_q(v_e)$ satisfies some of the symmetry properties discussed in Sec. II .4 : Hermiticity of ρ, the axial symmetry, and the symmetries under reflections. Furthermore, as we have used the approximations of the electrostatic interaction and classical-linear-path, and the nondigenerate ground state of the perturber (one-level perturber), the system is invariant with time reversal, which yields another relation between the components of the relaxation matrix. Here, we summarize these properties as follows :

$$\tilde{\Gamma}^{kk'}_q(v_e) = \tilde{\Gamma}^{kk'}_{-q}(v_e)^* \qquad \text{(Hermiticity of } \rho\text{)}, \tag{3.62a}$$

$$= (-1)^{k+k'} \tilde{\Gamma}^{kk'}_{-q}(v_e) \qquad \text{(reflection)}, \tag{3.62b}$$

$$= (-1)^{k+k'} \tilde{\Gamma}^{k'k}_{q}(v_e)^* \qquad \text{(one-level perturber)}, \tag{3.62c}$$

$$= \tilde{\Gamma}^{k'k}_{q}(v_e) \qquad \text{(from above three relations)}. \tag{3.62d}$$

III.3.3 Isotropic Collisions

In this subsection, we consider the special case that emitters are at rest ($\vec{v}_e=0$). In this case, all collision directions of perturbers with respect to the emitters are equally possible. Thus, the situation is isotropic, so that the relaxation matrix $\tilde{\Gamma}_q^{kk'}(0)$ is diagonal with respect not only to q but also to k, and the diagonal elements with the same k are independent of q, as described in Sec. II.4.3.

Substituting $v_e=0$ into Eq.(3.52), we obtain the relaxation matrix for emitters at rest :

$$\tilde{\Gamma}_q^{kk'}(0) = -\delta_{kk'} \sum_{\substack{\mu\mu' \\ \nu\nu' N}} (-1)^{\nu-\mu} \langle jj\mu-\mu' | kN \rangle \langle jj\nu-\nu' | kN \rangle M_{\mu\mu'}^{\nu\nu'} , \tag{3.63}$$

where $M_{\mu\mu'}^{\nu\nu'}$ is defined by Eq.(3.57) for nonresonant collisions or by Eq.(3.60) for resonant collisions. For resonant collisions, as one can see in Eq.(3.60), $\tilde{\Gamma}_q^{kk}(0)$ is independent of the mass of perturber. On the other hand, for nonresonant collisions, $\tilde{\Gamma}_q^{kk}(0)$ depends on the mass of perturber through the factor $\langle v_p^{3/5} \rangle$ in Eq.(3.57).

It is worthwhile noting that this result can be extended to the case of general isotropic collisions in which the emitter velocity distribution is an isotropic Maxwellian. Then, we must replace only $\langle v_p^{3/5} \rangle$ in Eq.(3.57) by $\langle v_R^{3/5} \rangle$. This corresponds to replacing m_p in Eq.(3.57) with the reduced mass $m_e m_p/(m_e+m_p)$ where m_e is the mass of emitter. In fact, $\tilde{\Gamma}_q^{kk'}(0)$ is formally the same as those obtained by D'yakonov and Perel'[17] and Berman

and Lamb[22] for general isotropic collisions.

III.3.4 Numerical Calculations of the Relaxation Matrix for Emitters Moving with a Definite Velocity

In the preceding subsections, we have derived the relaxation matrix $\tilde{\Gamma}_q^{kk'}(v_e)$ for emitters moving with a definite velocity by averaging the time evolution of the density matrix caused by a single collision. In order to calculate the dependence of $\tilde{\Gamma}_q^{kk'}(v_e)$ on the emitter velocity, we must calculate the behavior of the matrix $M_{\mu\mu'}^{\nu\nu'}(\xi,\Omega_1')$ [$\equiv M_{\mu\mu'}^{\nu\nu'}(b,v_R,\Omega_1')$] which is related to the time evolution matrix $M_{mm'}(t)$ after a single collision. The problem is now reduced to finding the solution of the differential equation (3.25) at $t=\infty$. This cannot be done analytically. Many authers used either the scalar approximation[16),21)] or the asymptotic approximation accompanied with a cutoff procedure[19),34)]. On the other hand, we make fully numerical calculations for non-resonant collisions of emitters in the excited state with j=1. Although Berman and Lamb[22] have made the same calculations, their results are insufficient for the case of anisotropic collisions.

In the first place, we integrate the Eq.(3.27) and obtain $M_{mm'}^{nn'}(\xi,\Omega_0)$ [$\equiv M_{mm'}^{nn'}(b,v_R,\Omega_0)$] in the reference frame Ω_0 by using Eq.(3.37). We integrate Eq.(3.27) in three different ways according to the magnitude of ξ[$=B/b^5v_R$] in order to avoid unnecessarily long time for machine calculations.

I) Region I: $0 \leq \xi \leq 0.01$

This region corresponds to collisions with very large impact parameters or with very large velocity. During such collisions, the collisional change in the wave function is thought to be small because of the small interaction V and short interaction time. Using the perturbation method , we have obtained the elements of the time evolution matrix $M_{mn}(\theta=\pi/2)$ up to the second order of ξ :

$$M_{mn}(\theta=\pi/2)=\begin{pmatrix} 1+i\frac{15}{8}\pi\xi-\frac{117}{64}\pi^2\xi^2 & -\frac{315}{128}\sqrt{2}\pi^2\xi^2 & -i\frac{3}{8}\pi\xi+\frac{45}{64}\pi^2\xi^2 \\ \frac{315}{128}\sqrt{2}\pi^2\xi^2 & 1+i\frac{21}{4}\pi\xi-\frac{441}{32}\pi^2\xi^2 & -\frac{315}{128}\sqrt{2}\pi^2\xi^2 \\ -i\frac{3}{8}\pi\xi+\frac{45}{64}\pi^2\xi^2 & \frac{315}{128}\sqrt{2}\pi^2\xi^2 & 1+i\frac{15}{8}\pi\xi-\frac{117}{64}\pi^2\xi^2 \end{pmatrix} \tag{3.64}$$

II) Region II : $0.01 \leq \xi \leq 5.0$

In this region, we have carried out the numerical intrgration of Eq.(3.27) with the Runge-Kutta-Gill's method. As the parameter ξ becomes larger, i.e. the impact parameter b becomes smaller, the collisional interaction becomes stronger. Consequently, the solutions of Eq.(3.27) becomes rapidly oscillating as θ is varied. Then the step size of the numerical integration must be taken smaller for larger ξ. Therefore, we divided this region into three regions $0.01 \leq \xi \leq 0.1$, $0.1 \leq \xi \leq 2.0$, and $2.0 \leq \xi \leq 5.0$ where the step size of integration over θ are 0.01 rad, 0.005 rad, and 0.0025 rad, respectively. Substituting $M_{mn}(\theta=\pi/2)$ into

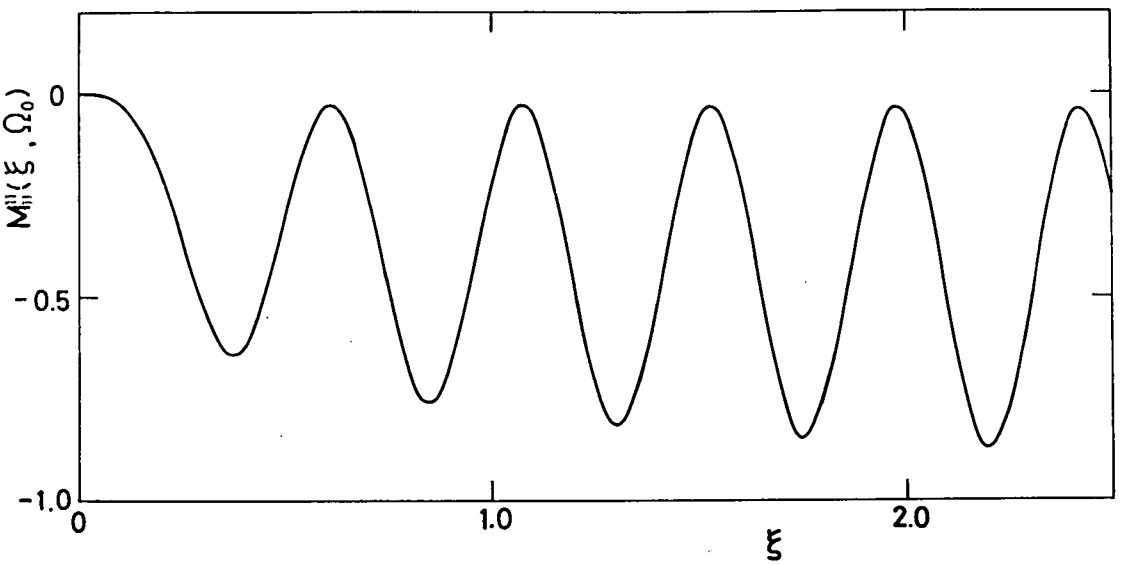

Fig. 3.5 Typical result of numerical calculations of the relaxation matrix element $M_{mm'}^{nn'}(\xi,\Omega_0)$ for a single collision in the reference frame Ω_0.

Eq.(3.37), we obtain $M^{nn'}_{mm'}(\xi,\Omega_0)$. A typical example of $M^{nn'}_{mm'}(\xi,\Omega_0)$ is shown in Fig.3.5. We can see in Fig.3.5 that the element $M^{nn'}_{mm'}(\xi,\Omega_0)$ oscillates sinusoidally with an approximately constant period in the region $\xi \geq 1$

III) Region III : $\xi \geq 5.0$

This region corresponds to very close collisions or very slow collisions. In fact, the parameter $\xi=5.0$ corresponds to the impact parameter of about 0.6 of the Weisskopf radius[22]. In this region, as the time evolution matrix $M_{mn}(\theta)$ oscillates drastically with θ, we must diminish the step size of the numerical integration in proportional to ξ^{-1}. For larger value of ξ, the smallness of the step size desperately lengthens the machine calculation time. Setting this difficulty aside, as the electrostatic dipole-dipole approximation becomes less valid for such close collisions, it is meaningless to proceed with exact numerical calculations in this region. Then, we adopted the same procedure as that used by Berman and Lamb[22].

As seen in Fig.3.5, the element $M^{11}_{11}(\xi,\Omega_0)$ oscillates sinusoidally with an approximately constant period of about 0.45 in ξ, and so do the other elements $M^{nn'}_{mm'}(\xi,\Omega_0)$ with the same period. The average value of the elements $M^{nn'}_{mm'}(\xi,\Omega_0)$over a period was estimated by means of machine calculations for two regions ξ= [4.00,4.45] and ξ=[9.00,9.45]. The average values obtained are tabulated in the first two columns in Table 3.3. We used the step size of integration 0.0025 rad for the region [4.00,4.45] and 0.001 for [9.00,9.45]. Other elements required for our problem

Table 3.3 Average Values of $M_{mm'}^{nn'}(\xi,\Omega_0)$ for Periods ξ=[4.00,4.45] and ξ=[9.00,9.45] in the Reference Frame Ω_0 and Its Asymptotic Form for the Region III

	ξ=[4.00,4.45]	ξ=[9.00,9.45]	ASYMPTOTIC FORM
$M_{11}^{11}(\xi,\Omega_0)$	-0.480	-0.491	-0.500
$Re[M_{1\,1}^{1-1}(\xi,\Omega_0)]$	0.106	0.0879	0.123exp(-0.0377ξ)
$Im[M_{1\,1}^{1-1}(\xi,\Omega_0)]$	0.0759	0.0563	0.0978exp(-0.0600ξ)
$Re[M_{10}^{10}(\xi,\Omega_0)]$	-1.46	-1.50	-1.50
$Im[M_{10}^{10}(\xi,\Omega_0)]$	0.270	-0.207	-0.338exp(-0.0530ξ)
$M_{11}^{00}(\xi,\Omega_0)$	0.212	0.176	0.245exp(-0.0357ξ)
$M_{1\,1}^{-1-1}(\xi,\Omega_0)$	0.268	0.315	0.5[1-0.560exp(-0.0462ξ)]
$Re[M_{1\,0}^{-10}(\xi,\Omega_0)]$	-0.194	-0.251	-0.5[1-0.728exp(-0.0414ξ)]
$Im[M_{1\,0}^{-10}(\xi,\Omega_0)]$	0.0471	0.0350	0.0605exp(-0.0592ξ)
$M_{00}^{00}(\xi,\Omega_0)$	-0.425	-0.352	-0.490exp(-0.0357ξ)

can be obtained from the elements in Table 3.3 by using following relations, which can be derived from the unitarity of $M_{mn}(\theta=\pi/2)$ and from the properties of Eq.(3.27) :

$$M^{nn'}_{mm'}(\xi,\Omega_0) = M^{n'n}_{m'm}(\xi,\Omega_0)^* \tag{3.65a}$$

$$= (-1)^{m+m'+n+n'} M^{mm'}_{nn'}(\xi,\Omega_0) \tag{3.65b}$$

$$= (-1)^{m+m'+n+n'} M^{-n-n'}_{-m-m'}(\xi,\Omega_0) \tag{3.65c}$$

$$= (-1)^{m+n} M^{mn'}_{nm'}(\xi,\Omega_0) \tag{3.65d}$$

$$= (-1)^{m+n} M^{-nn'}_{-mm'}(\xi,\Omega_0). \tag{3.65e}$$

Taking account of the adiabatic nature of collisions within Zeeman multiplet for very close collisions due to the large separation of the energy levels of the instantaneous eigenfunctions, Berman and Lamb showed that, when the parameter ξ becomes large, the average values of $M^{nn'}_{mm'}(\xi,\Omega_0)$ asymptotically approach some final values given by

$$M^{11}_{11}(\infty,\Omega_0) = M^{-10}_{10}(\infty,\Omega_0) = 0.5, \quad M^{10}_{10}(\infty,\Omega_0) = -1.5$$

$$M^{-1-1}_{11}(\infty,\Omega_0) = 0.5, \; M^{1-1}_{11}(\infty,\Omega_0) = M^{00}_{11}(\infty,\Omega_0) = M^{00}_{00}(\infty,\Omega_0) = 0. \tag{3.66}$$

From these final values and the average values in the two regions tabulated in Table 3.3, we can obtain the asymptotic behaviors of the average values in exponential forms by using the least-

Table 3.4 Averaged Relaxation Matrix Elements $M_{mm'}^{nn'}$, for Three Regions of Integrations and the Total Values of $M_{mm'}^{nn'}$, Defined by Eq.(3.57) in the Reference Frame Ω_0 in Units of $(2\pi/5)n_p B^{2/5}\langle v_p^{3/5}\rangle$

	$\xi=[0,0.01]$	$\xi=[0.01,0.50]$	$\xi=[0.50,\infty)$	$\xi=[0,\infty)$	
				UNCORRECTED	CORRECTED
M_{11}^{11}	-0.001	-1.603	-0.657	-2.261	-2.261
$Re(M_{1\,1}^{1-1})$	0.000	0.496	0.107	0.603	0.555
$Im(M_{1\,1}^{1-1})$	0.124	1.045	0.125	1.294	1.294
$Re(M_{10}^{10})$	-0.022	-6.506	-1.970	-8.499	-8.499
$Im(M_{10}^{10})$	-1.115	-5.551	-0.379	-7.046	-7.046
M_{11}^{00}	0.000	0.992	0.118	1.110	1.109
$M_{1\,1}^{-1-1}$	0.001	0.612	0.539	1.152	1.152
$Re(M_{1\,0}^{-10})$	-0.005	-0.822	-0.324	-1.152	-1.152
$Im(M_{1\,0}^{-10})$	-0.124	-0.160	0.076	-0.218	-0.218
M_{00}^{00}	0.000	-1.984	-0.237	-2.221	-2.221

squares method. This asymptotic forms are tabulated in the last column of Table 3.3.

In the next step, in order to estimate the values of $M_{\mu\mu'}^{\nu\nu'}$ in Eq.(3.59), we must carry out the integration over ξ in Eq. (3.57). In the region I, the integration over ξ was analitically performed by using the perturbation sólution Eq.(3.64). In the region II , we numerically integrated the obtained values of $M_{mm'}^{nn'}(\xi,\Omega_0)$ multiplied by $\xi^{-7/5}$. In this process, we used the Simpson's one-third rule. In the region III, we adopted the exponential asymptotic forms given in Table 3.3 in place of $M_{mm'}^{nn'}(\xi,\Omega_0)$. One may easily find that the integrations of the asymptotic forms multiplied by $\xi^{-7/5}$ can be expressed by the incomplete gamma functions[98]. The estimations of the incomplete gamma functions were done by machine calculations. The results obtained for these three regions are shown in the first three columns of Table 3.4 with $M_{mm'}^{nn'}$ defined by Eq.(3.57) in the fourth column. The matrix elements $M_{mm'}^{nn'}$ should satisfy the conditions for the conservation of the total population ($\propto \rho_0^0$) within the Zeeman multiplet :

$$M_{11}^{00} = -\frac{1}{2}M_{00}^{00} = 2\mathrm{Re}(M_{1\,1}^{1-1}) = -(M_{11}^{11} + M_{1\,1}^{-1-1}). \qquad (3.67)$$

The obtained results satisfy approximately this condition, but there exists a small amount of error although it is less than 10%. This error seems to come from the procedure used in the region III. Then we corrected some of the elements in order that

Table 3.5(a) Averaged Relaxation Matrix Elements in the Ω_0' Frame for Nonresonant Collisions in Units of $(2\pi/5)n_p B^{2/5}\times$ $\langle v_p^{3/5}\rangle$ Together with the Values Calculated by Chamoun et al.

	M_{00}^{00}	M_{00}^{11}	M_{11}^{11}	$\mathrm{Re}(M_{10}^{10})$	$\mathrm{Im}(M_{10}^{10})$	$M_{-1-1}^{1\,1}$
Present work	-2.21	1.11	-5.38	-5.38	2.21	4.27
Chamoun et al.[a)]	-2.11	1.05	-4.93	-4.51	1.58	3.36

a) Ref. 50.

Table 3.5(b) Averaged Relaxation Matrix Elements in the Ω_0' Frame for Nonresonant Collisions in Units of $(2\pi/5)n_p B^{2/5}\times$ $\langle v_p^{3/5}\rangle$ Together with the Values Calculated Previously

	$\tilde{\Gamma}_0^{11}$	$\tilde{\Gamma}_1^{11}$	$\tilde{\Gamma}_1^{12}$	$\tilde{\Gamma}_0^{22}$	$\tilde{\Gamma}_1^{22}$	$\tilde{\Gamma}_2^{22}$
Present work	9.65	4.27	-i2.12	3.33	6.49	5.38
Chamoun et al.[a)]	8.80	3.61	-i1.58	3.16	5.42	5.42
Lombardi[b)]			-i3.05	2.66	5.33	4.36

a) Ref. 50.

b) Ref. 97.

they satisfy the condition by using Eqs.(3.67). These corrected values are tabulated in the last column of Table 3.4.

So far, the calculations have been carried out in the reference frame Ω_0. As described before, this reference frame is not convenient to our problem, so that we have to transfer from the reference frame Ω_0 to Ω_0'. The matrix elements $M^{nn'}_{mm'}$ in the Ω_0' frame can be obtained by using the relation given by Eq.(3.40), and are tabulated in Table 3.5(a). Chamoun et al [50] calculated the relaxation matrix in irreducible basis for the case that emitters at rest are undergoing collisions with perturbers moving with a definite velocity. Consequently, their relaxation matrix $P^{kk'}_q$ (given in Table I of Ref. 50) should essentially gives the values of $M^{nn'}_{mm'}$ by changing the basis. The values $P^{kk'}_q$ defined by Chamoun et al. are related with our $M^{nn'}_{mm'}$ according to following relation :

$$\tilde{\tilde{\Gamma}}^{kk'}_q = n_p v_p P^{kk'}_q, \tag{3.68}$$

where $\tilde{\tilde{\Gamma}}^{kk'}_q$ is the irreducible relaxation matrix derived from our $M^{nn'}_{mm'}$. The tabulated $P^{kk'}_q$ in Ref. 50 is given in units of $2\pi b_0^2$ where b_o is the impact parameter defined by[99]

$$b_0 = \left(\frac{\sqrt{7}\beta'}{4v_p \hbar \Delta E}\right)^{1/2}, \tag{3.69}$$

and β' is given by Carrington and Corney[34]:

$$\beta' = \frac{(-1)^{2j} p_g^{\,2} \alpha_b}{\sqrt{j(2j-1)(2j+1)(j+1)(2j+3)}}, \tag{3.69}$$

and α_b is the polarizability of the perturber and p_g is the dipole moment of the emitter. The relation between the parameter B and the impact parameter b_0 is easily obtained[22),34)]. Especially for the case of j=1, we obtain

$$b_0^2 = \frac{6.80}{2.48}\left(\frac{56}{15\pi^2}\right)^{1/5} v_p^{-2/5} B^{2/5}. \qquad (3.70)$$

Thus we can compare their $P_q^{kk'}$ with our $M_{mm'}^{nn'}$, by changing the basis. The values calculated from their $P_q^{kk'}$ are also tabulated in Table 3.5(a).

Lombardi also made similar calculations. We can compare their results with ours by integrating the curves in the figure of Ref. 99. Since they have not shown the decay rates of orientation, we cannot compare in magnetic quantumnumber representation. Then, we compare their results with ours and those of Chamoun et al. in the irreducible representation [see Table 3.5(b)].

Substituting these values of $M_{mm'}^{nn'}$ in the Ω_0' frame, which are shown in Table 3.5(a), into Eqs.(3.52) and (3.59), we obtain the relaxation matrix elements $\tilde{\Gamma}_q^{kk'}$ as functions of emitter velocity whose direction is fixed in the Z direction. The results of these calculations are shown in Fig. 3.6. All other nonvanishing elements are related to tabulated elements by Eq.(3.62). As mentioned in Sec. II .4.4, all diagonal elements $\tilde{\Gamma}_q^{kk}$ are real, while nondiagonal elements which cause the coupling between orientation and alignment are pure imaginary. It should be noted that, when emitters are at rest (v_e=0), the situation is isotropic,

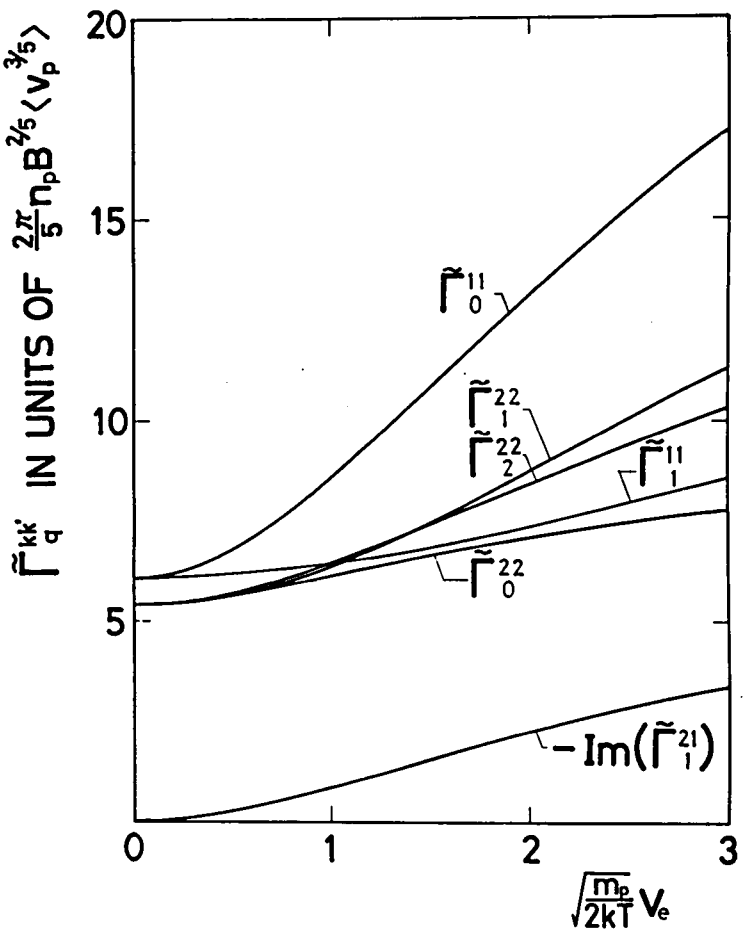

Fig. 3.6 Relaxation matrix elements for emitters moving with a definite velocity along the Z axis as functions of the emitter velocity normalized by $(2kT/m_p)^{1/2}$.

so that the nondiagonal element $\tilde{\Gamma}^{21}_{1}(0)$ becomes zero, the values of all diagonal elements with the same k become equal, which give the collisional decay rates of alignment or orientation for isotropic collisions. From Fig. 3.6, we can obtain the ratio of the decay rate of orientation to that of alignment for isotropic collisions as

$$\tilde{\Gamma}^{11}_{q}(0)/\tilde{\Gamma}^{22}_{q}(0) = 1.12, \tag{3.71}$$

which agrees with the theory of Berman and Lamb[22].

When we increase the emitter velocity from zero, the situation becomes anisotropic. Then, the coupling between alignment and orientation becomes nonzero and increases with the increase of emitter velocity. The emitter velocity in the abscissa of Fig. 3.6 is expressed in units of the most probable velocity $(2kT/m_p)^{1/2}$ of "perturber". Then we find that the effects of anisotropy are more significant for collisions with heavier perturbers as one might expect.

The second feature of anisotropic collisions is the splittings of the diagonal elements $\tilde{\Gamma}^{kk}_{q}(v_e)$ (the collisional decay rates of multipole components) with different $|q|$. The splittings become larger when the emitter velocity is increased, but they are not so serious for the relaxations of alignment than for those of orientation. On the other hand, we can also find in Fig. 3.6 that each diagonal element becomes larger with the increase of the emitter velocity. This feature must be mainly due rather

to the increase of the mean relative velocity than to the anisotropy of collisions.

III.4 Collisional Depolarizations of Emitters Excited by a Single-Mode Laser

In the preceding section, we have considered the simple case that the emitters with a definite velocity undergo collisions with perturbers with an isotropic velocity distribution. However, in general situations, emitters have some velocity distribution. Then, the relaxation matrix given by Eq.(3.52a) must be averaged over the velocity distribution of the excited emitters with respect not only to the velocity v_e but also to its direction. In this section, we consider the case that the emitters excited by a single-mode laser collide with perturbers which have an isotropic velocity distribution. In this case, the emitter velocity distribution has an axial symmetry and symmetries under plane reflections.

III.4.1 Averaging over the Velocity Distribution of Emitters

We consider a single-mode laser beam with angular frequency ω_L propagated along the z direction in the laboratory frame (x,y,z). We will assume that the emitter atoms , which are in the ground state before excitation, have an isotropic velocity distribution given by a Maxwellian function. If the frequency ω_L is close to the resonant frequency of the transition of the

excitation, this laser beam excites only the emitters with velocities whose projections v_{ez} on the z axis are nearly equal to $v_0[=c\{(\omega_L/\omega_0)-1\}]$. Therefore, we shall consider only the case that the distribution function of v_{ez} is much narrower than that of the transverse component which is given by a Maxwellian, and hence it can be regarded approximately as a delta function. In this case, the velocity distribution function of the excited emitters can be expressed as

$$f_e(\vec{v}_e) = \frac{\alpha_e}{\pi}\exp\{-\alpha_e(v_e^2-v_0^2)\}\delta(v_{ez}-v_0), \qquad (3.72)$$

where $\alpha_e=m_e/2kT$, m_e is the mass of the emitter, and the factor $(\alpha_e/\pi)\exp(\alpha_e v_0^2)$ is the normalization constant.

The relaxation matrix for emitters whose velocity is in the direction with polar angles (Θ,Φ) can be obtained by using the rotational transformation given by Eq.(2.28) from the relaxation matrix for emitters moving in the Z direction with the same velocity. The transformation from the (X,Y,Z) frame to the (x,y,z) frame is performed through a rotation with the Euler angles $\Omega_3=(\Theta,\Phi,0)$ as shown in Fig. 3.7. After performing this transformation and averaging it over the emitter velocity distribution given by Eq.(3.72), we obtain the averaged relaxation matrix $\Gamma^{kk'}_{qq'}(v_0)$ for emitters whose velocity projected on the z axis is v_0:

$$\Gamma^{kk'}_{qq'}(v_0) = \sum_{q_1}\int d^3v_e f_e(\vec{v}_e)\,\mathcal{D}^{k}_{qq_1}(\Omega_3)\tilde{\Gamma}^{kk'}_{q_1}(v_e)\mathcal{D}^{k'*}_{q'q_1}(\Omega_3). \qquad (3.73)$$

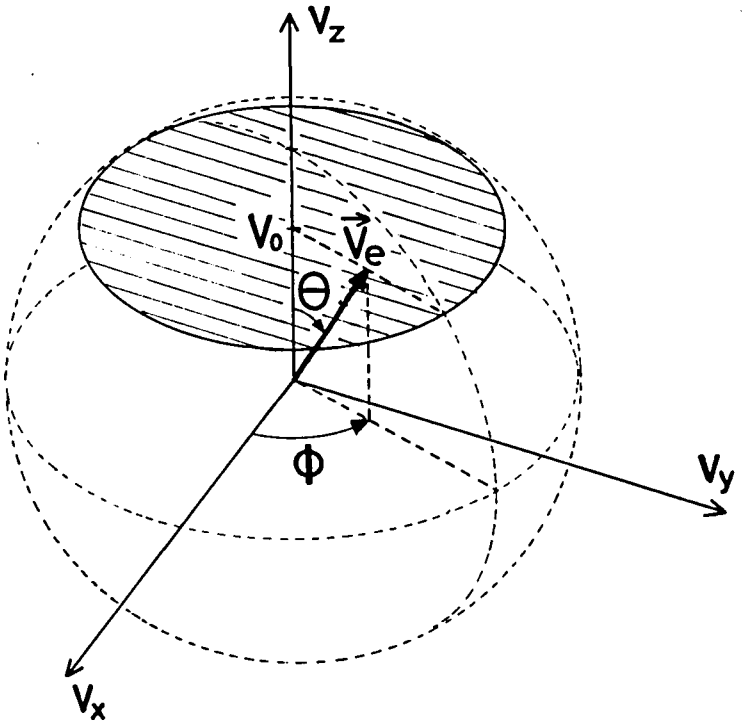

Fig. 3.7 Considered velocity distribution of emitters excited by a single-mode laser beam propagated along the z axis (shaded portion). The velocity distribution perpendicular to the z axis is given by a Maxwellian.

From axial symmetry of the system, we find that $\Gamma_{qq'}^{kk'}(v_0)$ vanishes when $q \neq q'$ as described before. Then, by expanding the product of two elements of the rotation matrix by the Clebsch-Gordan series, we obtain

$$\Gamma_q^{kk'}(v_0) = \sum_{Lq_1} (-1)^{q-q_1} \langle kk' q-q | L0 \rangle \langle kk' q_1 - q_1 | L0 \rangle \times \int d^3 v_e f_e(\vec{v}_e) P_L(\cos\Theta) \tilde{\Gamma}_{q_1}^{kk'}(v_e), \qquad (3.74)$$

where $\Gamma_q^{kk'}(v_0) \equiv \Gamma_{qq}^{kk'}(v_0)$ and $P_L(\cos\Theta)$ [$\equiv \mathcal{D}_{00}^{L}(0,\Theta,0)$] is the Legendre's polynomial. Substituting $\tilde{\Gamma}(v_e)$ given by Eq.(3.52a) into Eq.(3.74), and using the orthogonality relation of the Clebsch-Gordan coefficients, we obtain

$$\Gamma_q^{kk'}(v_e) = -\sum (-1)^{K-q+\nu-\mu'} \langle jj\mu-\mu' | kN \rangle \langle jj\nu-\nu' | k'N \rangle \times \langle kk' q-q | K0 \rangle \langle kk' N-N | K0 \rangle \mathcal{M}_{\mu\mu' K}^{\nu\nu'}(v_0), \qquad (3.75a)$$

where

$$\mathcal{M}_{\mu\mu' K}^{\nu\nu'}(v_0) = \int d^3 v_e f_e(\vec{v}_e) P_K(\cos\Theta) \tilde{\mathcal{M}}_{\mu\mu' K}^{\nu\nu'}(v_e), \qquad (3.75b)$$

and $\tilde{\mathcal{M}}_{\mu\mu' K}^{\nu\nu'}(v_e)$ is given by Eq.(3.59) for nonresonant collisions and by Eq.(3.61) for resonant collisions.

In order to perform the averaging over $\vec{v}_e$ in Eq.(3.75b), we introduce a function $G_{mK}(v_0)$ defined as

$$G_{mK}(v_0) \equiv (-2)^K \int d^3 v_e f_e(\vec{v}_e) P_K(\cos\Theta) e^{-\alpha_p v_e^2} (4\alpha_p v_e^2)^{m+\frac{K}{2}}. \qquad (3.76)$$

Using this function, we can obtain an infinite series expression of Eq.(3.75b).

For nonresonant collisions,

$$\mathcal{M}^{\nu\nu'}_{\mu\mu',K}(v_0)=M^{\nu\nu'}_{\mu\mu'}\sum_{m=0}^{\infty}\frac{(m+K)!\,\Gamma(m+\frac{K}{2}+\frac{9}{5})}{(2m+2K+1)!\,m!\,\Gamma(9/5)}\,G_{mK}(v_0), \qquad (3.77)$$

where $M^{\nu\nu'}_{\mu\mu'}$ is given by Eq.(3.57).

For resonant collisions,

$$\mathcal{M}^{\nu\nu'}_{\mu\mu',K}(v_0)=M^{\nu\nu'}_{\mu\mu'}\sum_{m=0}^{\infty}\frac{(m+K)!\,\Gamma(m+\frac{K}{2}+\frac{3}{2})}{(2m+2K+1)!\,m!\,\Gamma(3/2)}\,G_{mK}(v_0), \qquad (3.78)$$

where $M^{\nu\nu'}_{\mu\mu'}$ is given by Eq.(3.60).

In order to obtain the explicit form of $G_{mK}(v_0)$, we substitute the emitter velocity distribution given by Eq.(3.72) into Eq.(3.76). After integrating Eq.(3.76) over the angle Φ, we obtain

$$G_{mK}(v_0)=-(-2)^{K+1}\alpha_e\exp(\alpha_e v_0^2)\int_0^{\infty}v_e^2dv_e\int_0^{\pi}\sin\theta d\theta\,(4\alpha_p v_e^2)^{m+\frac{K}{2}} \times e^{-(\alpha_e+\alpha_p)v_e^2}P_K(\cos\theta)\,\delta(v_e\cos\theta-v_0). \qquad (3.79)$$

Performing the integration over the angle θ in Eq.(3.79), we have

$$G_{mK}(v_o)=-(-2)^{K+1}\alpha_e(4\alpha_p)^{m+\frac{K}{2}} \times\int_0^{\infty}dv_e v_e^{2m+K+1}e^{-(\alpha_e+\alpha_p)v_e^2}P_K(v_0/v_e). \qquad (3.80)$$

It is convenient to expand the Legendre's polynomial on the right-hand side of Eq.(3.80) as

$$P_K(v_0/v_e) = \sum_{r=0}^{[K/2]} \frac{(2K-2r-1)!!}{(-2)^r r!\,(K-2r)!} (v_0/v_e)^{K-2r}. \qquad (3.81)$$

where [K/2] is the largest integer that does not exceed K/2. Using Eq.(3.81) and the incomplete gamma function[98] defined as $\Gamma(n,x) \equiv \int_x^\infty t^{n-1}e^{-t}dt$, we obtain

$$G_{mK}(v_0) = (-4)^K(1-x)\left[\frac{x}{1-x}\right]^{K/2}\zeta^2 e^{\zeta^2}(4x)^m \times \sum_{r=0}^{[K/2]} \frac{(2K-2r-1)!!}{r!\,(K-2r)!}\left[-\frac{1-x}{2\zeta^2}\right]^r \Gamma\left(m+r+1,\frac{\zeta^2}{1-x}\right), \qquad (3.82)$$

where $x \equiv m_p/(m_e+m_p)$, and ζ is given by $\zeta=\sqrt{\alpha_e}v_0$ which is the projection of the velocity of the excited emitters onto the direction of the incident laser beam, hence ζ is proportional to the detuning of the laser frequency from the center of the absorption line.

Because the whole system has the same symmetry as in the case described in the previous section, the relations (3.62) are still valid for $\Gamma_q^{kk'}(v_0)$.

III.4.2 Numerical Calculations of the Relaxation Matrix for Emitters Excited by a Single-Mode Laser

Numerical calculations were carried out for nonresonant col-

lisions of the emitters (j=1) excited by a single-mode laser with perturbers in the ground state. We can calculate the relaxation matrix $\Gamma_q^{kk'}$ by substituting the matrix elements $M_{\mu\mu'}^{\nu\nu'}$ into Eq.(3.78) [$M_{\mu\mu'}^{\nu\nu'}$ in the Ω_0' frame are shown in Table 3.5(a)]. The dependence of $\Gamma_q^{kk'}(v_0)$ on the axial component v_0 of the emitter velocity and on the normalized perturber mass x appears through the function $G_{mK}(v_0)$. Therefore, we must calculate the infinite series on the right-hand side of Eq.(3.77) for given values of ζ and x. This infinite series is convergent if $0 \leq x < 1$. As a matter of course, this condition is always satisfied for any combination of emitter and perturber. This convergence is good except for the case that the mass of perturber is much larger than that of emitter ($x \simeq 1$).

At first, in order to clarify the dependence of the relaxation matrix on the mass ratio x, we show in Fig.3.8 the typical result calculated for the case that the emitters are excited by a single-mode laser tuned to the line center, and hence only the emitters whose axial components of velocities are equal to zero are excited ($v_0=0$). In Fig.3.8, solid curves represent the elements $\Gamma_q^{kk'}(0)$, while two dotted curves represent the relaxation rates of orientation and alignment for emitters having an isotropic Maxwellian distribution. It should be noted that the relaxation rates in Fig.3.8 are not shown in units of $(2\pi/5)n_p \times B^{2/5}\langle v_R^{3/5}\rangle$ but in units of $(2\pi/5)n_p B^{2/5}\langle v_p^{3/5}\rangle$ even for the case of isotropic collisions. As seen in Fig.3.8, the relaxation rates $\Gamma_q^{kk}(0)$ are always smaller than those for the isotropic case.

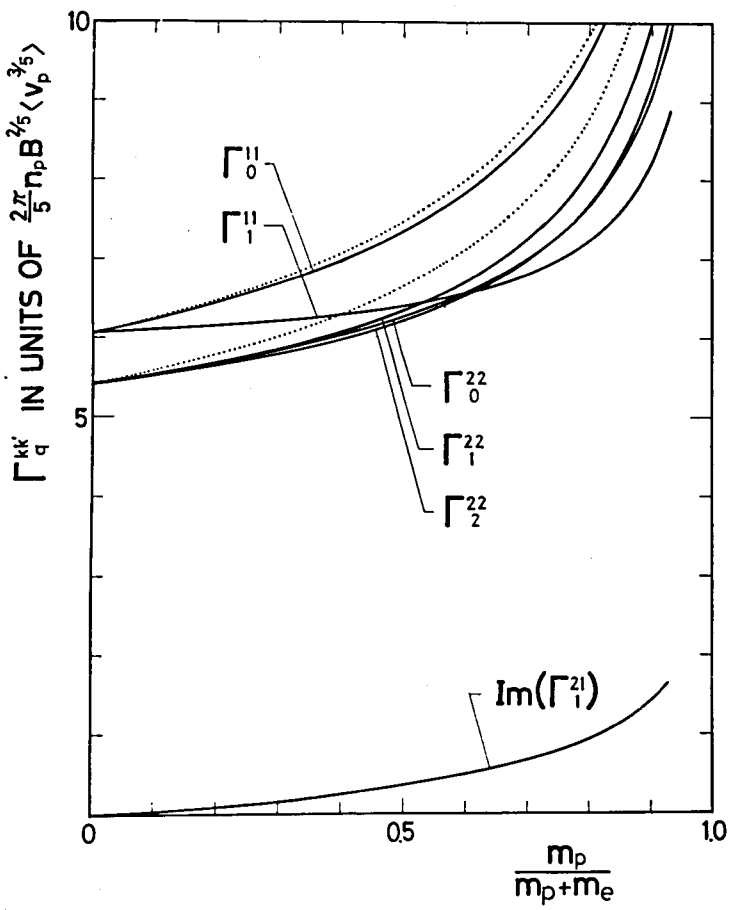

Fig. 3.8 Relaxation matrix elements for emitters excited by a single-mode laser tuned to the center of the absorption line, as functions of $x \equiv m_p/(m_p+m_e)$. Two dotted curves show the case that emitters have an isotropic Maxwellian distribution.

This is not surprising because the average relative velocity of emitters excited by a zero-detuning laser is always smaller than that of isotropically excited emitters. If the mass of the emitter is much larger than that of perturber, the system is nearly isotropic.

In the next place, we shall consider the case that the laser frequency is detuned from the line center. Figures 3.9 show the elements of the relaxation matrix as functions of the axial velocity component of the emitters which is proportional to the detuning of the single-mode laser frequency from the line center. The relaxation rates of orientation and alignment for isotropic collisions are also shown by two dotted lines. Figure 3.9(a) shows the case that $m_e:m_p=4:1$, which corresponds to collisions between neon and helium atoms. In this case, the isotropic velocity distribution of perturbers (helium atoms) is considerably wider than that of emitters (neon atoms), so that the effect of the detuning on the relaxation matrix is not so remarkable. Figure 3.9(b) shows the case of nonresonant collisions between atoms of the same species ($m_e=m_p$). Figure 3.9(c) shows the case that $m_e:m_p=3:17$, which corresponds to the case of sodium atoms (emitters) perturbed by xenon atoms (perturbers). In this case, the velocity distribution of emitters spreads much wider than the isotropic velocity distribution of perturbers, so that the effect of the detuning is remarkable.

It is worthwhile noting that the transfer rates between alignment and orientation, which are pure imaginary, change

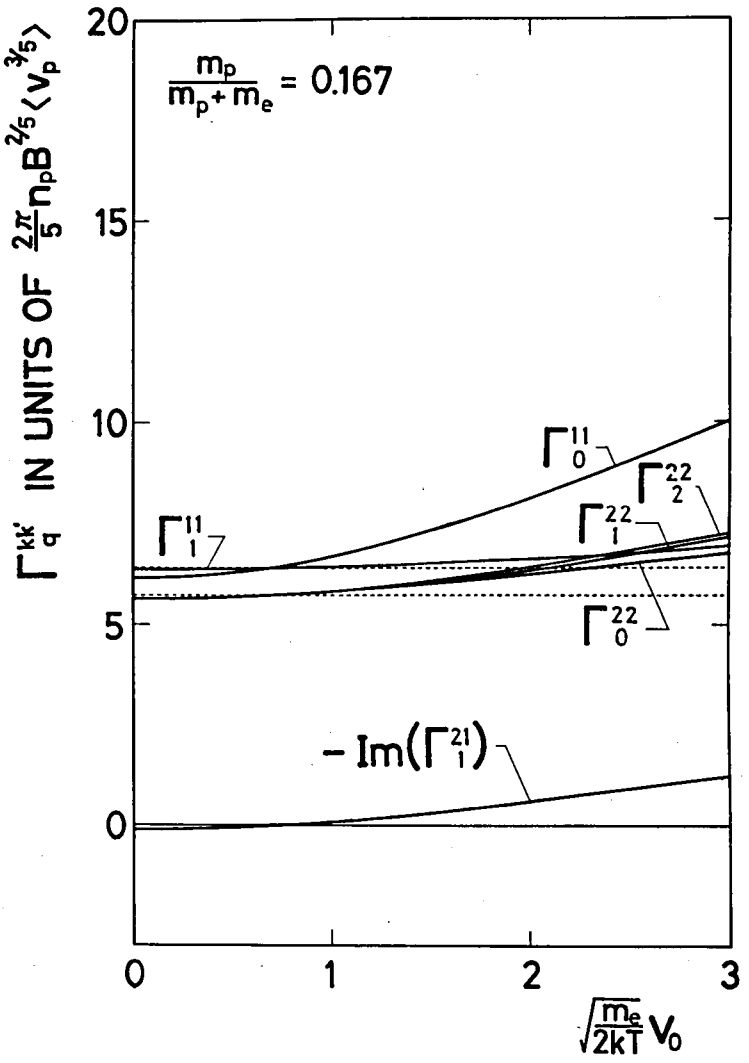

Fig. 3.9(a) Relaxation matrix elements for emitters excited by a single-mode laser as functions of the normalized axial emitter velocity, for x = 0.167, which corresponds to the case of neon atoms perturbed by helium atoms.

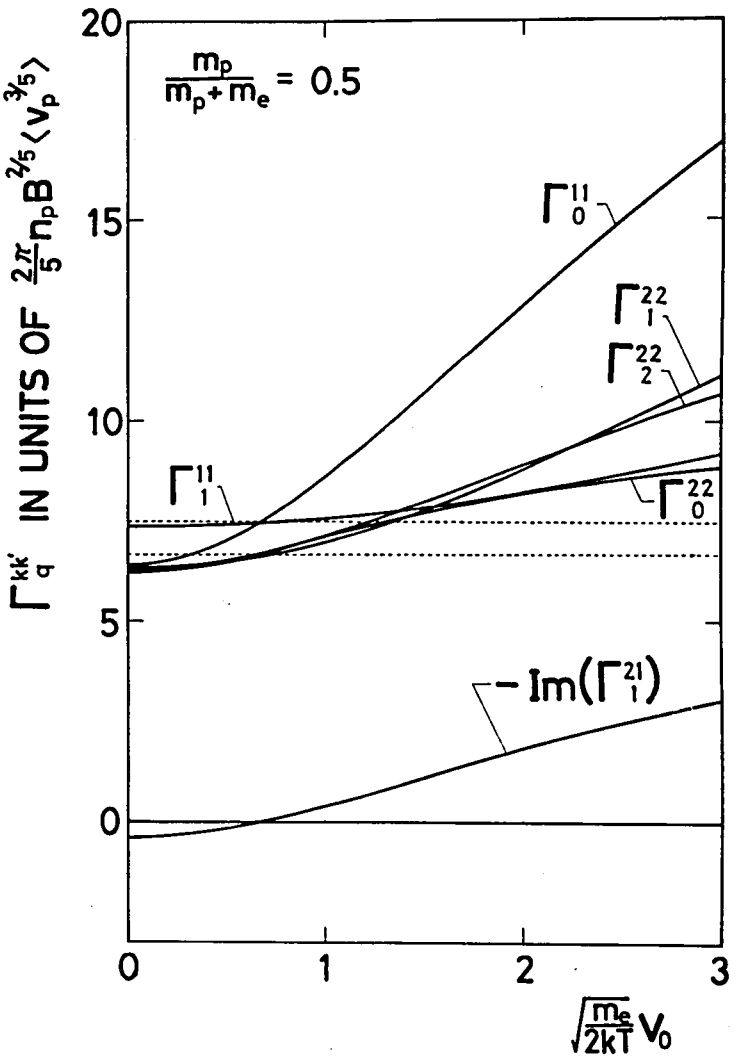

Fig. 3.9(b) As for Fig. 3.9(a), but for x = 0.5, which corresponds to the case of nonresonant collisions between the same species.

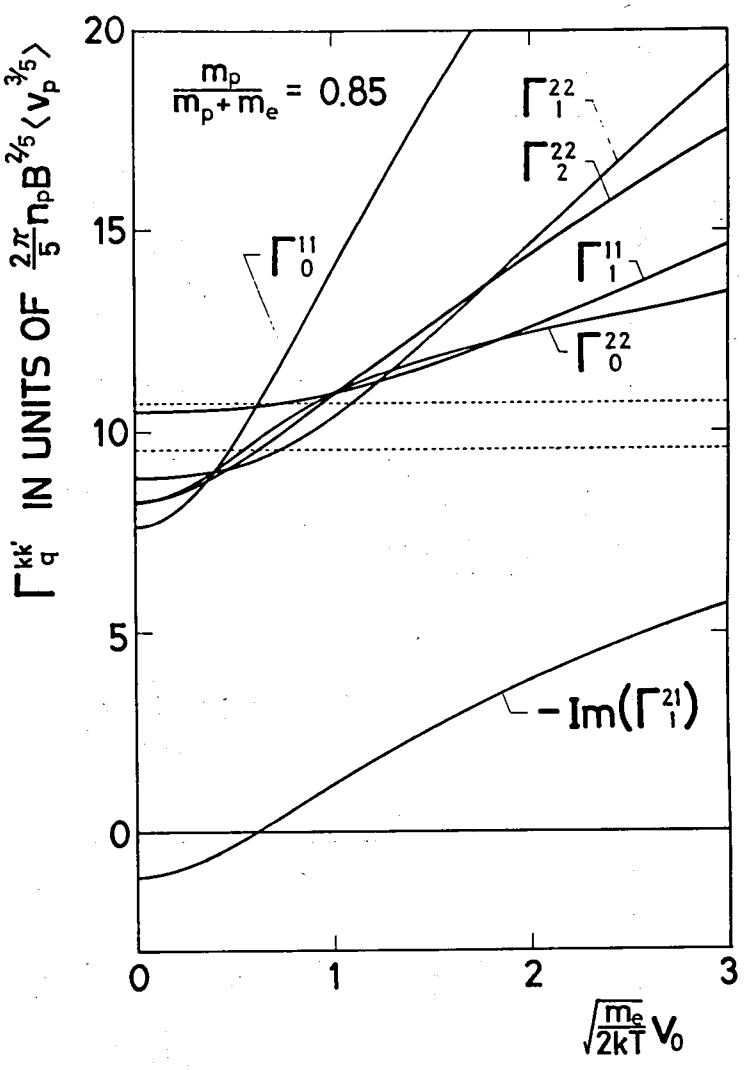

Fig. 3.9(c) As for Fig. 3.9(a), but for x = 0.85, which corresponds to the case of sodium atoms perturbed by xenon atoms.

their signs when the detuning is increased through the frequency at which the corresponding axial emitter velocity is equal to 60~70% of $(2kT/m_e)^{1/2}$ (the most probable velocity of emitters with an isotropic velocity distribution). Furthermore, at about this detuning, the diagonal elements $\Gamma_q^{kk}(v_0)$ are equal to those for isotropic collisions which are shown by two dotted lines (the upper is for orientation, the lower is for alignment). When the matrix elements shown in Figs.3.9 are averaged with respect to v_0 over the one-dimensional Maxwellian function given by $(m_e/2\pi kT)^{1/2}\exp(-m_e v_0^2/2kT)$, the diagonal elements $\Gamma_q^{kk}(v_0)$ are reduced to the relaxation rates of the 2^k-pole momemt for isotropic collisions and the off-diagonal elements are reduced to zero, as one might expect.

Although our calculations have been carried out for the case that the emitters are excited by a single-mode laser beam, our results are applicable for the emitters excited by a light beam with an arbitrary spectral profile. In this case, the distribution of v_{ez} is no longer given by a delta function. Therefore, the relaxation matrix should be obtained by averaging $\Gamma_q^{kk'}(v_0)$ obtained in this section over the velocity distribution of v_{ez} as follows :

$$\Gamma_q^{kk'} = \int_{-\infty}^{\infty} f(v_{ez})\Gamma_q^{kk'}(v_{ez})dv_{ez} \ , \qquad (3.83)$$

where $f(v_{ez})$ is the distribution function of v_{ez}. Especially when the emitters are excited by a multi-mode laser, the integral

in Eq.(3.83) is reduced to a simple summation of $\Gamma_q^{kk'}(v_{ez})$ weighted by the intensity of each mode.

III.5 Discussion and Conclusions

In this chapter, we have investigated the collisional relaxation among Zeeman substates by nonresonant collisions where the velocity distribution of emitters is anisotropic, especially in the case that the emitters are excited by a single-mode laser beam. The relaxation matrix elements for emitters excited by a single-mode laser have been obtained by averaging the relaxation matrix for emitters moving with a definite velocity over the emitter velocity distribution whose projection onto the direction of the laser propagation has been assumed to be a delta function.

The most remarkable feature of anisotropic collisions is the appearance of the transfer between multipole components with different k. The transfer rates becomes larger with an increase in the ratio of the mass of perturber to that of emitter. Even when the single-mode laser is tuned to the line center, the transfer between alignment and orientation is sufficiently large to be observed experimentally. For example, the ratio of the transfer rate to the collisional broadening is about 6% when the mass of emitter is equal to that of perturber [i.e. $x \equiv m_p/(m_p+m_e)=0.5$]. When the emitters are sodium atoms and the perturbers are xenon atoms ($x \simeq 0.85$), this ratio amounts to about 12%, as seen in Fig.3.8.

Another feature of anisotropic collisions is the fact that the decay rate of a multipole moment is also dependent on $|q|$. Furthermore, in the case of single-mode laser excitation, the decay rates increase as the detuning is increased. Therefore, the decay rates obtained in the experiments with a single-mode laser are not the same as those for isotropic collisions. Even when the laser is tuned to the line center, the observed decay rates should be smaller than those for isotropic collisions. As one dutunes the laser frequency from the absorption line center, the decay rates increase and finally become greater than the values for isotropic collisions. Consequently it must be emphasized that one cannot in principle calculate the cross sections for destructions of multipole moments by comparing the experimental results with the isotropic collision theory. The error in the calculation of cross sections is, however, small when the perturber is not heavier than the emitter, and when the laser is tuned around the absorption line center.

In the optical-rf double-resonance experiments, the shift of the magnetic resonance line becomes important as well as its broadening. It has been shown by Happer [100] that a weak isotropic fluctuating perturbation in a strong magnetic field such that the Larmor precession cannot be neglected compared with the correlation time of the perturbation induces anisotropic relaxations of multipole moments and causes energy shifts of Zeeman substates as if a fictitious magnetic field is present. Namely, the energy level with the magnetic quantum number m and that with -m are

shifted by the same amount but to opposite directions, so that the magnetic resonance line is shifted as a whole. Recently, Gay[58),59)] has shown that, even if the velocity distribution is isotropic, similar shifts are caused by collisional perturbations in such a strong magnetic field. In their cases, due to the presence of a strong magnetic field, the system is not symmetric under plane reflections. On the contrary, our system has symmetries with respect to planes in addition to the axial symmetry. Using the relations (3.62), we find that the imaginary eigenvalues of the relaxation matrix are always accompanied by their complex conjugates. It follows that the energy levels with the magnetic quantum number m and -m are shifted to the same direction by the same amount as if a fictitious electric field inducing the Stark shift is present. Consequently, it is expected that, when one considers the emitter atoms with j=1, the magnetic resonance line is decomposed into two components which are shifted to opposite directions by the same amount. However, as the shifts are expected to be smaller than the broadening of each component, the overall resonance line to be observed might never split and have only unshifted peak at the center. So far we neglected the power broadening due to the rf magnetic field. If it is taken into account, the magnetic resonance signal of alignment is given by the well-known Majorana formula which has two peaks symmetric with respect to the resonance frequency ω_0 even when collisions are isotropic :

$$S \propto \frac{\omega_1^2\{4(\omega-\omega_0)^2+\gamma_2^2+\omega_1^2\}}{\{(\omega-\omega_0)^2+\gamma_2^2+\omega_1^2\}\{4(\omega-\omega_0)^2+\gamma_2^2+4\omega_1^2\}}$$

$$= -\frac{\omega_1^2}{(\omega-\omega_0)^2+\gamma_2^2+\omega_1^2} + \frac{3\omega_1^2}{4(\omega-\omega_0)^2+\gamma_2^2+4\omega_1^2} \quad , \qquad (3.84)$$

where ω is the angular frequency of the rf field, $\omega_1=g\mu_B H_{rf}$, and γ_2 is the decay rate of alignment for isotropic collisions. Nedelec et al. have theoretically shown the probability that the two peaks become more prominent for the case of anisotropic collisions due to the difference between $\Gamma^{22}_{\pm1}$ and $\Gamma^{22}_{\pm2}$. They observed experimentally this anomalous behavior, and attributed it to anisotropic collisions due to the convection of emitters caused by the temperature gradient in the cell[45]. However, this anisotropic effect of the convection is thought to be too small to be observable. Lombardi[46] has shown that the anomalous signal observed by Nedelec et al. is the effect of anisotropic relaxation due to the presence of strong external electric field rather than to anisotropic collisions. Hence, the overall magnetic resonance line to be observed might never shifted by anisotropic collisions. Therefore, it is impossible to explain the pressure-induced g_J-shift observed by Yabuzaki et al.[36] by the anisotropy, since the magnetic field is not too strong to break the plane-reflection symmetry.

CHAPTER IV

OBSERVATIONS OF THE EFFECTS OF ANISOTROPIC COLLISIONS ON MAGNETIC DEPOLARIZATION SIGNALS

IV.1 Introduction

The above-mentioned effects of anisotropic collisions on emitters excited by a single-mode laser may be possible to be investigated by observing the collisional broadening in some optical-pumping experiments (e.g., Hanle effect, magnetic resonance, etc.). In optical-pumping experiments with a single-mode laser, the anisotropy of the emitter velocity distribution is not, however, so large that the effect of anisotropic collisions on the broadening of the Hanle curve or magnetic resonance signal may not be so remarkable.

On the other hand, the transfer between alignment and orientation, which is absent for the case of isotropic collisions, increases with increasing degree of anisotropy. The averged collisional interaction for emitters excited by a single-mode laser, which has been discussed in Chapter III, has alignment-like symmetry; i.e., axial symmetry and symmetries under reflection with respect to any planes containing the axis of symmetry, which is the same as the symmetry of a system in an electric field. Lombardi has shown that, when the excited atoms are

aligned in a direction neither parallel nor perpendicular to the axis of anisotropy, orientation is created in the direction perpendicular to the plane which contains the principal axis of alignment and the axis of anisotropy[46]. Conversely, when the excited atoms are oriented in a direction which is not parallel to the axis of anisotropy, alignment is created in the plane containing the axis of anisotropy, which is perpendicular to the plane containing both of the axes of orientation and anisotropy. In this plane, the principal axis of the created alignment is neither parallel nor perpendicular to the axis of anisotropy.

Recently, Chamoun et al.[50] have investigated the transfer from alignment to orientation by observing partially circularly polarized fluorescences emitted by excited helium atoms initially aligned by collisions with an accelerated heavy-ion beam. In their experiment, the velocities of excited helium atoms are restrained on a conical surface in the velocity space[48], so that the collisions with helium atoms in the ground state are anisotropic. Furthermore, this anisotropic excitation also creates alignment in the excited state, but orientation is by no means created in the excited state. Therefore, it is impossible to observe directly the transfer from orientation to alignment by the collisional excitation.

On the other hand, in optical-pumping experiments using a single-mode laser, it is possible to create not only alignment but also orientation in the excited state by linearly and circularly polarized light beams respectively, and the degree of

anisotropy in the velocity distribution can easily be varied by varying the detuning of the single-mode laser frequency. Thus it is possible to observe both transfers from alignment to orientation and from orientation to alignment.

In this chapter, it shall be considered how the effects of anisotropic collisions are expected to appear in the magnetic depolarization signals in such experiments as the Hanle experiment using a single-mode laser. By the term " magnetic depolarization", we mean the phenomenon that the macroscopic polarization such as alignment or orientation which is stationarily excited by external light is depolarized under the influence of external static magnetic field (i.e., Larmor precession of the multipole moments). In the course of the magnetic depolarization, no transfer between multipole moments with different k occurs, as in the case of isotropic collisions. Consequently, if the collisions are isotropic, the fluorescence emitted by initially aligned atoms has no circularly polarized component. On the other hand, if the collisions are anisotropic, the fluorescence should be partially polarized circularly due to the transfer from alignment to orientation. Conversely, the transfer from orientation to alignment can be observed in linearly polarized fluorescence emitted by initially oriented atoms.

The first half of this chapter is devoted to derive analytically the signal profile of magnetic depolarization experiments under the influence of anisotropic collisions for the atoms excited by a linearly or circularly polarized light beam.

Stationary solutions of the master equation for the density matrix is solved by taking account of the anisotropic relaxation discussed in Chap. III. In this calculation, couplings with higher order multipole moments ($k \geq 3$) are neglected, since only the orientation and alignment can be directly excited or observed optically. In fact, the lowest order contribution of these couplings to orientation or alignment appears in the second order, which is good contrast with the coupling between orientation and algnment appearing in the first order. Under this approximation, the analyzed signal profiles are applicable to the excited state with an arbitrary total angular momentum j.

Experimentally the effects of anisotropic collisions are studied for the $2p_4$ state (j=2) of neon atoms excited by a single-mode laser from the metastable $1s_5$ state. The latter half of this chapter is devoted to discuss about the experiments which we have made.

IV.2 Priciples of Experiments

In the optical-pumping experiments, the multipole moments are created in a given atomic state by a polarized light beam. On the other hand, the information about the multipole moment in the excited Zeeman multiplet can be obtained by detecting the light emitted in a given direction with some polarization. The purpose of this section is to derive the formulae for the intensity and polarization of the light emitted by atoms in a

magnetic field under the influence of anisotropic collisions. In this process, we neglect the higher order effects of the laser excitation.

IV.2.1 Polarizations of the Excitation and Emission

As described in Sec.II.3, the time evolution of the density matrix for the q-component of the 2^k-pole moment is governed by Eq.(2.16). In this equation, the effect of optical pumping $(d\rho_q^k/dt)_{pump}$ is represented by the term F_q^k given by Eq.(2.23b). Especially, its dependence on the polarization is contained in the factor $\Phi_q^k(\vec{e})$. On the other hand, the intensity of the fluorescence with polarization $\vec{e}$ is related to the density matrix of the excited state by the relation

$$I_{\vec{e}} = I_0' \sum_{\substack{mm' \\ m_0}} \langle j_0 m_0 | \vec{e}^* \cdot \vec{d} | jm \rangle \rho_{mm'} \langle jm' | \vec{e} \cdot \vec{d} | j_0 m_0 \rangle, \qquad (4.1)$$

where I_0' is a proportionality constant, j_0 and m_0 are the quantum numbers specifying the state to which the transition terminates. Using the irreducible representation of the density matrix and $\Phi_q^k(\vec{e})$ given by Eq.(2.24), we can transform Eq.(4.1) to

$$I_{\vec{e}} = (-1)^{j-j_0} I_0 \sum_k \sqrt{2k+1} \begin{Bmatrix} 1 & 1 & k \\ j & j & j_0 \end{Bmatrix} \sum_q (-1)^q \rho_q^k \Phi_q^k(\vec{e}), \qquad (4.2)$$

where

$$I_0 = I_0' |\langle j \| d \| j_0 \rangle|^2. \qquad (4.3)$$

Both of excitation and emission are dependent on the polarization of the light through the factor $\phi_q^k(\vec{e})$.

In our experiments, the linear polarization is selected by a linear polarizer, while the circular polarization is selected by the combination of a linear polarizer and a quarter-wave plate.

Here, we shall derive the expressions of $\phi_q^k(\vec{e})$, for the light beam propagated in the Z direction in the (X,Y,Z) frame, which passes through a linear polarizer and an anisotropic retarder. When the principal axis of the linear polarizer is directed to the $(0,\psi)$ direction and the retardation axis of the retarder is directed to the $(0,\gamma)$ direction with phase retardation η, the polarization vector $\vec{e}$ is given by

$$\begin{pmatrix} e_X \\ e_Y \end{pmatrix} = \begin{pmatrix} \cos\gamma & \sin\gamma \\ -\sin\gamma & \cos\gamma \end{pmatrix} \begin{pmatrix} e^{i\eta} & 0 \\ 0 & 1 \end{pmatrix} \begin{pmatrix} \cos\gamma & -\sin\gamma \\ \sin\gamma & \cos\gamma \end{pmatrix} \begin{pmatrix} \cos\psi \\ \sin\psi \end{pmatrix}$$

$$= e^{i\eta/2} \begin{pmatrix} \cos(\eta/2)\cos\psi + i\sin(\eta/2)\cos(2\gamma-\psi) \\ \cos(\eta/2)\sin\psi + i\sin(\eta/2)\sin(2\gamma-\psi) \end{pmatrix}. \quad (4.4)$$

When the light is propagated in the (θ,ϕ) direction in the laboratory frame (x,y,z), we can obtain the polarization vector in this frame by rotating Eq.(4.4) by the Euler angles $(\phi,\theta,0)$. Thus we obtain the standard components of $\vec{e}$ in the laboratory frame :

$$e_{\pm 1} = \frac{1}{\sqrt{2}} e^{i(\frac{\eta}{2}\pm\phi)} [\sin\tfrac{\eta}{2}\sin(2\gamma-\psi) \mp \cos\theta\cos\tfrac{\eta}{2}\cos\psi$$

$$-i\{\cos\tfrac{\eta}{2}\sin\psi \pm \cos\theta\sin\tfrac{\eta}{2}\cos(2\gamma-\psi)\}],$$

$$e_0 = -e^{i\frac{\eta}{2}}\sin\theta\{\cos\tfrac{\eta}{2}\cos\psi + i\sin\tfrac{\eta}{2}\cos(2\gamma-\psi)\}. \qquad (4.5)$$

Substituting these standard components into Eq.(2.24), we obtain the general form of $\Phi^k_q(\vec{e})$:

$$\Phi^0_0 = -\frac{1}{\sqrt{3}}, \quad \Phi^1_0 = -\frac{1}{\sqrt{6}}\cos\theta\sin\eta\sin(2\gamma-2\psi),$$

$$\Phi^1_{\pm1} = \mp\frac{1}{2\sqrt{3}}e^{\pm i\phi}\sin\theta\sin\eta\sin(2\gamma-2\psi),$$

$$\Phi^2_0 = -\frac{1}{\sqrt{30}}(1-\frac{3}{2}P\sin^2\theta), \quad \Phi^2_{\pm1} = \mp\frac{1}{2\sqrt{5}}e^{\pm i\phi}\sin\theta(P\cos\theta\pm iQ),$$

$$\Phi^2_{\pm2} = -\frac{1}{4\sqrt{5}}e^{\pm i2\phi}\{2-P(1+\cos^2\theta)\mp i2Q\cos\theta\}, \qquad (4.6)$$

where

$$P = 1 + \cos^2(\eta/2)\cos2\psi + \sin^2(\eta/2)\cos(4\gamma-2\psi),$$

$$Q = \cos^2(\eta/2)\sin2\psi + \sin^2(\eta/2)\sin(4\gamma-2\psi). \qquad (4.7)$$

To get a light beam with linear polarization, the retarder is not required ($\eta=0$). In this case, only the alignment is created or observed. On the other hand, to get a circularly polarized light beam, the retardation $\eta=\pm\pi/4$ is necessary. In this case, the orientation is also created or observed , in addition to the alignment.

IV.2.2 Excitation with Linearly Polarized Light Beam

When the single-mode laser beam is propagated in the z direction ($\theta=\phi=0$), and is linearly polarized ($\eta=0$), only the excitations F^0_0, F^2_0, and $F^2_{\pm 2}$ are different from zero, as seen in Eq.(4.6) and (2.23b). We consider the case that a static magnetic field $\vec{H}$ is applied in the x direction. According to Eq.(2.17), the term representing the interaction with the magnetic field $\vec{H}$ becomes

$$(-i/\hbar)\,[\,\mathcal{H}_F,\rho]^k_q = -i\frac{\omega}{2}\{\sqrt{k(k+1)-q(q+1)}\,\rho^k_{q+1} + \sqrt{k(k+1)-q(q-1)}\,\rho^k_{q-1}\}, \qquad (4.8)$$

where $\omega=g\mu_B H$.

Next, we shall consider the relaxation which is caused by anisotropic collisions and spontaneous emission. The relaxation term in Eq.(2.16) is given by

$$\left(\frac{d\rho^k_q}{dt}\right)_{rel} = -\gamma_{nat}\rho^k_q - \sum_{k'} \Gamma^{kk'}_q \rho^{k'}_q \quad , \qquad (4.9)$$

where γ_{nat} is the spontaneous decay rate and $\Gamma^{kk'}_q$ is the collisional relaxation matrix obtained in Chap. III.

After substituting these termes into the right-hand side of Eq.(2.16), the stationary solutions are obtained :

$$\mathrm{Re}(\rho^1_1) = -\frac{1}{\Delta_1}\Gamma\omega A \quad , \qquad \rho^1_0 = -\frac{\sqrt{2}}{\Delta_2}\Gamma\omega^2\,\mathrm{Im}(F^2_2) \quad ,$$

$$\rho_0^2 = \frac{1}{\gamma_0^2}F_0^2 - \frac{\sqrt{6}}{\Delta_1}\frac{\gamma_1^1}{\gamma_0^2}\omega^2 A \ , \qquad \mathrm{Im}(\rho_1^1) = -\frac{1}{\Delta_2}\gamma_0^1\Gamma\omega\mathrm{Lm}(F_2^2) \ ,$$

$$\mathrm{Im}(\rho_1^2) = -\frac{1}{\Delta_1}\gamma_1^1\omega A \ , \qquad \mathrm{Re}(\rho_1^2) = \frac{1}{\Delta_2}\omega(\gamma_0^1\gamma_1^1+\omega^2)\,\mathrm{Im}(F_2^2) \ ,$$

$$\mathrm{Re}(\rho_2^2) = \frac{1}{\gamma_2^2}\mathrm{Re}(F_2^2) - \frac{1}{\Delta_1}\frac{\gamma_1^1}{\gamma_2^2}\omega^2 A \ ,$$

$$\mathrm{Im}(\rho_2^2) = \frac{1}{\Delta_2}\{\gamma_1^2(\gamma_0^1\gamma_1^1+\omega^2) + \gamma_0^1\Gamma^2\}\mathrm{Im}(F_2^2) \ , \qquad (4.10)$$

where

$$\Delta_1 = (3\gamma_2^2 + \gamma_0^2)\gamma_1^1\omega^2 + \gamma_0^2\gamma_2^2(\gamma_1^1\gamma_1^2 + \Gamma^2) \ ,$$

$$\Delta_2 = (\omega^2 + \gamma_0^1\gamma_1^1)(\omega^2 + \gamma_1^2\gamma_2^2) + \Gamma^2\gamma_1^1\gamma_2^2 \ ,$$

$$A = \gamma_0^2\mathrm{Re}(F_2^2) + \frac{\sqrt{6}}{2}\gamma_2^2F_0^2 \ ,$$

$$\gamma_q^k = \gamma_{nat} + \Gamma_q^{kk} \ , \quad i\Gamma = \Gamma_1^{21} = \Gamma_1^{12} = -\Gamma_{-1}^{21} = -\Gamma_{-1}^{12} \ . \qquad (4.11)$$

In the case of isotropic collisions (Γ=0), each alignment component shows the ordinary Hanle effect, which appears as dispersion type functions for $\rho_{\pm1}^2$ and as Lorentzian functions for ρ_0^2 and $\rho_{\pm2}^2$ when the magnetic field is swept through zero. Since all orientation components disappear in the isotropic case, the orientation components in Eq.(4.10) are attributed to the transfer from alignment to orientation caused by anisotropic collisions.

It is easily found from Eqs.(4.2)and (4.6) that, when we

observe the difference in the intensity between right-handed and left-handed circularly polarized fluorescences emitted in the x direction, the transverse orientation ρ_1^1 can be observed :

$$I_{\sigma+} - I_{\sigma-} = (-1)^{j+j_0} I_0 \begin{Bmatrix} 1 & 1 & 1 \\ j & j & j_0 \end{Bmatrix} 2\mathrm{Re}(\rho_1^1). \tag{4.12}$$

Substituting the stationary solution for $\mathrm{Re}(\rho_1^1)$ given by Eq.(4.10) into Eq.(4.12), we obtain

$$I_{\sigma+} - I_{\sigma-} = (-1)^{j+j_0} I_0 \begin{Bmatrix} 1 & 1 & 1 \\ j & j & j_0 \end{Bmatrix} \frac{2\omega\Gamma A}{(3\gamma_2^2+\gamma_0^2)\gamma_1^1\omega^2+\gamma_0^2\gamma_2^2(\gamma_1^1\gamma_1^2+\Gamma^2)}. \tag{4.13}$$

This intensity difference for circularly polarized emissions can be explained as follows. The alignment, which is transverse with respect to $\vec{H}$, created by laser light, precesses in the y-z plane under the influence of $\vec{H}$. Then the alignment ρ_1^2 is created along the direction $(\pi/4,\pi/2)$, which is neither parallel nor perpendicular to the axis of anisotropy (i.e. the z axis). The anisotropic collisions transfer the alignment ρ_1^2 to the transverse orientation ρ_1^1 directed along the x axis. The transfer process is very similar to the creation of orientation by the combination of alignment and oscillating electric field which are neither parallel nor perpendicular discussed in Ref. 83. As seen in Eq.(4.13), this orientation signal is in dispersion shape when the magnetic field is swept through zero.

On the other hand, the difference in the intensities of

linearly polarized fluorescences emitted in the x direction and polarized along the z and y directions shows the ordinary Hanle signal in a Lorentzian shape as ω is varied in the vicinity of zero magnetic field :

$$I_{\parallel} - I_{\perp} = (-1)^{j+j_0} \begin{Bmatrix} 1 & 1 & 2 \\ j & j & j_0 \end{Bmatrix} \{\sqrt{3/2}\rho_0^2 + \mathrm{Re}(\rho_2^2)\} I_0$$

$$= (-1)^{j+j_0} I_0 \begin{Bmatrix} 1 & 1 & 2 \\ j & j & j_0 \end{Bmatrix} \frac{(\gamma_1^1\gamma_1^2+\Gamma^2)A}{(3\gamma_2^2+\gamma_0^2)\gamma_1^1\omega^2+\gamma_0^2\gamma_2^2(\gamma_1^1\gamma_1^2+\Gamma^2)}, \tag{4.14}$$

Especially when collisions are isotropic, the values of all decay rates of alignment components become the same and the transfer rate Γ vanishes, so that Eq.(4.14) shows the ordinary Hanle signal given by

$$I_{\parallel} - I_{\perp} = (-1)^{j+j_0} I_0 \begin{Bmatrix} 1 & 1 & 2 \\ j & j & j_0 \end{Bmatrix} \frac{A}{4\omega^2 + (\gamma_{iso}^2)^2}, \tag{4.15}$$

where γ_{iso}^2 is the decay rate of alignment for isotropic collisions. Then, the half width of the Hanle signal for anisotropic collisions is larger or smaller than that for isotropic collisions by a factor

$$\frac{\Delta\omega(\mathrm{aniso})}{\Delta\omega(\mathrm{iso})} = \{4\gamma_0^2\gamma_2^2(\gamma_1^1\gamma_1^2+\Gamma^2)/\gamma_{iso}^2\gamma_1^1(3\gamma_2^2+\gamma_0^2)\}^{1/2}. \tag{4.16}$$

From Eqs.(4.13) and (4.14), the ratio of the orientation signal to the alignment signal is given by

$$\frac{A_{or}}{A_{al}} = \left|\frac{\begin{Bmatrix} 1 & 1 & 1 \\ j & j & j_0 \end{Bmatrix}}{\begin{Bmatrix} 1 & 1 & 2 \\ j & j & j_0 \end{Bmatrix}}\right| \frac{|\Gamma|}{\gamma_1^1}\left\{\frac{4\gamma_1^1\gamma_0^2\gamma_2^2}{(\gamma_1^1\gamma_1^2+\Gamma^2)(3\gamma_2^2+\gamma_0^2)}\right\}^{1/2}, \qquad (4.17)$$

where A_{or} and A_{al} are the amplitudes as depicted in Fig.4.1. For instance, for j=1 and j_0=0, Eq.(4.17) becomes

$$\frac{A_{or}}{A_{al}} = \frac{|\Gamma|}{\gamma_1^1}\left\{\frac{4\gamma_1^1\gamma_0^2\gamma_2^2}{(\gamma_1^1\gamma_1^2+\Gamma^2)(3\gamma_2^2+\gamma_0^2)}\right\}^{1/2}. \qquad (4.18)$$

Furthermore, when the anisotropy is small ($\gamma_0^2 \simeq \gamma_1^2 \simeq \gamma_2^2$, $\Gamma \ll \gamma_q^k$), we obtain for j=1 and j_0=0

$$A_{or}/A_{al} \simeq |\Gamma|/\gamma_1^1, \qquad (4.19)$$

and for j=2 and j_0=1

$$A_{or}/A_{al} \simeq \sqrt{15/7}\,|\Gamma|/\gamma_1^1. \qquad (4.20)$$

IV.2.3 Excitation with Circularly Polarized Light Beam

When the laser beam propagated along the z axis is circularly polarized and $\vec{H}$ is directed along the x axis, only the longitudinal orientation F_0^1 and alignment F_0^2 are excited. Then the solutions of Eq.(2.16) can be obtained as follows :

$$\mathrm{Re}(\rho_1^1) = -\frac{\sqrt{6}}{2}\frac{1}{\Delta_1}\gamma_2^2\Gamma\omega F_0^2, \quad \rho_0^1 = \frac{1}{\Delta_2}\{\gamma_1^1\omega^2+\gamma_2^2(\gamma_1^1\gamma_1^2+\Gamma^2)\}F_0^1,$$

$$\rho_0^2 = \frac{1}{2}F_0^2 - \frac{3}{\Delta_1}\frac{\gamma_1^1\gamma_2^2}{\gamma_0^2}\omega^2 F_0^2, \quad \mathrm{Im}(\rho_1^1) = -\frac{\sqrt{2}}{2}\frac{1}{\Delta_2}\omega(\gamma_1^2\gamma_2^2+\omega^2)F_0^1,$$

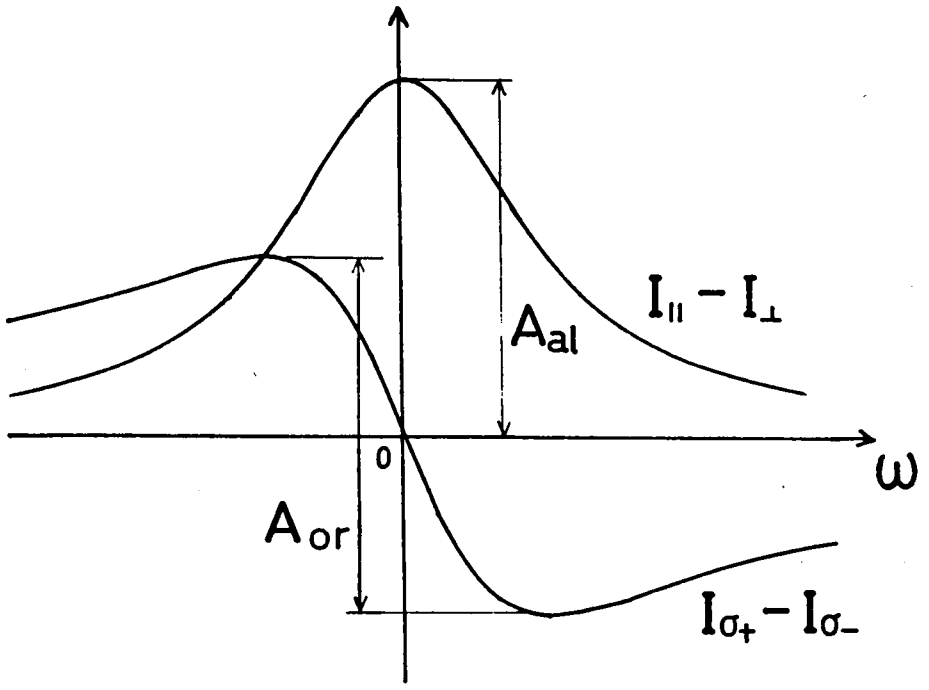

Fig. 4.1 Ordinary Hanle signal ($I_{\parallel} - I_{\perp}$) and orientation signal ($I_{\sigma+} - I_{\sigma-}$) as functions of $\omega(\equiv g\mu_B H)$ for excitation with a linearly polarized laser beam.

$$\mathrm{Im}(\rho_1^2) = -\frac{\sqrt{6}}{2}\frac{1}{\Delta_1}\gamma_1^1\gamma_2^2\omega F_0^2 \ , \qquad \mathrm{Re}(\rho_1^2) = -\frac{\sqrt{2}}{2}\frac{1}{\Delta_2}\gamma_2^2\Gamma\omega F_0^1 \ ,$$

$$\mathrm{Re}(\rho_2^2) = -\frac{\sqrt{6}}{2}\frac{1}{\Delta_1}\gamma_1^1\omega^2 F_0^2 \ , \qquad \mathrm{Im}(\rho_2^2) = \frac{\sqrt{2}}{2}\frac{1}{\Delta_2}\Gamma\omega^2 F_0^1 \ , \qquad (4.21)$$

where the relations given by Eqs.(4.11) are used.

In these results, $\mathrm{Re}(\rho_1^1)$, ρ_0^2, $\mathrm{Im}(\rho_1^2)$, and $\mathrm{Re}(\rho_2^2)$ show essentially the same results as in the case of the excitation by a linearly polarized light beam (Sec.IV.2.2), because these results can be obtained as well by substituting $F_2^2=0$ into Eqs. (4.10) and (4.11). Here, it should be noted that circularly polarized light also creates alignment in addition to orientation as mentioned in Sec.IV.2.1. Therefore, ρ_0^2, $\mathrm{Im}(\rho_1^2)$, and $\mathrm{Re}(\rho_2^2)$ show the ordinary Hanle effect of alignment, and $\mathrm{Re}(\rho_1^1)$ shows the transfer from alignment to orientation. On the other hand, the solutions for ρ_0^1 and $\mathrm{Im}(\rho_1^1)$ give the ordinary Hanle signal of orientation. It is $\mathrm{Re}(\rho_1^2)$ and $\mathrm{Im}(\rho_2^2)$ that should be attributed to the effect of transfer from orientation to alignment.

When we observe the fluorescence which is polarized linearly in the direction with the polar angles $(\pi/4,0)$, the observed intensity is derived from Eq.(4.2) by substituting $\theta=\phi=\pi/2$, $\psi=\pi/4$, and $\eta=0$ into Eq.(4.6). We then obtain

$$I = (-1)^{j+j_0} I_0 \left[\frac{1}{\sqrt{3}}\begin{Bmatrix} 1 & 1 & 0 \\ j & j & j_0 \end{Bmatrix}\rho_0^0 + \begin{Bmatrix} 1 & 1 & 2 \\ j & j & j_0 \end{Bmatrix}\left\{\frac{1}{2\sqrt{6}}\rho_0^2 - \mathrm{Re}(\rho_1^2) + \frac{1}{2}\mathrm{Re}(\rho_2^2)\right\}\right]. \qquad (4.22)$$

In order to extract the pure effect of the transfer, we must

change the sense of the circular polarization of the exitation, which may result in the change in the sign of F_0^1 but no change of F_0^2. Accordingly, we can see the effect of transfer by observing the difference in the intensity of the fluorescence for the right- and left-handed circularly polarized excitations :

$$\Delta I = (-1)^{j+j_0} I_0 \begin{Bmatrix} 1 & 1 & 2 \\ j & j & j_0 \end{Bmatrix} \frac{\sqrt{2}\omega\gamma_2^2\Gamma}{(\omega^2+\gamma_0^1\gamma_1^1)(\omega^2+\gamma_1^2\gamma_2^2)+\Gamma^2\gamma_0^1\gamma_2^2} F_0^1 . \quad (4.23)$$

If we neglect the small term $\Gamma^2\gamma_0^1\gamma_1^2$ in the denominator of Eq.(4.23), we can make clear the physical processes involved in Eq.(4.23) as follows. The excitation with circularly polarized light creates continuously the longitudinal orientation F_0^1 in the z direction, which begins to precess in the y-z plane under the influence of $\vec{H}$ directed along the x axis. Consequently, the stationary transverse orientation $\rho_{\pm 1}^1$ is created in the y direction (the ordinary Hanle effect of orientation), the ω dependence of $\rho_{\pm 1}^1$ being expressed as $\omega/(\omega^2+\gamma_0^1\gamma_1^1)$. This transverse orientation is transferred to the transverse alignment $\rho_{\pm 1}^2$ under the influence of anisotropic collisions with the transfer rate Γ. This transverse alignment is created in the perpendicular direction to the orientation $\rho_{\pm 1}^1$ and in the direction neither parallel nor perpendicular to the axis of anisotropy. It shold be noted that this configuration is much the same as that in the preceding section. Finally, since the transferred algnment $\rho_{\pm 1}^2$ precesses about $\vec{H}$, $\rho_{\pm 1}^2$ is decreased by a factor $\gamma_2^2/(\omega^2+\gamma_1^2\gamma_2^2)$ (the Hanle effect of alignment). Thus the dependence of $\rho_{\pm 1}^2$

on ω becomes $\omega\gamma_2^2/(\omega^2+\gamma_0^1\gamma_1^1)(\omega^2+\gamma_1^2\gamma_2^2)$. The remaining term $\Gamma^2\gamma_0^1\gamma_2^2$ in the denominator of Eq.(4.23) is caused by the secondary transfer to orientation from the alignment created by anisotropic collisions, i.e., orientation→alignment→orientation.

IV.3 Broadening of the Hanle Signal

As mentioned in Sec. IV.2.2, the most important collisional effect on atoms excited by a single-mode laser should be manifested in the broadening of the Hanle signal. In order to investigate this effect, we made a Hanle experiment of alignment in the $2p_4$ state (j=2) of neon atoms. The associated energy level diagram of neon is shown in Fig.4.2. In the positive column of a glow discharge, the metastable $1s_5$ state (j=2) is well populated ($\sim 10^{-11}$ cm^{-3}) by collisions with electrons[101),102)], so that we can align the $2p_4$ state by exciting with a linearly polarized single-mode dye laser beam tuned around the $1s_5$–$2p_4$ absorption line. The linearly polarized component of the fluorescence from this state to the $1s_4$ state (j=1) (609.6 nm) is observed. In order to eliminate the fluorescence originating in the population ρ_0^0, the differential technique described in Sec. IV.2.2 is used.

IV.3.1 Experimental Setup

The schematic diagram of the experimental setup is shown in

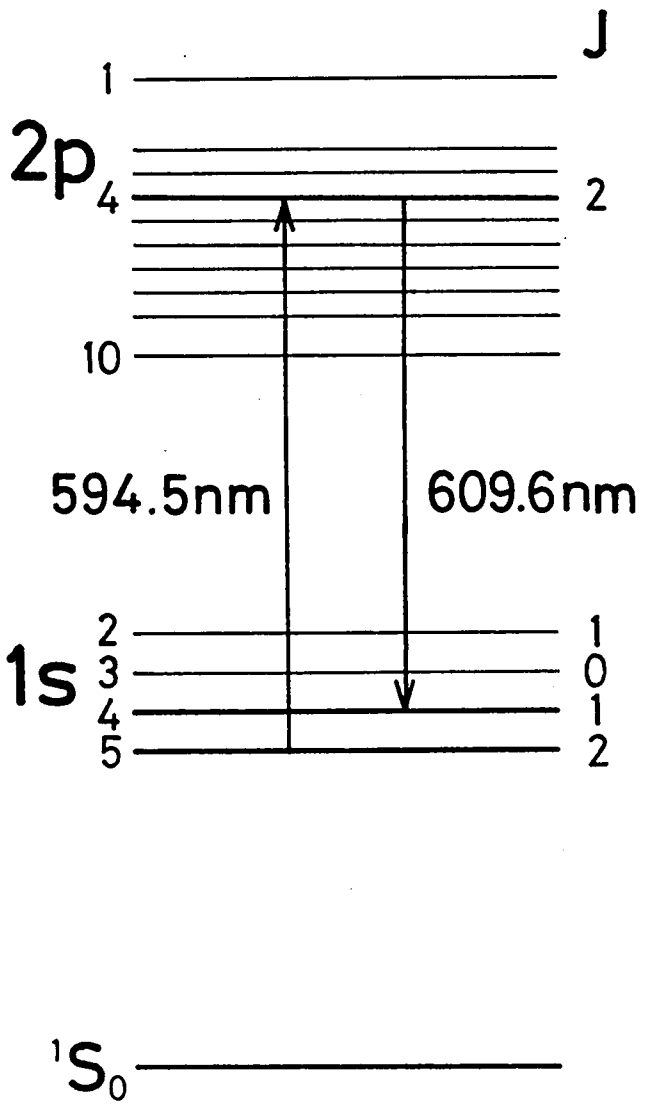

Fig. 4.2 Energy level diagram of neon and transitions of excitation (594.5 nm) and observation (609.6 nm).

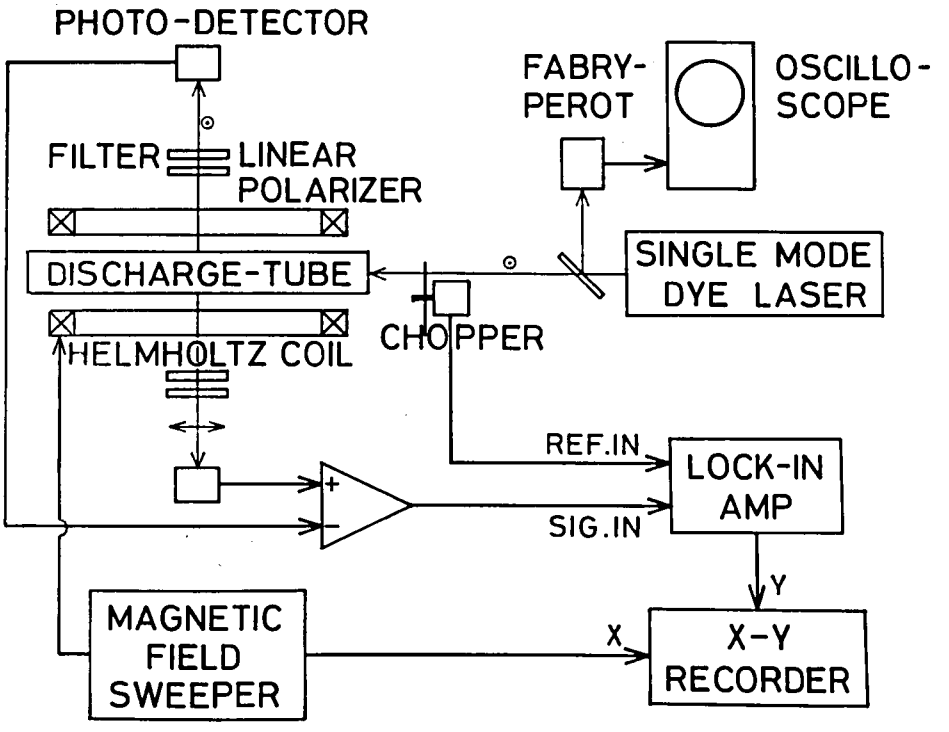

Fig. 4.3 Schematic diagram of the arrangement for Hanle experiment.

Fig.4.3. The single-mode operation of the dye laser pumped by an argon ion laser is attained by inserting a Faraday filter into the dye laser cavity. The Faraday filter used consists of a discharge tube filled with neon of natural abundance and a solenoid coil which produce an axial magnetic field[103),104)]. The single-mode operation in the center region of the absorption line at 594.5 nm was used and the frequency can easily be varied around the line center by changing the axial magnetic field strength. The single-mode frequency was monitored by a scanning Fabry-Perot interferometer. This single-mode output was fed into the positive column of a glow discharge tube with a bore of 8 mm filled with neon of natural abundance [i.e, the relative abundances are 90.92% for Ne^{20}, 0.257% for Ne^{21}, and 8.82% for Ne^{22}][105)]. The pressure of neon was 1.3 Torr, and the discharge current was kept constant at 8 mA by a regulated current supply. This discharge tube was placed in a set of Helmholtz coils.

The spatial arrangement of the exciting light beam and the signal detection is schematically in Fig. 4.4 together with the direction of an applied magnetic field $\vec{H}$. The magnetic field $\vec{H}$ along the x direction was provided by a Helmholtz pair of diameter 100 cm. The magnetic field $\vec{H}$ was varied continuously from -3.2 to +16.1 G by a regulated current supply controlled by a microcomputer. Stray magnetic fields perpendicular to $\vec{H}$ were compensated by two pairs of Helmholtz coils of diameters of 80 and 90 cm at right angles. The incident laser beam was propagated along the z direction, and its polarization plane was chosen to

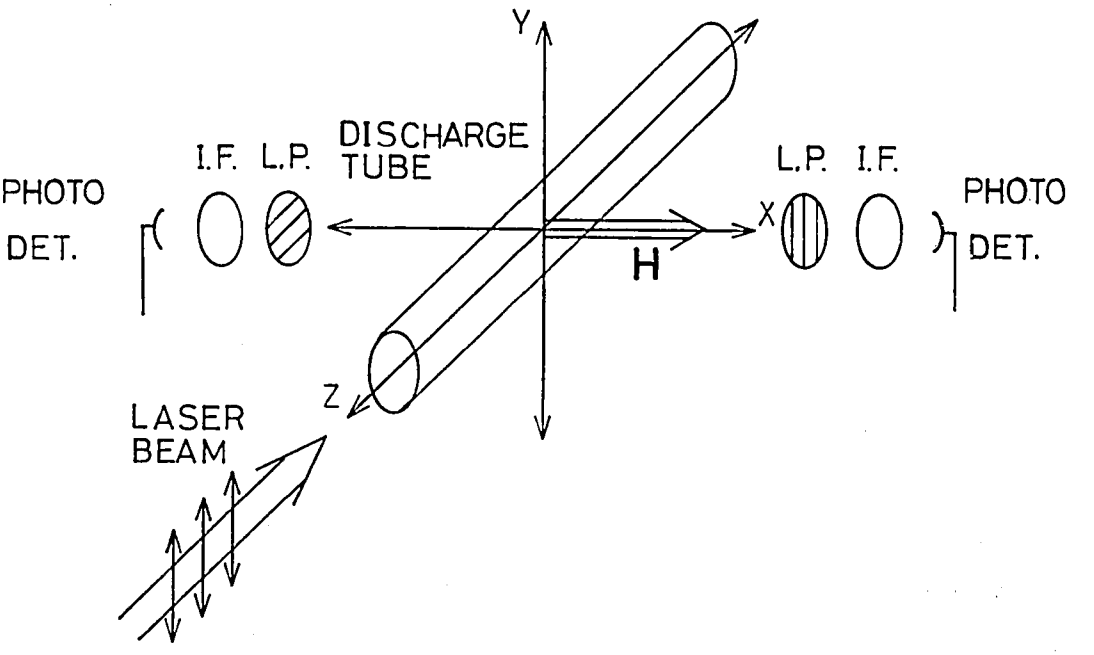

Fig. 4.4 Schematic diagram of the arrangements of magnetic field H and polarizations of excitation and detection, for the Hanle experiment.

be in the direction of the y axis. The position of the discharge tube was so arranged that the portion just behind the entrance of the laser light was placed at the center of the Helmholtz coils. Fluorescences emitted from this portion to the x and -x directions were focussed onto silicon solar cells after passing through linear polarizers and interference filters of transmission wavelength 609.6 nm. The linear polarizers were arranged so that we could observe the two fluorescences $I_{\parallel}$ and $I_{\perp}$ linearly polarized along the y and z directions respectively.

The intensity difference $I_{\parallel}-I_{\perp}$ was obtained by applying the outputs of two solar cells to a differential amplifier. We are only interested in the laser-induced component in the intensity difference $I_{\parallel}-I_{\perp}$. Therefore, in order to improve the signal-to-noise ratio, the incident laser beam was periodically chopped by an mechanical chopper, and the modulated component at the chopping frequency in the output of the differential amplifier was synchronously detected by a lock-in amplifier. The time constant of the lock-in amplifier was chosen to be 1 sec, while it took about 88 sec for a single sweep of the static magnetic field. The chopping frequency of the incident laser light was 30 Hz.

IV.3.2 Experimental Results and Discussions

A typical recorder trace for the case that the single-mode laser was tuned to the absorption line center is shown in Fig.4.5.

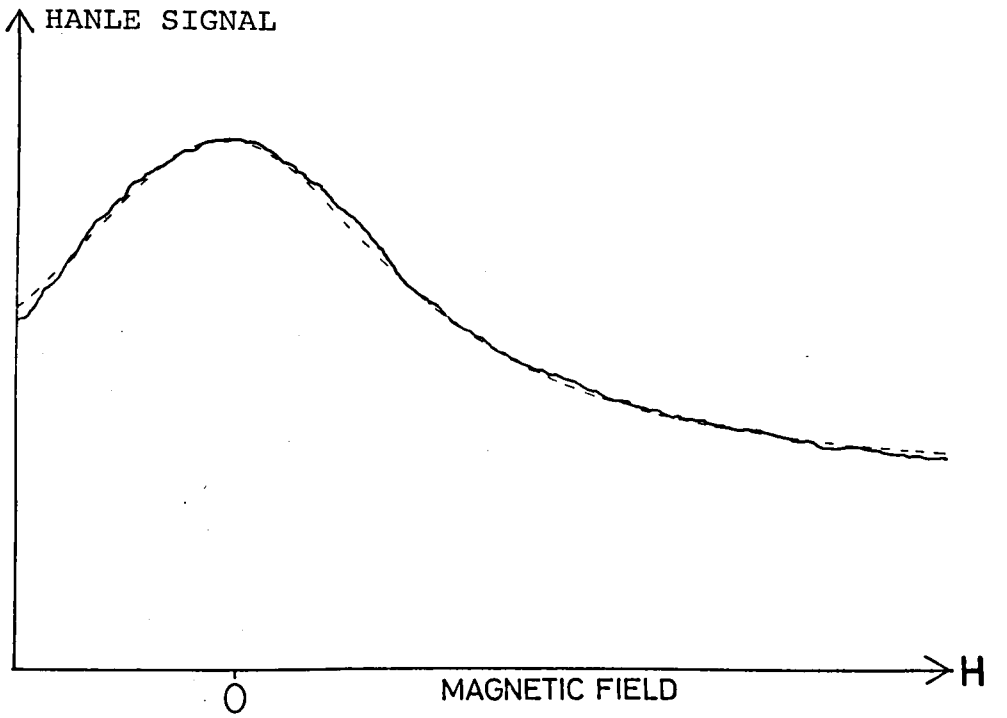

Fig. 4.5 Typical recorder trace of the Hanle signal.

We could obtain similar recorder traces for the cases that the detunings $\Delta\nu$ from the line center were 180, 360, and 540 MHz. For the detuning larger than 540 MHz, we could not obtain the Hanle signal with high signal-to-noise ratio. One of the reasons is that the intensity of the single-mode laser becomes rather weak in such a large detuning region due to the transmission characteristics of the Faraday filter. Furthermore, the excitation rate to the $2p_4$ state is relatively small for such a large detuning, since the velocities of neon atoms in the $1s_5$ state interacting with the single-mode laser light are given by a Maxwellian distribution with the half width of 800 MHz, and as the result the excitation of alignment in the $2p_4$ state becomes ineffective.

The Hanle curves obtained experimentally had the Lorentzian shape as the magnetic field was swept through zero even for the case of the single-mode excitation as expected from the discussion in Sec. IV.2.2. In order to obtain the accurate values of the full-width at half-maximum (FWHM), we made the best fit of the experimental Hanle signal to the Lorentzian function superposed upon a constant offset by using the Levenberg's damped least-squares method[106),107)]. Figure 4.6 shows the dependence of the measured FWHM on the detuning of the single-mode laser frequency. The detuning $\Delta\nu$ is related to the axial emitter velocity v_0 by the relation $\Delta\nu=(\nu/c)v_0$. It can be seen in Fig.4.6 that the width of the Hanle signal is slightly broadened when the detuning is increased. Although our theoretical calculations in Chap. III

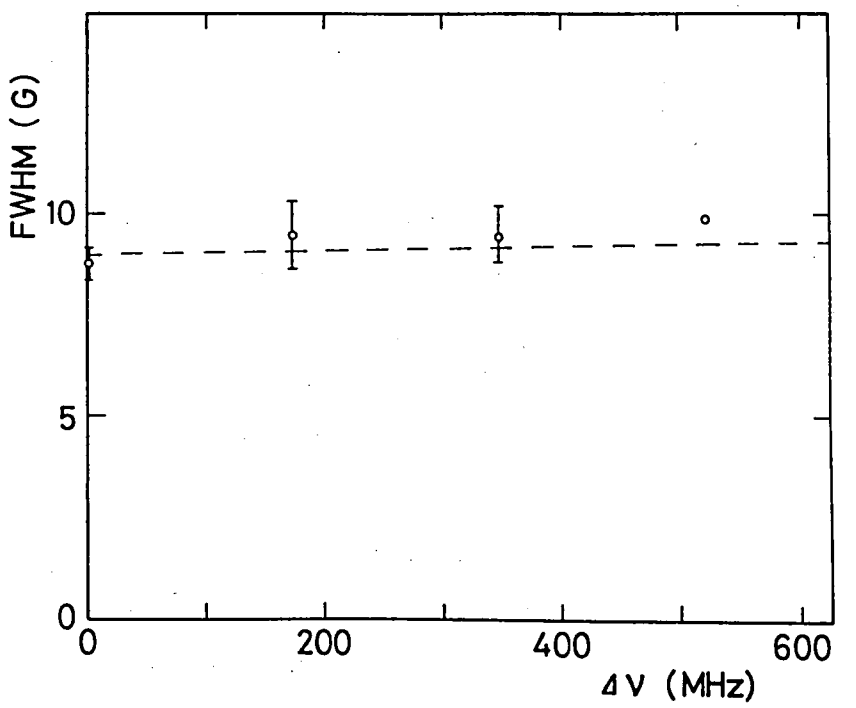

Fig. 4.6 Half-width at half-maximum of the Hanle signal as a function of the detuning of the single-mode laser frequency from the line center.

are made for the excited state with j=1, we shall compare the experimental results for the $2p_4$ state with the theoretical results. The theoretical estimation of FWHM ΔH is made as follows. From Eq.(4.14), the FWHM is given by

$$\Delta H = \frac{2}{g\mu_B}\left\{\frac{\gamma_0^2\gamma_2^2(\gamma_1^1\gamma_1^2+\Gamma^2)}{\gamma_1^1(3\gamma_2^2+\gamma_0^2)}\right\}^{1/2}, \qquad (4.24)$$

where $\gamma_q^k = \gamma_{nat} + \Gamma_q^{kk}$. We adopt the value of the natural decay rate $\gamma_{nat}=5.9\times10^7$ rad/sec for the $2p_4$ state measured by Decomps and Dumont[89),91)], and the g-value g = 1.298 measured by Giacobino-Fournier[108)]. The values of Γ_q^{kk} and Γ is derived from Fig.3.9(b), and the constant factor $(2\pi/5)n_pB^{2/5}\langle v_p^{3/5}\rangle$ is so determined that the calculated value of ΔH for $v_0=0$ coinsides with the experimental FWHM for $\Delta\nu=0$. The obtained value of $(2\pi/5)n_pB^{2/5}\langle v_p^{3/5}\rangle$ is 6.8×10^6 rad/sec. This theoretical width ΔH is also shown in Fig. 4.6 by a dotted curve. As seen in this figure, when the detuning is varied from zero to 500 MHz, the theoretical width increases about 1.5 percent, while the experimental increase of ΔH seems to be a little larger than the theoretical one, though experimental errors are not negligible. The discrepancy between the theoretical and experimental results may be partly due to the fact that the theoretical calculations have been made for the case of j=1 while the experiment has been made for the state with j=2. However, the difference in the dependence of $\Gamma_q^{kk'}$ on detuning between the cases of j=1 and j=2 is thought to be rather small as long as only alignment and orientation are considered.

Another reason for the discrepancy may be due to the ambiguity in the detuning of the laser frequency. We shall make detailed discussions on this point in the next section.

Ⅳ.4 Transfer from Alignment to Orientation

The most remarkable feature of the effect on multipole moments caused by anisotropic collisions is the appearance of transfer between different multipole moments. In this section, we deal with the experiment which was made in order to observe the transfer from alignment to orientation by using the same transitions of neon as described in the previous section. As described in Sec. Ⅳ.2.2, the transfer from alignment to orientation can be observed as the difference in the intensity of left-handed and right-handed circularly polarized fluorescences emitted by atoms excited by a linearly polarized light beam.

Ⅳ.4.1 Experimental Setup

The essential part of the experimental setup is schematically shown in Fig.4.7. The single-mode laser used in this experiment was the same as used in the Hanle experiment described in the previous section. The single-mode output at 594.5 nm with linear polarization along the y direction was applied to the positive column of the glow discharge tube filled with natural neon. In contrast to the experiment described in the previous section,

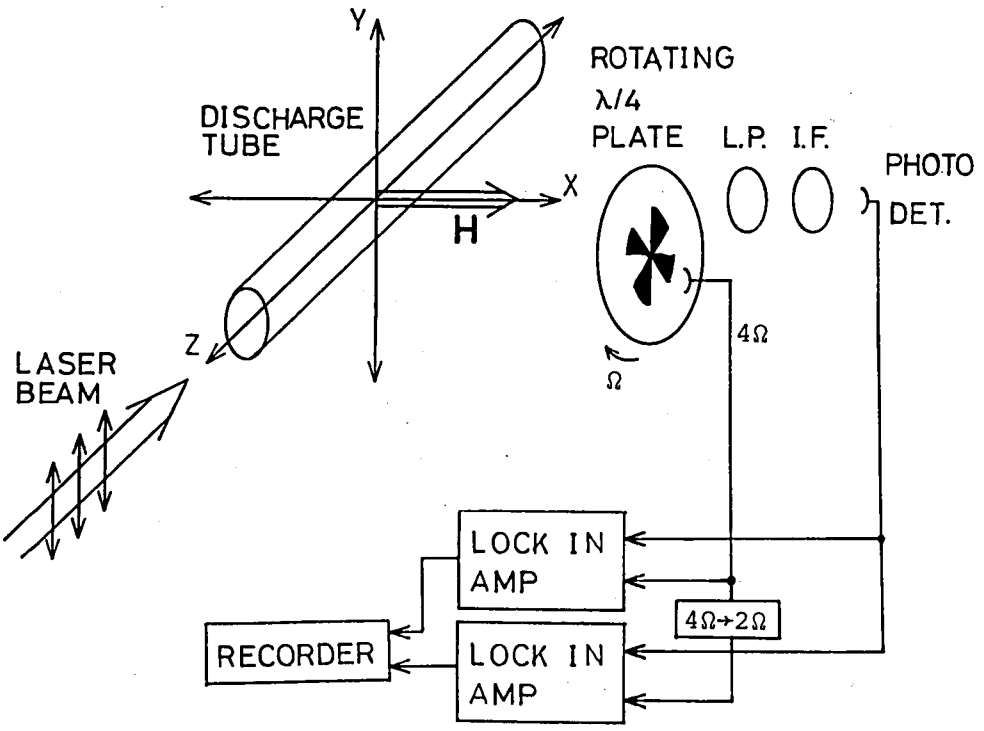

Fig. 4.7 Schematic diagram of the experimental arrangement for simultaneous observations of the transfer from alignment to orientation and the ordinary Hanle effect.

the incident laser beam was not chopped. The pressure of neon was 1.3 Torr, and the discharge current was kept constant at 8 mA.

The static magnetic field $\vec{H}$ was applied in the x direction and swept from -19.3 to +19.3 G through zero in 68 sec. Stray magnetic fields were cancelled out.

We observed the fluorescence emitted to the x direction. In order to analyze the circularly polarized component of the fluorescence which was expected to be much smaller than the linearly polarized component, we used the technique devised by Pavlovic and Laloë[109]. That is, the fluorescence emitted to the x direction was passed through a rotating quarter-wave plate and then through a linear polarizer. When the angular frequency of the rotation of the quarter-wave plate is Ω and the polarization axis of the linear polarizer makes an angle ψ from the z axis, we can obtain Φ_q^k by substituting $\theta=\pi/2$, $\phi=0$ and $\gamma=\Omega t$ into Eq.(4.6)

$$\Phi_0^0 = -\frac{1}{\sqrt{3}}, \quad \Phi_0^1 = 0, \quad \Phi_{\pm1}^1 = \pm\frac{1}{2\sqrt{3}}\sin\eta\sin(2\Omega t-2\psi),$$

$$\Phi_0^2 = \frac{1}{2\sqrt{30}}[1+3\{\cos^2(\eta/2)\cos2\psi+\sin^2(\eta/2)\cos(4\Omega t-2\psi)\}],$$

$$\Phi_{\pm1}^2 = -i\frac{1}{2\sqrt{5}}\{\cos^2(\eta/2)\sin2\psi+\sin^2(\eta/2)\sin(4\Omega t-2\psi)\},$$

$$\Phi_{\pm2}^2 = -\frac{1}{4\sqrt{5}}[1-\{\cos^2(\eta/2)\cos2\psi+\sin^2(\eta/2)\cos(4\Omega t-2\psi)\}], \quad (4.25)$$

where η is the retardation of the quarter-wave plate ($\eta=\pi/2$ for

a perfect quarter-wave plate). It should be noted that the circularly polarized component of the fluorescence from orientation $\rho^1_{\pm 1}$ is modulated at 2Ω after passing through this analyzing system, while the linearly polarized component from alignment is modulated at 4Ω, whether the quarter-wave plate is perfect or not. Therefore, the amplitude of the fluorescence $I_{2\Omega}$ modulated at 2Ω is proportional to the difference $I_{\sigma+}-I_{\sigma-}$:

$$I_{2\Omega} = (I_{\sigma+} - I_{\sigma-})\sin\eta\sin(2\Omega t - 2\psi), \qquad (4.26)$$

where $I_{\sigma+}-I_{\sigma-}$ is given by Eq.(4.13). In particular, when the quarter-wave plate is perfect ($\eta=\pi/2$), the amplitude $I_{2\Omega}$ is exactly equal to the difference $I_{\sigma+}-I_{\sigma-}$. In our experiment, we obtained the orientation signal $I_{\sigma+}-I_{\sigma-}$ by using a lock-in amplifier tuned to the frequency 2Ω. On the other hand, the fluorescence modulated at 4Ω is related to the alignment signal:

$$I_{4\Omega} = I_{4\Omega}(C)\cos(4\Omega-2\psi) + I_{4\Omega}(S)\sin(4\Omega-2\psi), \qquad (4.27)$$

where the quadrature amplitudes are given by

$$I_{4\Omega}(C) = (-1)^{j+j_0} I_0 \begin{Bmatrix} 1 & 1 & 2 \\ j & j & j_0 \end{Bmatrix} \frac{\gamma^1_1\gamma^2_1+\Gamma^2}{2\Delta_1} A\sin^2(\eta/2)$$

$$= \frac{1}{2}(I_{\parallel} - I_{\perp})\sin^2(\eta/2), \qquad (4.28)$$

$$I_{4\Omega}(S) = (-1)^{j+j_0} I_0 \begin{Bmatrix} 1 & 1 & 2 \\ j & j & j_0 \end{Bmatrix} \frac{\gamma^1_1\omega}{\Delta_1} A\sin^2(\eta/2) \qquad (4.29)$$

In partcular, when the quarter-wave plate is perfect, the quadrature amplitude $I_{4\Omega}(C)$ is 1/4 of $I_{\parallel}-I_{\perp}$. In order to compare the orientation signal with the alignment signal (see Sec. IV.2.2), we obtained the alignment signal $I_{4\Omega}(C)$ by using another lock-in amplifier tuned to the frequency 4Ω.

The quarter-wave plate was rotated by a dc moter at about 1200 rpm. The reference signal which should be applied to the lock-in amplifier tuned at 4Ω was obtained by chopping the light beam from an LED which passed through the rotating quarter-wave plate with four shaded portions as seen in Fig.4.7. On the other hand, the reference signal at 2Ω was obtained from the 4Ω signal by passing through a frequency divider. The time constant of both of the lock-in amplifiers were chosen to be 3 sec.

IV.4.2 Experimental Results and Discussions

Using the setup described in Sec.IV.4.1, we observed simultaneously the orientation signal which is due to the transfer from alignment caused by anisotropic collisions and the alignment signal (the ordinary Hanle effect). We show typical recorder traces in Fig. 4.8 obtained for the case that the detuning of the single-mode laser from the line center was 900 MHz. The upper and lower traces show the signals of orientation $I_{\sigma^+}-I_{\sigma^-}$ and alignment $I_{\parallel}-I_{\perp}$, respectively. Since the gain of the detection system for orientation was ten times as large as that for alignment, the upper trace is magnified by 40 tines compared with the

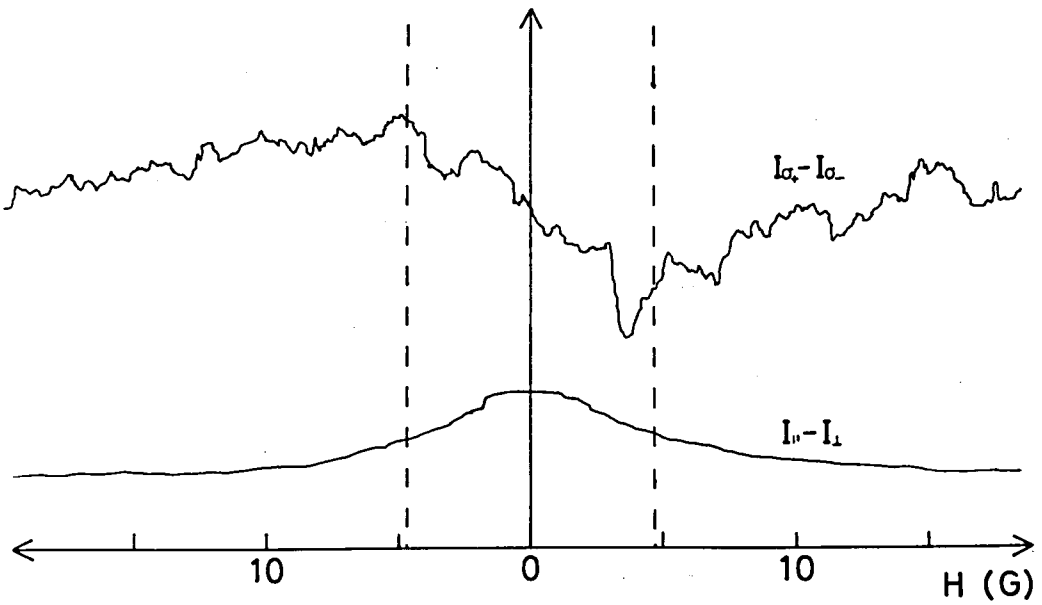

Fig. 4.8 Typical recorder traces for orientation signal $I_{\sigma+} - I_{\sigma-}$ (the upper trace) and alignment signal $I_{\parallel} - I_{\perp}$ (the lower trace). The upper trace is magnified by 40 times as compared with the lower trace.

lower trace as described in Sec. IV.4.1. We could obtain the similar recorder traces for the cases that the detunings from the line center were 360, 540, 720, 900, and 1080 MHz. These detunings correspond to the normalized axial velocities $(m_e/2kT)^{1/2}v_0$ of 0.37, 0.56, 0.75, 0.93, and 1.12, respectively.

In order to ascertain that the dispersion-shaped signal in Fig. 4.8 is not the signal from alignment but that from orientation, we observed the signal by changing the phase of the lock-in amplifier. If the fluorescence $I_{4\Omega}$ is perfectly suppressed by the lock-in amplifier tuned at 2Ω, the output signal of this lock-in amplifier always should have a dispersion shape and only the amplitude should be changed by the change in the phase of the lock-in amplifier [see Eq.(4.26)]. On the other hand, if the alignment signal is not perfectly suppressed, it is possible that the output of the lock-in amplifier tuned at 2Ω shows a dispersion type dependence on the magnetic field H even when anisotropic collisions are not present. If we assume so, the change of the phase by 90° must give rise to the change in the shape of the output signal; from a dispersion shape to a Lorentzian shape [see Eq.(4.27)]. In Fig. 4.9, we show the experimental results for different phases of the lock-in amplifier tuned at 2Ω, in the case that the detuning of the single-mode laser is 360 MHz. We can confirm that the signal from alignment were sufficiently suppressed since no Lorentzian signal is superposed on any traces in Fig. 4.9. From Eqs.(4.26) and (4.27), we see that changing the phase of the lock-in amplifier by 2ψ is equi-

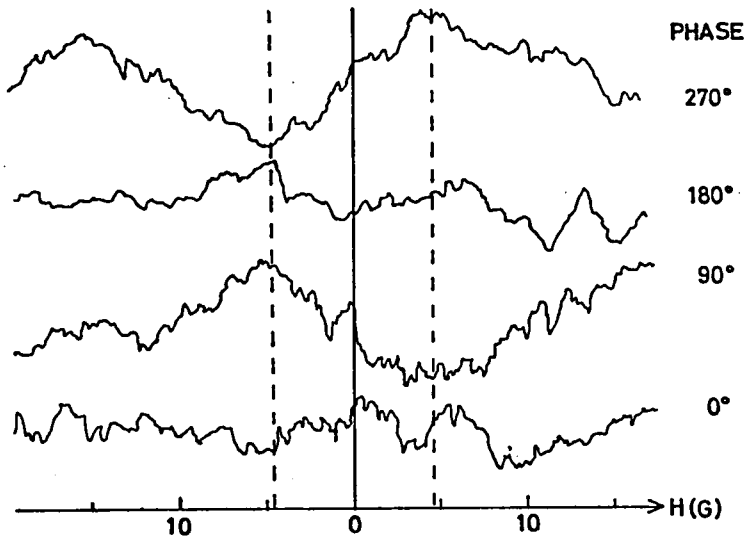

Fig. 4.9 Orientation signals for different values of the phase of the lock-in amplifier.

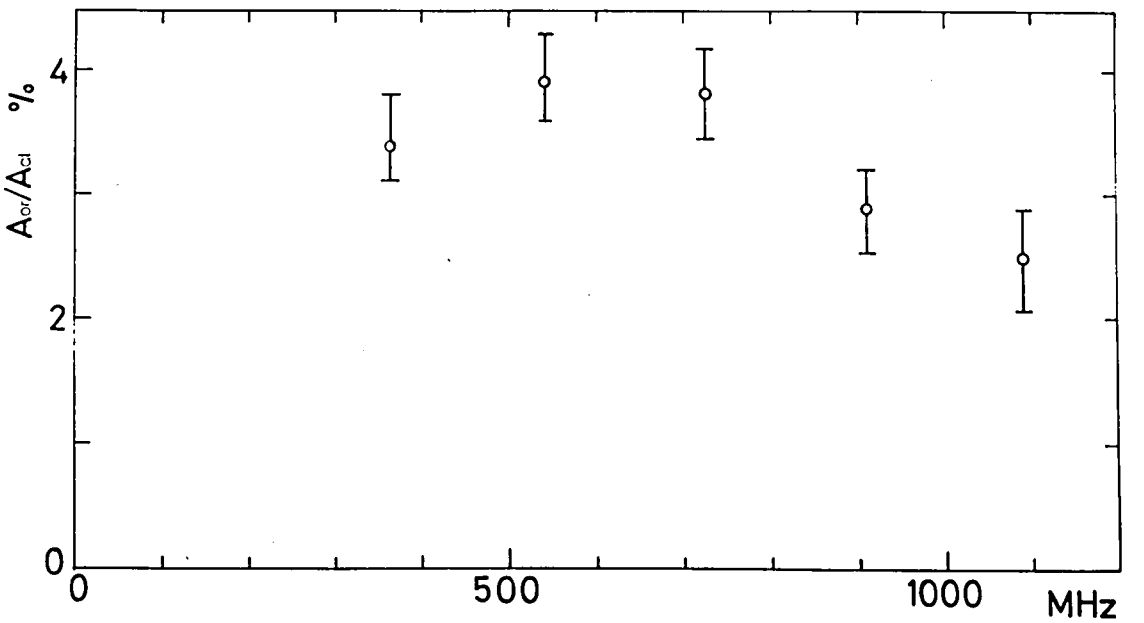

Fig. 4.10 Experimental plots of the ratio A_{or}/A_{al} as a function of the detuning of the frequency of the single-mode laser from the frequency at which the laser began to oscillate.

valent to changing the polarization direction of the linear polarizer placed in front of the photodetectot by the angle ψ. By changing the polarization direction, we could obtain similar recorder traces as in Fig. 4.9. The inhomogeneity of the rotating quarter-wave plate may produce the 2Ω modulation of the alignment signal. However, we can also find in Fig.4.9 that it excerted no serious influence on our experimental results.

From the experimental results shown in Fig. 4.8, we can obtain the ratio A_{or}/A_{al} defined by Eq.(4.17), and this result are shown in Fig. 4.10. In this experiment, the oscillation of the single-mode laser was very unstable, we could not obtain the orientation signals with high signal-to-noise ratio in the range of detuning 0 ~ 300 MHz.

Since the dependence of $\Gamma_q^{kk'}$ for the excited state with j=2 on $(m_e/2kT)^{1/2}v_0$ is considered not to differ largely from that for the excited state with j=1, we will compare the experimental results for the $2p_4$ state of neon (j=2) with the theoretically estimated values of A_{or}/A_{al} for the state with j=1. We have made theoretical estimations of A_{or}/A_{al} by substituting the values of γ_q^k and Γ into Eq.(4.17). In this calculation, we have used the values of $\Gamma_q^{kk'}$ given in Fig. 3.9(b), $\gamma_{nat} = 5.9\times10^7$ rad/sec [91], and $(2\pi/5)n_p B^{2/5}\langle v_p^{3/5}\rangle = 6.8\times10^6$ rad/sec estimated from the Hanle experiment described in the previous section. The factor $\begin{Bmatrix} 1 & 1 & 1 \\ j & j & j_0 \end{Bmatrix} / \begin{Bmatrix} 1 & 1 & 2 \\ j & j & j_0 \end{Bmatrix}$ in Eq.(4.17) has been considered for the actual case that j=2 and j_0=1, and calculated as $(15/7)^{1/2}$. The results of this calculation is shown in Fig. 4.11. This theoretical

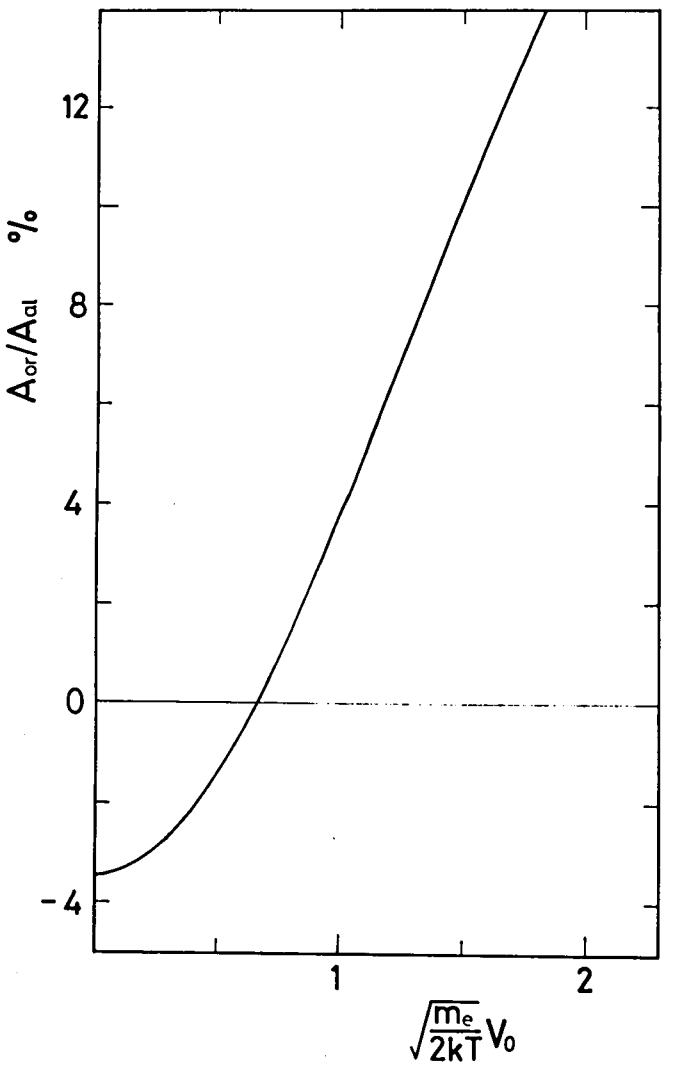

Fig. 4.11 Theoretically calculated ratio A_{or}/A_{al} for the case of pure isotope of neon, as a function of the normalized emitter velocity which is proportional to the detuning of the single-mode laser.

calculations show that the ratio A_{or}/A_{al} increases monotonically with the increase of $\Delta\nu$, while we can see a gentle peak in the experimental results (Fig. 4.10). This discrepancy between the theoretical and experimental results was found to come frome the fact that we did not take the isotope effect into account in our theoretical calculations, although we used natural neon in the experiment.

Natural neon have three stable isotopes (Ne^{20}, Ne^{21}, and Ne^{22}). Since the relative abundance of Ne^{21} (0.257%) is small compared with those of Ne^{20} (90.92%) and Ne^{22} (8.82%), we will neglect the presence of Ne^{21} in the present discussions. The isotope shift between Ne^{20} and Ne^{22} for the transition $1s_5-2p_4$ (594.5 nm) is 1.72 GHz [110]. Due to this isotope shift, velocities of Ne^{22} atoms excited by a single-mode laser are different from those of excited Ne^{20} atoms. The isotope shift of 1.72 GHz corresponds to the difference in the normalized axial velocity $x[=(m_e/2kT)^{1/2}v_0]$ of 1.78 for T = 400 K. Therefore, the effect of anisotropic collisions on Ne^{22} is not the same as that on Ne^{20}, which are excited by the light with the same frequency, so that the relaxation matrix elements $\Gamma_q^{kk'}$ have different values for Ne^{20} and Ne^{22}.

We can estimate the ratio of the orientation signal to the alignment signal using the relation

$$\frac{A_{or}}{A_{al}} = \frac{10A_{or}^{(20)}e^{-y^2} + A_{or}^{(22)}e^{-(y-1.78)^2}}{10A_{al}^{(20)}e^{-y^2} + A_{al}^{(22)}e^{-(y-1.78)^2}} \qquad (4.30a)$$

where $A^{(20)}_{or,al}$ and $A^{(22)}_{or,al}$ are the signal amplitudes defined in Fig. 4.1 for Ne^{20} and Ne^{22}, respectively. The parameter y in Eq.(4.30a) is the quantity, which is proportional to the detuning $\Delta\nu_{20}$ from the center of the absorption line of Ne^{20} :

$$y = c\frac{\Delta\nu_{20}}{\nu}(m_e/2kT)^{1/2} \qquad (4.30b)$$

Using the approximate value of the relative abundance of Ne^{20} and Ne^{22} (Ne^{20}: Ne^{22} = 10 : 1), we can calculate the ratio A_{or}/A_{al} from Eq.(4.30a). The calculated ratio A_{or}/A_{al} is shown in Fig. 4.12 as a function of the detuning from the absorption line center of Ne^{20} (solid curve) together with $A^{(20)}_{or}/A^{(20)}_{al}$ and $A^{(22)}_{or}/A^{(22)}_{al}$ for pure isotopes (two dotted curves). As seen in Fig. 4.12, the presence of Ne^{22} gives a significant influence upon the ratio A_{or}/A_{al} in spite of its small relative abundance, when the laser is tuned around the absorption line center of Ne^{22}. This is due to the large change in the collisional transfer rate Γ as the detuning is increased. On the other hand, since the width of the Hanle signal for pure isotope increases by only a few percent when one detune the laser from the line center of this isotope to that of the other isotope, the width of the Hanle signal is not so drastically affected by the presence of two isotopes as long as the g-factors of these isotopes are the same.

It should be noted that the position of the zero detuning $\Delta\nu$=0 in Fig. 4.10 has been determined to be the frequency at which the shingle-mode dye laser with a Faraday filter began

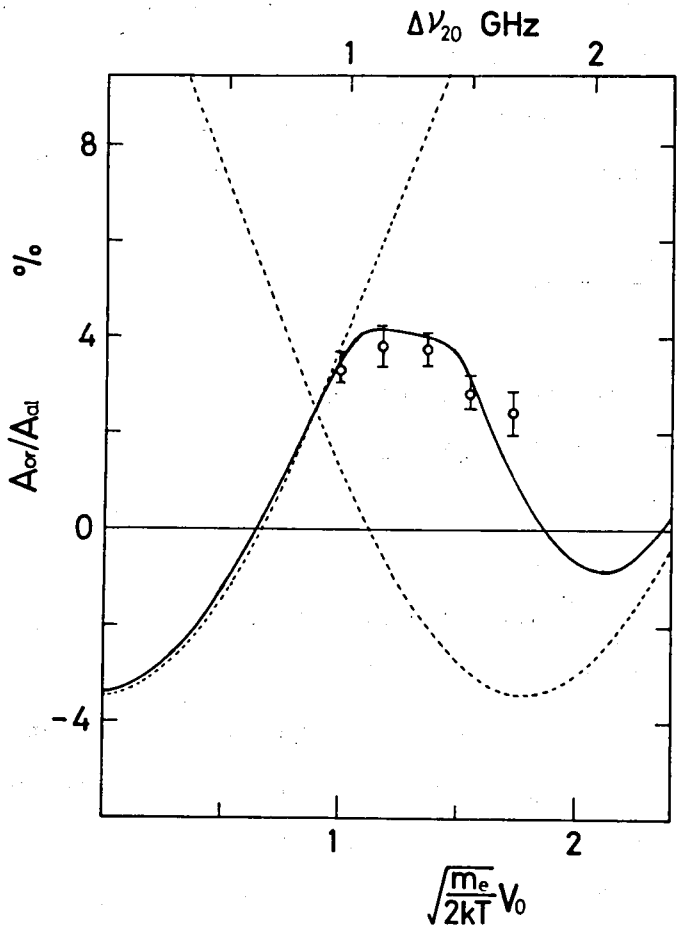

Fig. 4.12 Theoretically calculated ratio A_{or}/A_{al} for the case of natural abundance neon (solid curve), and the ratios for the cases of pure isotopes Ne^{20} and Ne^{22} (two dotted curves), as functions of detuning from the center of the absorption line of Ne^{20}. Experimental plots fitted to the theoretical curve are also shown.

to oscillate when the magnetic field applied to the Faraday filter was increased. Since we used the Faraday filter of natural neon, the single-mode dye laser began to oscillate at the frequency shifted from the center of the Ne^{20} absorption line toward the Ne^{22} absorption line center[104], so that we could not know the absolute detuning from the line center of Ne^{20}. Comparing our experimental result (Fig. 4.10) with the theoretical calculations taking the isotope effect into account (Fig. 4.12), the experimental plots are well fitted to the theoretical curve if we assume that the detunig $\Delta\nu = 0$ in Fig. 4.10 corresponds to the detuning $\Delta\nu_{20} = 600$ MHz from the line center of Ne^{20}. Thus corrected plots are also shown in Fig. 4.12. In this figure, we can see a fairly good agreement between theory and experiment which have been made for emitters with j=1 and j=2, respectively, in spite of the difference in the value of j. This might indicate the fact that the dependence of the collisional relaxation matrix $\Gamma_q^{kk'}$ on v_0 is not so dependent on the values of the total angular momentum j of the emitter.

So far, we have assumed that the velocity distribution of the emitters along the direction of the laser beam is a delta function. However, as a matter of fact, the velocity distribution must be given by a Lorentzian function, whose width is determined by the decay rate of the optical coherence and the saturation of the exciting transition. In the case of the weak laser intensity, the full width of the velocity distribution of emitters is given by $c\gamma_{ab}/(\pi\nu)$ where γ_{ab} is the decay rate of

the optical coherence between the $2p_4$ state and the $1s_5$ state. At the low pressure limit, γ_{ab} is $(\gamma_a+\gamma_b)/2$ where γ_a and γ_b are the decay rates of the $2p_4$ and the $1s_5$ states ($\gamma_a \sim 10^6$ Hz, $\gamma_b \sim 10^4$ Hz [111]). But, at the gas pressure in the present experiment, the optical coherence is more strongly destroyed by the dephasing collisions compared with the population. The pressure dependence of γ_{ab} for the $1s_5$–$2p_4$ transition has not been reported as yet. However, there have been many experimental results on laser transitions of He-Ne laser[112),113),114)]. If we assume that the collisional decay of optical coherence is not so different for these transitions, γ_{ab} is roughly estimated to be ~100 MHz. Moreover, the optical saturation further broadens the velocity distribution of emitters. Then, the observed A_{or} and A_{al} are considered to be the average values over the broadened velocity distribution. In fact, as seen in Fig. 4.12, the experimentally obtained dependence of A_{or}/A_{al} upon the detuning is somewhat gentle compared with the theoretical results.

IV.5 Transfer from Orientation to Alignment

In this section, we report on the experimental evidence of the transfer from orientation to alignment, which is the inverse of the process discussed in the previous section. The experiment proposed in Sec. IV.2.3 was carried out for the same transitions of neon as in the previous section. Namely, a circularly

polarized single-mode laser beam was used to excite neon atoms from the $1s_5$ state to the $2p_4$ state, and the fluorescence originating from the $2p_4$ state at 609.6 nm was observed. The existence of this transfer in the $2p_4$ state can be monitored by detecting the change in the intensity of linearly polarized fluorescence when one change the sense of circular polarization of the exciting laser beam.

IV.5.1 Experimental Setup

The essential part of the experimental setup is schematically shown in Fig. 4.13. We used the same single-mode dye laser operating at 594.5 nm, discharge tube , and Helmholtz coils as those used in the previous experiment. The discharge tube was filled with natural neon at 1.3 Torr, and the discharge current was kept constant at 8 mA. As shown in Fig. 4.13, the laser beam was applied into the discharge tube along the z direction, the static magnetic field was applied in the x direction, and the fluorescence emitted in the y direction was observed.

In order to create the orientation along the z direction, the incident laser beam, which was linearly polarized along the y direction, was passed through a rotating quarter-wave plate. This rotating quarter-wave plate changes periodically the sense of circular polarization of the exciting light. In the present case, we can obtain Φ_q^k for the excitation by substituting $\theta = \phi = 0$, $\psi = \pi/2$, and $\gamma = \Omega t$ into Eqs.(4.6) and (4.7) :

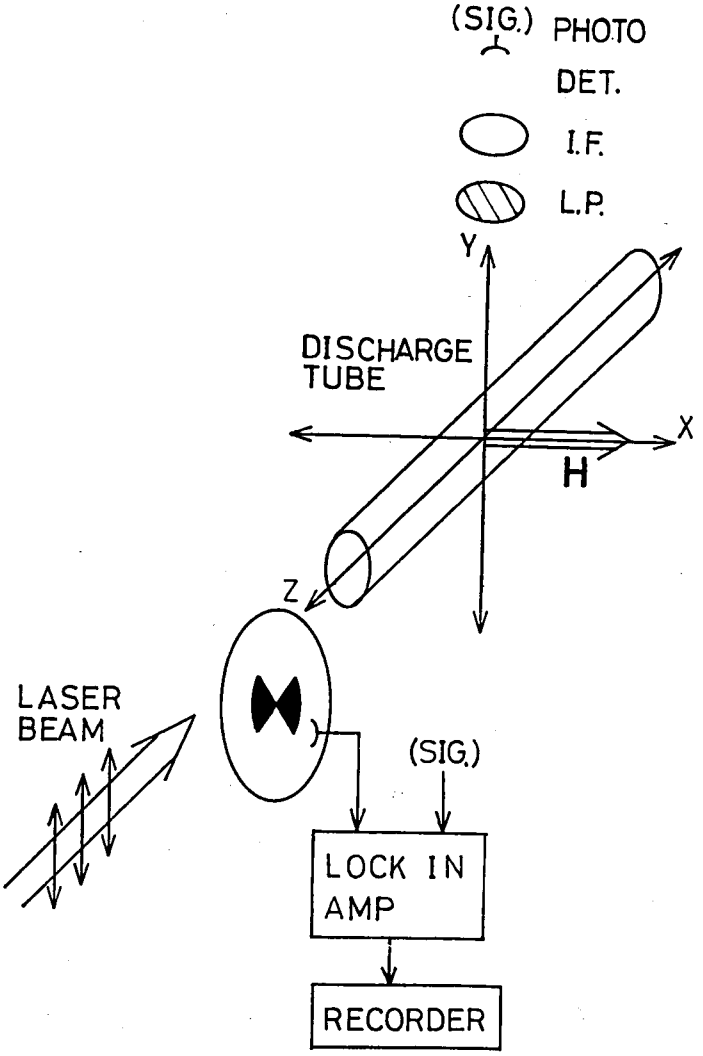

Fig. 4.13 Schematic diagram of the experimental arrangement for the observation of the transfer from alignment to orientation

$$\Phi_0^0 = -\frac{1}{\sqrt{3}} , \quad \Phi_0^1 = \frac{1}{\sqrt{6}}\sin\eta\sin 2\Omega t , \quad \Phi_{\pm 1}^1 = 0 , \quad \Phi_0^2 = -\frac{1}{\sqrt{30}} ,$$

$$\Phi_{\pm 1}^2 = 0 , \quad \Phi_{\pm 2}^2 = -\frac{1}{2\sqrt{5}}\{\cos^2(\eta/2) + \sin^2(\eta/2)e^{\pm i4\Omega t}\} , \tag{4.31}$$

where Ω is the angular frequency of the rotating quarter-wave plate and η is its phase retardation ($\eta=\pi/2$ for the perfect quarter-wave plate). From Eq.(4.31) and Eq.(2.23b), we see that only the excitation of the longitudinal orientation F_0^1 are modulated at 2Ω, while that of the alignment $F_{\pm 2}^2$ is modulated at 4Ω.

We observed the fluorescence linearly polarized in the direction with the polar angles $(\pi/4,0)$ or $(-\pi/4,0)$ by a silicon solar cell. This linearly polarized fluorescence consists of the signal from the alignment directly excited by the laser light and that from the alignment transferred from the orientation by anisotropic collisions, the former and the latter being modulated at 4Ω and 2Ω, respectively. Therefore, we obtained the signal of alignment transferred from orientation, by applying the output of the solar cell to a lock-in amplifier tuned at 2Ω. In contrast to the experiment described in Sec. IV.4, to modulate the incident laser beam has the advantages in reduction of the noise originating from the discharge.

The static magnetic field $\vec{H}$ was swept from -19.3 to +19.3 G in 68 sec, and the time constant of the lock-in amplifier was chosen to be 3 sec. The quarter-wave plate was rotated at about

1200 rpm.

IV.5.2 Experimental Results and Discussions

Using the setup described in IV.5.1, we observed the signal of alignment transferred from initially excited orientation. Typical recorder traces are shown in Fig. 4.14. The upper and the lower traces were obtained for fluorescence linearly polarized along the directions with the polar angles $(\pi/4,0)$ and $(-\pi/4,0)$, respectively. The signal-to-noise ratios of the obtained traces were not high due to the fluctuation in the intensity of the incident laser light, so that we could not make a quantitative comparison with theoretical results. However, can see in Fig. 4.14 that the experimental signals have the magnetic field dependence as expected from the theory [see Eq.(4.23)]. The polarity of the upper trace is the reverse of that of the lower trace because the directions of linear polarizations of the observed fluorescence for the upper and lower traces are perpendicular with each other.

As descrived in IV.5.1, only the signal of alignment, which is transferred from the initially excited orientation, is modulated at 2Ω, while the ordinary alignment signal (the Hanle signal of alignment) is modulated at 4Ω. Since the lock-in amplifier tuned at 2Ω eliminates highly the modulation at 4Ω, we can conclude that the signals obtained in the present experiment show the existence of the alignment transferred from the

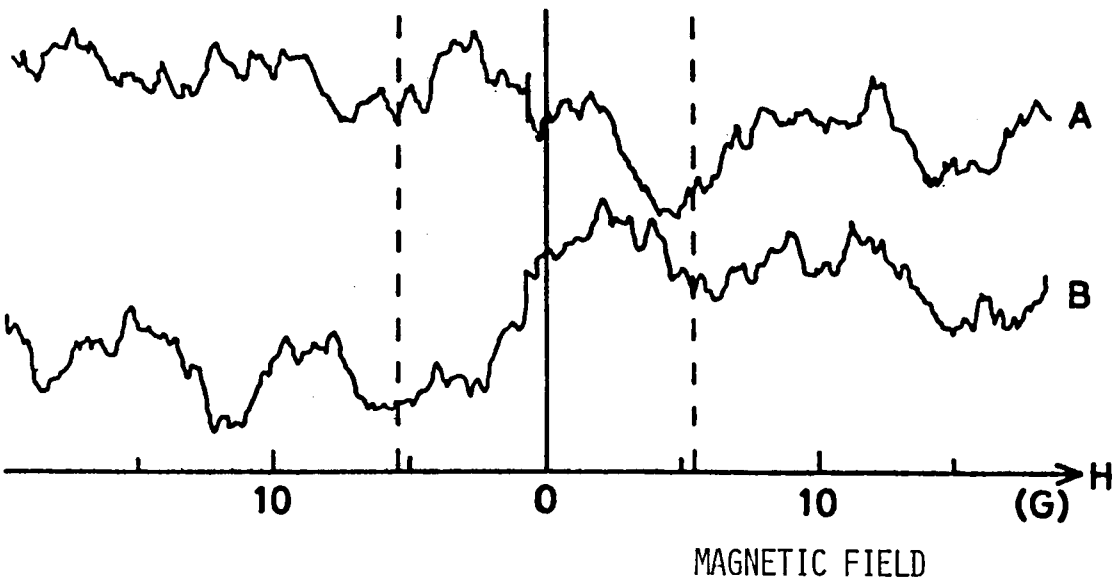

Fig. 4.14 Typical recorder traces of alignment signals for excitation with the linearly polarized single-mode laser beam.

initially excited orientation under the influence of anisotropic collisions.

IV.6 Discussion and Conclusions

In this chapter, we have investigated the effects of anisotropic collisions on emitter atoms excited by a single-mode laser light. We have analyzed the magnetic depolarization in the excited state with j=1 taking account of the splittings in different diagonal elements of the collisional relaxation matrix and the collisional transfer between alignment and orientation. It should be noted that anisotropic collisions give rise to some peculiar features in the magnetic depolarization signals : (i) the modification of the width of the Hanle signal; (ii) the difference in the intensity between the right- and left-handed circularly polarized fluorescences emitted by the atoms excited by linearly polarized light; (iii) the variation of the intensity of linearly polarized fluorescence by the change of the sense of circularly polarized excitation.

In order to verify our theory of anisotropic collisions, we have made defferent experiments of magnetic depolarizations of the $2p_4$ state of neon excited by a single-mode laser. Although the theoretical calculations in Chap. III have been made for the excited state with j=1, we compared the experimental results for the $2p_4$ state (j=2) with the theory, with respect

to (i) and (ii). We have found that the width of the Hanle signal is slightly broadened when the detuning of the single-mode laser is increased. The existence of the transfer from alignment to orientation has been experimentally verified from the observed magnetic field dependence of the orientation signal. The anomalous dependence of A_{or}/A_{al} on the detuning has been successfully explained by taking the isotope effect into account. It should be noted that the presence of different isotope gives rise to an important effect on the transfer between alignment and orientation, while it gives rise to only a little effect on the width of the Hanle signal. Despite of the difference in the total angular momentum j, we have found a fairly good agreement with the theoretical A_{or}/A_{al}. This ratio amounts to about 4% in our experimental region of the detuning.

We have also observed the signal ΔI of the alignment transferred from orientation [case (iii)], and the existence of the transfer has been qualitatively verified. Since the signal-to-noise ratio was not so high in this experiment, we could not compare the experimental results with theory.

As seen in Fig. 3.9(b) or Fig. 4.12, when the laser frequency is detuned from the line center of Ne^{20}, the collisional transfer rates $\Gamma_{\pm 1}^{12}$ and $\Gamma_{\pm 1}^{21}$ begin to decrease, and at a detuning where the z component of normalized emitter velocity $(m_e/2kT)v_0$ is 0.6~0.7, the transfers disappear. When the detuning is increased further, the transfer rates increase, with the sign opposite to those for the small detuning case. This change of the sign should appear

as the change of the sign of the orientation signal in the case (ii), and as that of ΔI in the case (iii). However, we could not observe this change of sign, because we could not get the stable operation of the Faraday filter when the detuning of the laser frequency from the line center of Ne^{20} is less than 780 MHz $[(m_e/2kT)^{1/2}v_0 \sim 0.8]$.

All experiments described in this chapter have been made using a neon discharge tube without any foreign gas, so that all collisions occur between atoms of same species, i.e., $m_p/(m_p+m_e)=0.5$. Therefore, the effects of anisotropic collisions are not so large. As mentioned in Sec. III.4.2, the effects of anisotropic collisions become more remarkable when perturbers are heavier than emitters. In order to make the anisotropy larger, we have intended to carry out experiments using the discharge tube filled mixture of neon (emitter) and krypton (perturber) $[m_p/(m_p+m_e) \simeq 0.8]$. However, we could not observe the fluorescence emitted from the $2p_4$ state of neon with high signal-to-noise ratio, so that we could not investigate the effects of anisotropic collisions. As the reason, we think that the $2p_4$ state cannot be sufficiently populated by the laser light, because the metastable $1s_5$ state is quenched by collisions with krypton atoms in their ground state. [The ionization potential of krypton is 14.0 eV, which is less than the energy of the $1s_5$ state (16.6 eV).]

In order to avoid this difficulty in observing the large effects of anisotropic collisions of laser excited atoms, we

should make an experiment for the first excited P state of alkali-metal atoms perturbed by heavier rare-gas atoms.

CHAPTER V

ALIGNMENT DESTROYING CROSS SECTIONS OF NEON FOR COLLISIONS WITH RARE-GAS ATOMS

V.1 Introduction

Many experimental works have been made for these fifteen years on the mixing of Zeeman substates in the excited states of gaseos atoms by collisions with rare-gas atoms. In the experiments on alkali atoms in the first excited P states[25)-29)] and neon atoms in the 2p states[23),34),35)], it has been shown that the measured cross sections for destruction of alignment are anomalously large for collisions with helium atoms and disagree with theories[19),22)] which explain well the cross sections for collisions with other rare gases. In these theories, the same assumptions and approximations as descibed in Chap. III are used for the case of isotropic collisions. As the cause of this discrepancy for collisions with helium, it has been considered that the short-range interactions are important rater than the van der Waals interaction, because of the small polarizability of helium atom (~0.2 Å). This explanation is now widely accepted for alkali-helium collisions.

In this chapter, we investigate the alignment destroying cross sections for neon atoms in the $2p_4$ state colliding with helium, neon, argon, and krypton atoms in their ground states.

It might be expected that He^3 is better than He^4 to make clear the importance of the short-range interaction in the Ne-He collisions. Furthermore, the comparison of cross sections for He^3 and He^4 may give us more informations, because the collisional interaction is approximately the same for these two isotopes except for their masses. However, there have been few measurements of the cross section for Ne-He^3 collisions, although the discrepancy has been found between the measured cross section for Ne-He^4 collisions and the theoretical one calculated with the van der Waals interaction.

Measurements of these cross sections were performed by means of the optical-rf double resonance of a He-Ne laser. The use of double-resonance phenomena in optical-pumping experiments was first proposed by Brossel and Kastler[8], and the first experiment was made by Brossel and Bitter[9] for mercury vapor. In their experiment, the mercury atoms were optically pumped to the $^3P_1$ state, and the magnetic resonance in this state was monitored by detecting the intensity change of the spontaneous emission. On the other hand, Bell and Bloom observed the magnetic resonance in the ground state through the absorption of light[115]. An extensive theoretical treatment of double-resonance phenomena was made by Dodd and Series[116], who showed how the magnetic resonance in the excited state with j=1 appears in the intensity change and the modulation of the spontaneous emission. Culshaw extended their theory of double resonance to the atoms in a gaseous laser[117),118),119]. The double resonance in a gaseous

enables us to observe the magnetic resonance in the excited states which cannot be optically pumped directly from the ground state. Observations of the double resonance in the He-Ne laser have been performed by detecting the intensity change of the laser output at 1.15 μm[120),121)], 1.52 μm [122)], and 632.8 nm [36),123)], and of the spontaneous emissions from the laser levels[124)].

In this chapter, we deal with the double-resonance phenomena appearing as an intensity change of the output of a He-Ne laser operating at the transitions from the $3s_2$ state (J=1) to the $2p_4$ state (J=2), occurring at 632.8 nm. The alignment destroying cross sections of neon in the $2p_4$ state can be measured from the pressure broadening of the magnetic resonance line.

V.2 Theory of Double Resonance in He-Ne Laser

V.2.1 Principles of Double-Resonance Experiment of He-Ne Laser

In a double-resonance experiment, atoms are subjected simultaneously to optical and rf radiations, both of which are nearly resonant with optical and Zeeman transitions of atoms. The magnetic resonance signals are generally more complicated than the typical Hanle signals, because the interaction between atoms and magnetic field is no longer time independent. Furthermore, in the double resonance for atoms in a gaseous laser, the resonance signals become much complicated due to the saturation phenomena occurring in laser transitions.

The double resonance in a He-Ne laser can be phenomeno-

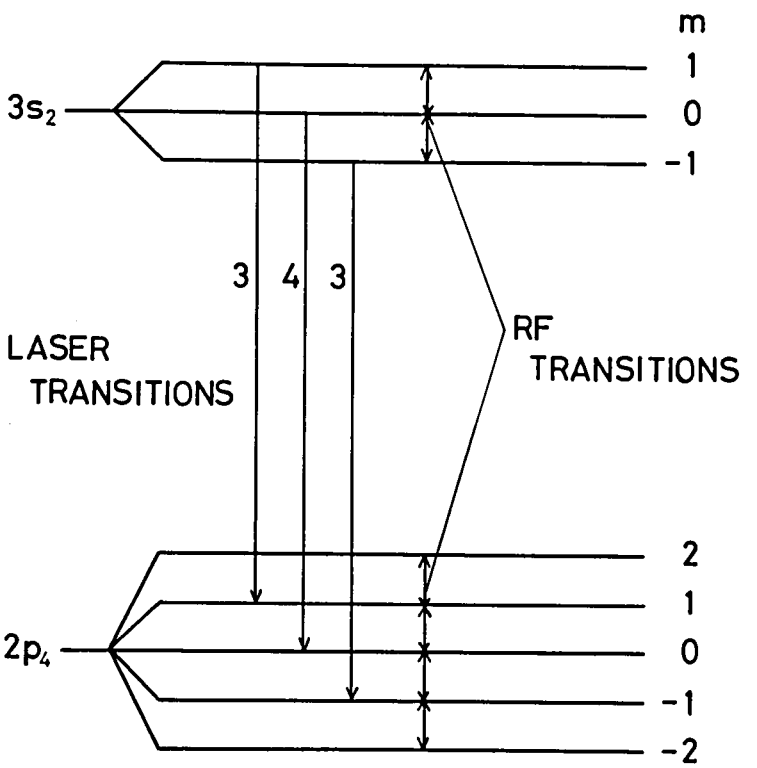

Fig. 5.1 Schematic energy level diagram of neon, associated with the rf transitions and the π-transitions of the He-Ne laser operating at 632.8 nm.

logically explained as follows. In the case of a He-Ne laser operating at 632.8 nm, the transition occurs between the $3s_2$ state (J=1) and the $2p_4$ state (J=2) of neon. The energy diagram is schematically shown in Fig. 5.1, taking account of the Zeeman splittings of laser levels due to a static magnetic field. When the laser light is linearly polarized in the direction parallel to the applied magnetic field (this direction is chosen to be the quantization axis), only the three π-transitions (Δm=0) occur as seen in Fig. 5.1. The transition probability for a π-transition (J=1 – J=2) connecting the Zeeman substates with magnetic quantum number m is given by[125)]

$$P(m,m) \propto |<1\ 1\ m\ 0 \mid 2\ m>|^2 = \frac{1}{6}(4 - m^2), \qquad (5.1)$$

Where $<j\ j'\ m\ m' \mid j''\ m''>$ is the Clebsch-Gordan coefficient. Accordingly, the relative transition probabilities for these three π-transitions can be written as

$$P(1,1) : P(0,0) : P(-1,-1) = 3 : 4 : 3. \qquad (5.2)$$

Due to these difference in the transition probability, the Zeeman substates of each laser level which is isotropically excited by discharge (i.e., the all Zeeman substates are equally populated), are populated differently by the laser π-transitions. This results in the population difference within each Zeeman multimultiplet. However, the substates $|m>$ and $|-m>$ are equally populated, so that the longitudinal alignment ρ_0^2 is created in

each laser level, while no orientation is created. On the other hand, a resonant magnetic field, which is oscillating in the plane perpendicular to the direction of the static magnetic field, induces transition between adjacent Zeeman substates so as to make smooth the population difference. As the result, the alignment created by laser transitions is destroyed by this magnetic resonance. This change of the alignment of each laser levels should be reflected in the change of the output intensity of the laser, because the intensity of the linearly polarized laser light depends not only on the population ρ_0^0 but also on the alignment ρ_0^2 of each laser level. It is the alignment ρ_0^2 that shows the resonant behavior when one varies the frequency of the rf field, or the Zeeman frequency by varying the strength of the static magnetic field. Therefore, informations about the relaxation of alignment can be obtained from the magnetic resonance signal manifested in the intensity change of the laser output. It is possible to extract the collisional contribution from the magnetic resonance signal by changing the partial gas pressure of perturber atoms in the laser tube.

In the next section, we shall analyze the magnetic resonance of alignment in a excited multiplet on the basis of irreducible representation. The result might be applicable to the double-resonance experiment in a gaseous laser. However, in the case of a He-Ne laser operating at 632.8 nm, the magnetic resonance in both laser levels are expected to occur simultaneously, because the g-factors of the $3s_2$ and $2p_4$ states are known to be close

to each other. Recently, Giacobino-Fournier has made quite accurate measurement of the g-factors of these states by observing the fluorescences emitted from these laser levels in double resonance experiments, and has obtained 1.2925 for the $3s_2$ state and 1.298 for the $2p_4$ state[108]. In Sec. V.2.3, we shall solve the rate equations for the π-transitions at 632.8 nm taking account of the interactions with magnetic fiels, and we show which magnetic resonance has dominant effect on the output of the laser.

V.2.2 Magnetic Resonance in a Laser Level

As mentioned in Chap. II , behaviors of multipole moments under the influence of external magnetic field can be well described by the master equation of the density matrix given by Eq.(2.16). Here we apply this equation to the upper or lower levels of a laser transition which are perturbed by an rf magnetic field. Linearly polarized laser light plays a role of pumping light as in the usual optical-pumping experiments. However, when the laser light is intense enough to change the populations of the upper and lower levels appreciably, the nonlinear effects with respect to the light intensity become important, so that the effects of the laser light might not be represented by a simple pumping term F_q^k as in Eq.(2.16). Then the coupled equations for density matrices of the upper and lower states and the optical coherence between these states should be solved

simultaneously. Nevertheless, as long as the magnetic field dependence of the laser intensity is considered , the resonant behavior appearing in the laser output is expected to be determined mainly by the resonant behaviors of alignments created by laser light in the upper and lower multiplets. In order to elucidate the magnetic resonance in each laser level, we will solve the master equation for each multiplet separately.

Consider the case that the static magnetic field $\vec{H}$ parallel to the electric field of the laser light is directed along the z axis (i.e. the quantization axis) and the rf magnetic field $\vec{H}_{rf}$ is rotating in the x-y plane at the angular frequency ω as seen in Fig. 5.2. Then the three standard components of the static and rf magnetic fields defined by Eq.(2.18) are given by

$$H_1 = -\frac{1}{\sqrt{2}} H_{rf} e^{i\omega t}, \quad H_0 = H , \quad H_{-1} = \frac{1}{\sqrt{2}} H_{rf} e^{-i\omega t}, \tag{5.3}$$

By substituting these three standard components into Eq.(2.17), the master equation for the density matrix can be written in the irreducible representation as follows :

$$\frac{d\rho_q^k}{dt} = -iq\omega_0 \rho_q^k - i\frac{\omega_1}{2}\{\sqrt{k(k+1)-q(q+1)}\, e^{i\omega t}\rho_{q+1}^k + \sqrt{k(k+1)-q(q-1)}\, e^{-i\omega t}\rho_{q-1}^k\} + \left(\frac{d\rho_q^k}{dt}\right)_{rel} + F_q^k , \tag{5.4}$$

where the first term in the right-hand side represents the interaction with the static magnetic field ($\omega_0 = g\mu_B H$) and the second

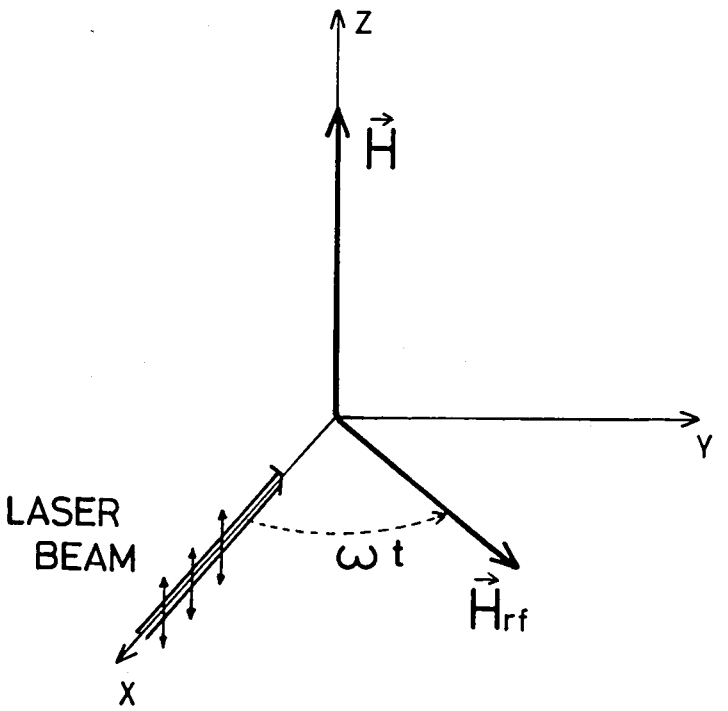

Fig. 5.2 Spatial arrangement of the orientations of the static and rotating magnetic fields, and the polarization of the laser light for the double resonance.

term describes the interaction with the rf magnetic field ($\omega_1 = g\mu_B H_{rf}$).

In contrast to the discussions in the preceding chapters, we here consider the case of the gaseous laser operating with multi-axial modes of the cavity. In the present experiments, since the separation between the output and end mirrors was about 100 cm, there are about ten axial modes within the Doppler width. Accordingly, the average collisional effects on the atoms interacting with the laser light can be approximately assumed to be isotropic. As a result, the collisional relaxation matrix $\Gamma^{kk'}_{qq'}$ is diagonal with respect to k and q, and is dependent only on the value of k, so that the third term in the right-hand side of Eq. (5.4) can be written as

$$\left(\frac{d\rho^k_q}{dt}\right)_{rel} = - \gamma_k \rho^k_q \qquad (5.5)$$

where the relaxation rate γ_k is given by

$$\gamma_k = \gamma_{nat} + \Gamma^{kk}_{qq} \, . \qquad (5.6)$$

As mentioned in the previous section, the laser light linearly polarized in the z direction creates no other than the population ρ^0_0 and the longitudinal alignment ρ^2_2, so that the non-vanishing pumping terms in the right-hand side of Eq.(5.4) are F^0_0 and F^2_0.

As seen in Eq.(5.4), the master equation is time-dependent

in the laboratory frame, but it becomes time-independent in a rotating frame in which the magnetic field $\vec{H}_{rf}$ is fixed in the x direction. In this rotating frame , the density matrix ρ_q^k is transformed into $\bar{\rho}_q^k$ according to the relation given by Eq.(2.10) :

$$\rho_q^k = \bar{\rho}_q^k \, e^{-iq\omega t}, \tag{5.7}$$

while the relaxation term and the pumping term F_0^2 remain invariant. It should be noted that, in this rotating frame, the total magnetic field becomes an effective magnetic field given by $\{(\omega_0-\omega)/\omega_0\}\vec{H}+\vec{H}_{rf}$, around which the alignment $\bar{\rho}_q^2$ precesses, as in the conventional theory of magnetic resonance (see, for instance, Ref. 126). Hence we can obtain the secular solutions ρ_q^k in the laboratory frame :

$$\rho_0^0 = F_0^0/\gamma_0 \ , \qquad \rho_1^1 = 0 \ , \qquad \rho_0^2 = \frac{F_0^2}{\gamma_2}\left\{ 1 - \frac{3\omega_1{}^2(4\delta^2+\gamma_2{}^2+\omega_1{}^2)}{D} \right\},$$

$$\rho_{\pm 1}^2 = -\sqrt{3/2}\,\frac{F_0^2}{\gamma_2}\,\frac{(2\delta \pm i\gamma_2)\{(\delta \mp i\gamma_2)(2\delta \mp i\gamma_2) - \omega_1{}^2\}}{D}\,\omega_1\, e^{\mp i\omega t},$$

$$\rho_{\pm 2}^2 = \sqrt{3/2}\,\frac{F_0^2}{\gamma_2}\,\frac{(\delta \mp i\gamma_2)(2\delta \mp i\gamma_2) - \omega_1{}^2}{D}\,\omega_1{}^2 e^{\mp i2\omega t} \ , \tag{5.8}$$

where

$$D = (\delta^2 + \gamma_2{}^2 + \omega_1{}^2)(4\delta^2 + \gamma_2{}^2 + 4\omega_1{}^2) \ ,$$

and $\delta=\omega-\omega_0$.

The magnetic field dependence of the longitudinal alignment ρ_0^2, which is time-independent, is reflected in the intensity change of the laser light. If the rf magnetic field H_{rf} is weak enough such that $\omega_1{}^2 \ll \gamma_2{}^2$, the magnetic field dependence becomes a Lorentzian function :

$$\rho_0^2 = \frac{F_0^2}{\gamma_2}\left\{ 1 - \frac{3\omega_1{}^2}{(\omega - \omega_0)^2 + \gamma_2{}^2} \right\}, \tag{5.9}$$

For a moderate value of ω_1, the resonance signal is no longer given by the Lorentzian function, but the half-width at half-maximum $\Delta\omega$ can be approximately calculated by using Eq.(5.8) as

$$\Delta\omega^2 = \gamma_2{}^2 + \frac{29}{5}\,\omega_1{}^2. \tag{5.10}$$

The first term in the right-hand side of Eq.(5.10) is the broadening due to the spontaneous and collisional relaxations, i.e,

$$\gamma_2 = \gamma_{nat} + n_p \langle v \rangle \sigma^{(2)}, \tag{5.11}$$

where n_p is the perturber density, $\langle v \rangle$ is the average relative velocity of colliding pair, and $\sigma^{(2)}$ is the cross section for isotropic alignment-destroying collisions. The second term in the right-hand side of Eq. (5.10) represents the power broadening due to the rf magnetic field. When $\Delta\omega$ is extrapolated to vanishing rf magnetic field strength, the half-width at half-

maximum becomes

$$\Delta\omega = \gamma_{nat} + n_p \langle v \rangle \sigma^{(2)} . \qquad (5.12)$$

Since the solutions given by Eq.(5.8) or (5.9) hold good for the Zeeman multiplet with an arbitrary total angular momentum J, both of the $3s_2$ state (J=1) and the $2p_4$ state (J=2) show the similar resonances with different widths and amplitudes. In the case of the double resonance of the He-Ne laser operating at 632.8 nm, these two resonances appear simultaneously in the change of the laser intensity at nearly the same resonance frequencies.

V.2.3 Double Resonance in a He-Ne Laser Operating at 632.8 nm

As mentioned in the previous section, the double-resonance signal in the He-Ne laser operating at 632.8 nm consists of the contributions from the upper laser level $3s_2$ (J=1) and the lower laser level $2p_4$, with approximately the same resonance frequency. In this section, we investigate which resonance of these two has a predominant contribution to the laser output. These contributions of the magnetic resonances to the laser intensity are estimated by solving the rate equation for the laser transitions combined with the results of Lamb's semiclassical laser theory[127), 128)].

Consider the same arrangement of the laser light and magnetic

fields as seen in Fig 5.2. We assume that both laser levels have approximately equal g-factors. For the sake of simplicity, the relaxation of each Zeeman substate is assumed to be characterized by a decay rate γ_a or γ_b for the $3s_2$ or $2p_4$ state, respectively. Furthermore, we assume that the discharge is isotropic, so that the excitation rate to each Zeeman substate is characterized by Λ_a and Λ_b for the $3s_2$ or $2p_4$ state, respectively. All transition rates for optical and Zeeman transitions necessary for the present calculations are shown in the energy diagram Fig. 5.3.

The rate equations for the populations of Zeeman substates can be written as

$$\begin{aligned}
\dot{n}_0^a &= -\gamma_a n_0^a + W_a(n_1^a+n_{-1}^a-2n_0^a) - A(n_0^a-n_0^b) + \Lambda_a \ , \\
\dot{n}_{\pm1}^a &= -\gamma_a n_{\pm1}^a - W_a(n_{\pm1}^a-n_0^a) - \tfrac{3}{4}A(n_{\pm1}^a-n_{\pm1}^b) + \Lambda_a \ , \\
\dot{n}_0^b &= -\gamma_b n_0^b + W_b(n_1^b+n_{-1}^b-2n_0^b) + A(n_0^a-n_0^b) + \Lambda_b \ , \\
\dot{n}_{\pm1}^b &= -\gamma_b n_{\pm1}^b + W_b(n_0^b+\tfrac{2}{3}n_{\pm2}^b-\tfrac{5}{3}n_{\pm1}^b) + \tfrac{3}{4}A(n_{\pm1}^a-n_{\pm1}^b) + \Lambda_b \ , \\
\dot{n}_{\pm2}^b &= -\gamma_b n_{\pm2}^b - \tfrac{2}{3}W_b(n_{\pm2}^b-n_{\pm1}^b) + \Lambda_b \ , \qquad (5.13)
\end{aligned}$$

where n_m^a and n_m^b are the populations of the Zeeman substates m of the upper and lower states, respectively, $W_a=\frac{1}{2}(g\mu_B H_{rf})^2$ and $W_b=\frac{3}{2}(g\mu_B H_{rf})^2$, A is the transition rate by the laser light and is proportional to its intensity.

In spite of the fact that our experiments were made by

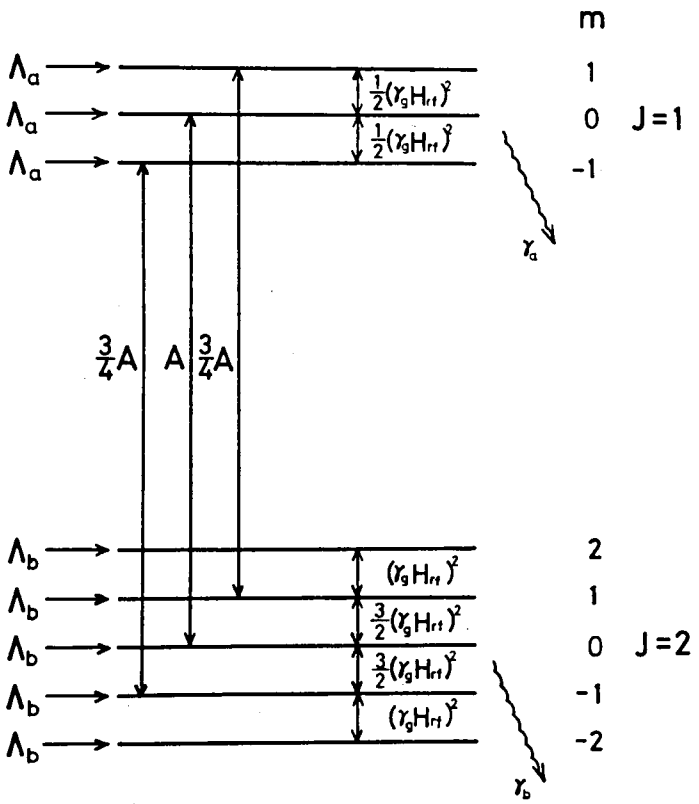

Fig. 5.3 Optical π-transitions and rf transitions which yield the double resonance in the He-Ne laser operating at 632.8 nm. Their transition probabilities are also shown.

using a multi-mode laser, we here consider the case of the single-mode operation with zero cavity detuning, for the sake of simplicity. The rate constant, which is defined by Eq.(35) in Ref. 128, can be expressed as

$$A = \frac{1}{2}(dE/\hbar)^2\gamma^{-1}|U(x)|^2, \tag{5.14}$$

where $d=e\langle a,m=0|z|b,m=0\rangle$, E is the electric field of the laser light, and γ is the decay rate of the optical coherence, and U(x) is the basis function of the cavity mode, i.e.the normalized amplitude distribution along the laser axis. On the basis of Lamb's semiclassical theory, we obtain a complex polarization of the medium :

$$P = -\frac{d^2E}{\hbar\gamma}\frac{2}{L}\int_0^L dx G(A,H_{rf})|U(x)|^2, \tag{5.15}$$

where L is the length of the cavity, and

$$G(A,H_{rf}) = \frac{3}{4}(n_1^a - n_1^b) + (n_0^a - n_0^b) + \frac{3}{4}(n_{-1}^a - n_{-1}^b). \tag{5.16}$$

Substituting the stationary solutions of Eq.(5.13) into Eq.(5.16), we obtain $G(A,H_{rf})$ upto the second order with respect to H_{rf} :

$$G(A,H_{rf}) \simeq N[X^{-1}+\frac{3}{2}Y^{-1}+\frac{1}{8}A_0(XY)^{-2}\left\{\frac{W_a}{\gamma_a}\right.$$

$$\left.+\frac{W_b}{\gamma_b}\left(7+12\frac{A_0}{\gamma_{ab}}+6\frac{A_0^2}{\gamma_{ab}^2}\right)\right\}], \tag{5.17}$$

where $N = \Lambda_a/\gamma_a - \Lambda_b/\gamma_b$, A_0 is the rate constant defined by Eq.(5.14) in the absence of rf magnetic field, and

$$X = 1 + \frac{A_0}{\gamma_{ab}}, \quad Y = 1 + \frac{3A_0}{4\gamma_{ab}}, \quad \gamma_{ab}^{-1} = \gamma_a^{-1} + \gamma_b^{-1} . \tag{5.18}$$

On the other hand, substituting the complex polarization P into the self-consistency equation[128], we obtain the relation for stationary state ($\dot{E}=0$):

$$\frac{2}{L}\int_0^L dx G(A, H_{rf}) |U(x)|^2 = \frac{\varepsilon_0 \hbar \gamma}{2Qd^2} . \tag{5.19}$$

Assuming that the rf field perturbation is small, we can expand Eq.(5.19) as

$$\int_0^L dx G(A_0, 0) |U(x)|^2 + \int_0^L dx \left(\frac{\partial G}{\partial A}\right) \frac{dA}{d(H_{rf})^2} H_{rf}^2 |U(x)|^2$$

$$+ \int_0^L dx \left(\frac{\partial G}{\partial W_a} W_a + \frac{\partial A}{\partial W_b} W_b\right) |U(x)|^2 \simeq \frac{\varepsilon_0 \hbar \gamma L}{4Qd^2} , \tag{5.20}$$

where all partial differentials must be estimated for $A=A_0$ and $H_{rf}=0$. The increase in the intensity of the laser light caused by the rf perturbation is proportional to

$$\frac{dA}{d(H_{rf})^2} H_{rf}^2 \simeq \frac{\int_0^L dx \left(\frac{\partial G}{\partial W_a} W_a + \frac{\partial G}{\partial W_b} W_b\right) |U|^2}{\int_0^L dx \left(\frac{\partial G}{\partial A}\right) |U|^2} . \tag{5.21}$$

From Eq.(5.21), we can estimate the ratio R of the contribution from the $2p_4$ state to that from the $3s_2$ state :

$$R = \frac{\int_0^L dx \frac{\partial G}{\partial W_b} W_b |U|^2}{\int_0^L dx \frac{\partial G}{\partial W_a} W_a |U|^2} \cdot \tag{5.22}$$

When we assume that the intensity of the laser light is small enough to approximate Eq.(5.22) upto the second order with respect to E_0 which is the electric field of the laser light in the absence of the rf perturbation, we find

$$R \simeq 21 \frac{\gamma_a^2}{\gamma_b^2} \left\{ 1 + \frac{6\gamma_{ab}}{7\gamma} \left(\frac{dE_0}{\hbar} \right)^2 \frac{\int_0^L N|U|^6 dx}{\int_0^L N|U|^4 dx} \right\}. \tag{5.23}$$

Since N varies little in a optical wavelength, so that, in the case of the standing wave with the basis $U(x)=\sin\{(n\pi/L)x\}$, we find

$$R \simeq 21 \frac{\gamma_a^2}{\gamma_b^2} \left\{ 1 + \frac{5\gamma_{ab}}{7} \left(\frac{dE_0}{\hbar} \right) \right\}. \tag{5.24}$$

In the case of the present experiment, the decay rates of the $3s_2$ and the $2p_4$ states are approximately equal ($\gamma_a \sim \gamma_b$). If we assume that $\gamma_a = \gamma_b$, the contribution from the $2p_4$ state is 21 times as large as that from the $3s_2$ state at the threshold of the laser ($E_0=0$). As the laser intensity is increased, this ratio R becomes larger. Therefore, the double-resonance signal appearing in the laser intensity is determined substantially by the magnetic resonance in the $2p_4$ state (J=2).

Carroll and Wolga have shown in a phenomenological way that the contribution from the state with J=2 to the double-

resonance signal in a He-Ne laser operating at 1.15 μm is more important than that from the state with J=1 [120]. Furthermore, Decomps and Dumont have shown experimentally for the case of saturation resonance of the 632.8 nm transition in a He-Ne laser, in which the fluorescence from each laser level was observed, that the resonance in the $2p_4$ state appears much stronger than that in the $3s_2$ state, even when the fluorescence emitted from the $3s_2$ state is observed[129].

V.3 Pressure Broadening of Magnetic Resonance Line of Neon

In this section, we investigate pressure effects on magnetic resonance line of neon by means of the double-resonance experiment in a He-Ne laser. The alignment destroying cross sections of the $2p_4$ state of neon for collisions with helium and neon were measured by observing the widths of magnetic resonance signals by changing the partial pressures of herium and neon, respectively. Besides, the cross sections for neon-argon and neon-krypton collisions were measured by adding small amounts of argon or krypton in the He-Ne laser tube.

V.3.1 Experimental Setup

The schematic diagram of the arrangement for the present experiments is shown in Fig. 5.4. Between two mirrors, which

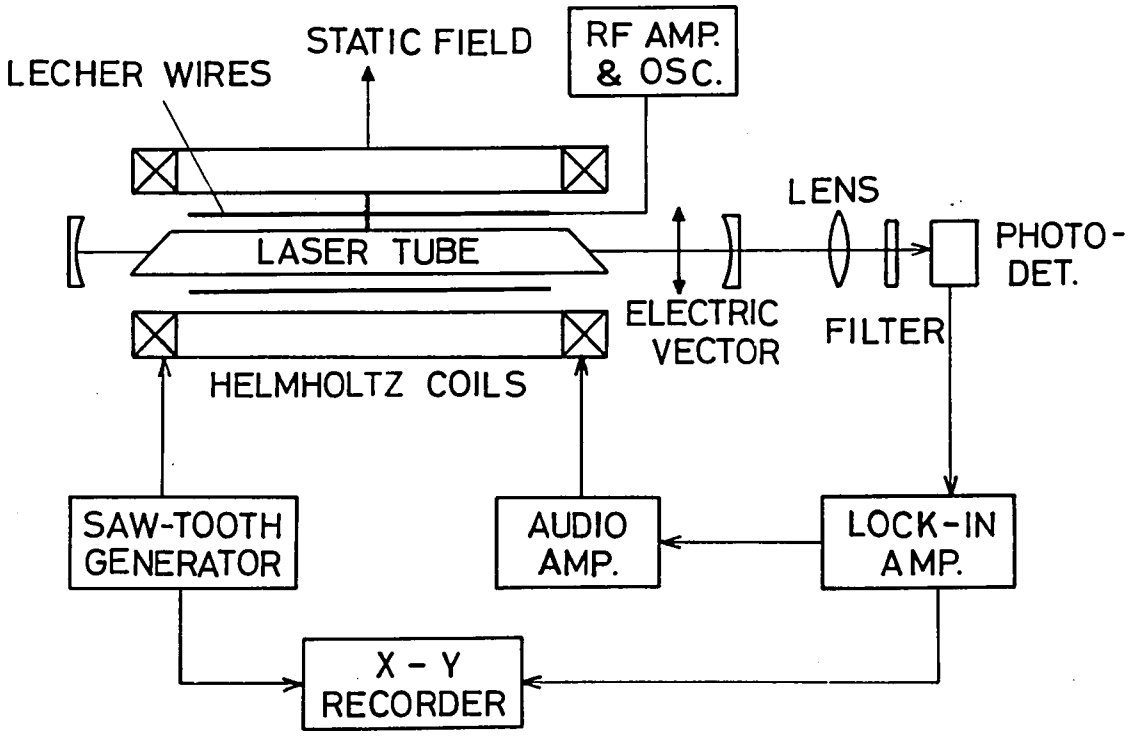

Fig. 5.4 Schmatic diagram of the experimental setup for double-resonance experiments.

insure laser oscillation on a single line at 632.8 nm, a dc-excited laser tube with Brewster-angle windows was inserted. The laser tube with a bore of 3 mm and an effective discharge length of 73 cm, can be connected to a vacuum system through a joint and can be filled with mixture of gases repeatedly. The discharge current was kept constant at 15 mA by a regulated current supply. The spacing between two mirrors was about 105 cm, which corresponds to the axial mode separation of about 140 MHz. The laser tube was submitted to a transverse magnetic field $\vec{H}$. The Brewster-angle windows were oriented so that the electric field of the laser light was pallalel to $\vec{H}$, and then only the π-transitions were allowed. The static field, applied by a set of double Helmholtz coils[130], was swept by a regulated current supply controlled by a saw-tooth generator. The spatial uniformity of the magnetic field $\vec{H}$ was better than 10^{-3} over the effective discharge length of the laser tube, so that the broadening of the resonance signal due to a inhomogeneous magnetic field might be neglected in the calculations of decay rates from the resonance widths. The oscillating rf magnetic field perpendicular to both the laser axis and the static magnetic field $\vec{H}$ was applied by Lecher wires between which the laser tube was placed. The frequency of the rf field was kept constant at 158.4 MHz by multiplying the original frequency of a crystal oscillator six times. The amplitude of the oscillating rf field was estimated as about 1.5 G at most. In spite of the use of oscillating field in place of rotating field utilized in the

theory described in Sec. V.2.2, we could neglect the Bloch-Siegert shift[131] due to the counter-rotating field because the amplitude of the rf field was small enough. Most of all apparatus, i.e. the optical bench, mirror holders, and the tube holders, which were placed in the double Helmholtz coils , were made of non-magnetic aluminum alloy in order to avoid perturbations due to residual magnetic fields.

The output of the laser was focussed on a silicon solar cell after passing through a interference filter of 632.8 nm transmission. In the present experiments, we used the field-modulation techniques[132] which are commonly used in NMR or ESR experiments. Hence, the modulation magnetic field of 400 Hz was superposed on the static field $\vec{H}$. This modulation field whose amplitude was kept constant at 0.8 G was applied by an audio-frequency power amplifier and additional windings on the double Helmholtz coils. The modulation in the output of the solar cell at the frequency 400 Hz was phase-sensitively detected by a lock-in amplifier, so that the output of the lock-in amplifier, which was traced by an X-Y recorder sweeping the static magnetic field H, showed the derivative of the Lorentzian resonance signal as a function of H. The horizontal axis of the X-Y recorder was driven by the current of the double Helmholtz coils, and the conversion factor of the value of H to the current was measured with accuracy of 0.1 % by an optically pumped cesium magnetometer[133].

V.3.2 Experimental Results

A typical recorder trace is shown in Fig. 5.5, where the horizontal axis is calibrated with the current of the double Helmholtz coils, and the conversion factor is 20 G/A. As expected in the previous section, we can see the double-resonance signal as the derivative of the Lorentzian resonance as a function of the strength of the static magnetic field H. We can estimate the half-width at half-maximum of the magnetc resonance from the separation ΔH between two peaks in Fig. 5.5 :

$$\Delta\omega = \frac{\sqrt{3}}{2} g\mu_B \Delta H. \qquad (5.25)$$

Since the double-resonance signal is thought to be determined by the magnetic resonance in the $2p_4$ state as discussed in Sec. V.2.3, we use the g-value of 1.298[108] in estimating $\Delta\omega$ by using Eq.(5.25).

We first investigate the effect of the rf magnetic field on the width of the magnetic resonance. The half-width at half-maximum was measured by changing the amplitude of the rf field which is thought to be proportional to the plate current I_{rf} of the final tube of the rf amplifier. We show in Fig. 5.6 the experimental results for the square of the half-width at half-maximum as a function of the square of the plate current. We can see apparently in this figure a linear dependence of $\Delta\omega^2$ on I_{rf}^2, which is consistent with the theoretical result given by Eq.(5.10). When $\Delta\omega^2$ is extrapolated to the limit of vanishing

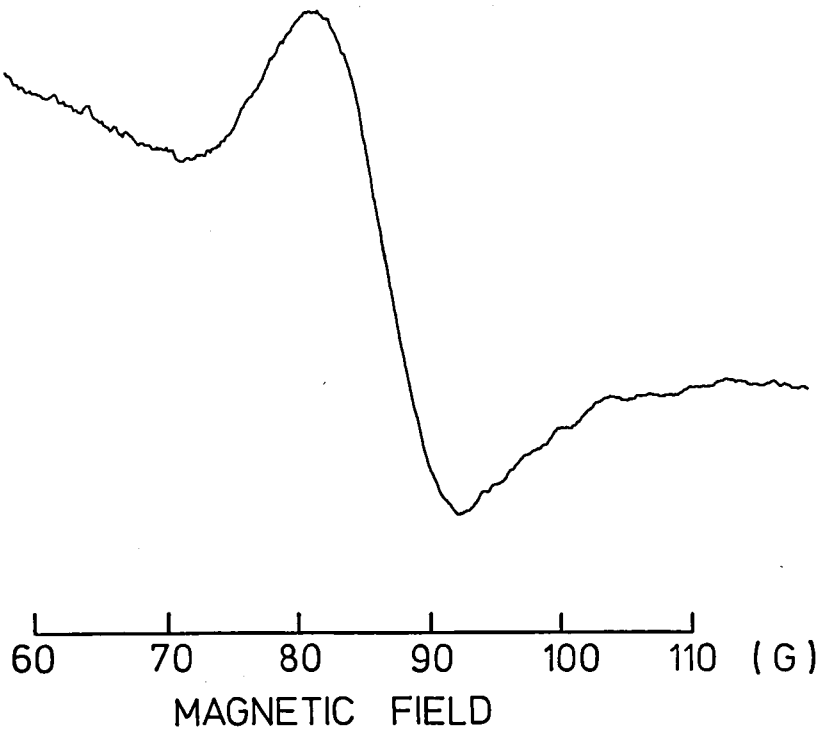

Fig. 5.5 Typical recorder trace of the double-resonance signal.

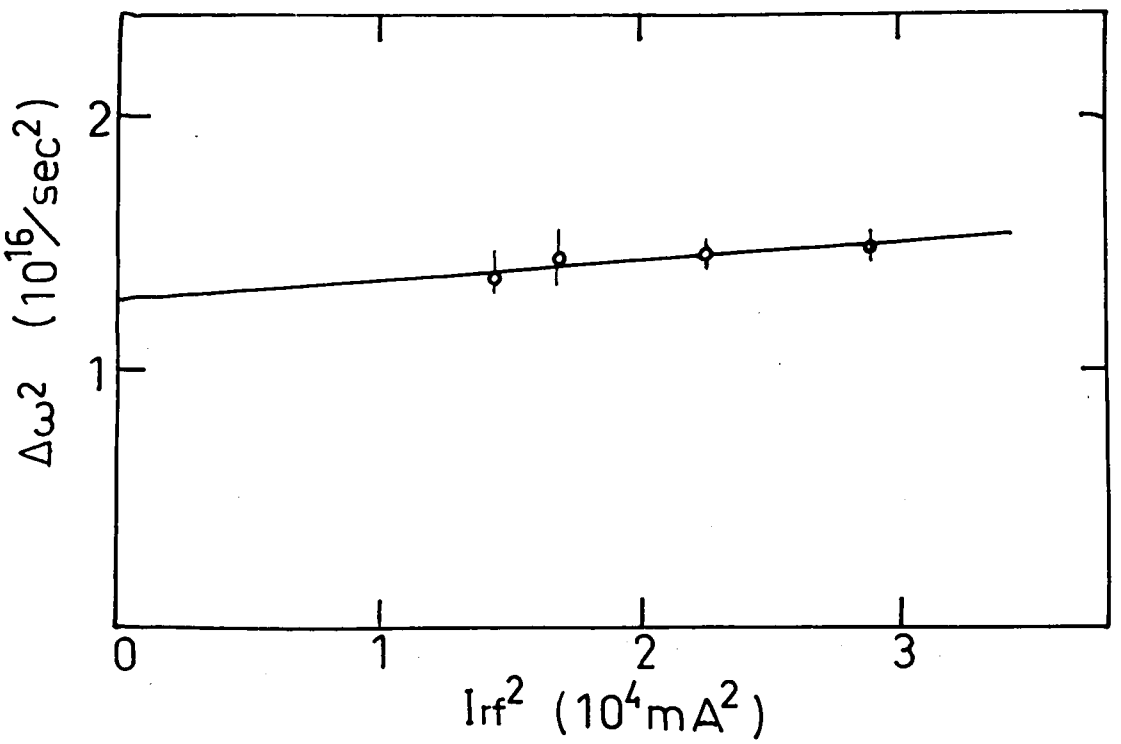

Fig. 5.6 The square of the half-width at half-maximum of the magnetic resonance signal as a function of the plate current I_{rf} of the rf amplifier.

I_{rf}^2, we can obtain the decay rate of alignment which consists of the spontaneous and collisional relaxations. However, throughout the following experiments measuring the pressue broadening, the amplitude of the rf magnetic field was kept constant at 1.5 G which was estimated from the power broadening seen in Fig. 5.6 for particular value of the plate current, so that the effect of power broadening due to the rf field can be subtracted through Eq.(5.10). Henceforth, we will denote the width as $\Delta\omega$ after subtracting the power broadening.

Now, we investigate the pressure broadening of the magnetic resonance line. In order to measure the broadening caused by collisions with helium, we made the double-resonance experiments by varying the partial pressure of helium in the laser tube while the partial pressure of neon was kept constant at 0.18 Torr. We carried out the present experiment by using different isotopes of helium, i.e. He^3 and He^4. In Fig. 5.7, the half-widths at half-maximum $\Delta\omega$ are shown as functions of partial pressures of He^3 and He^4. The least-squares fits of these plots in Fig. 5.7 to linear functions with respect to the partial pressures of He^3 and He^4 can be expressed as follows :

$$\Delta\omega = (5.40\pm0.22)\times10^7 P_{He^3} + (8.23\pm0.20)\times10^7 \text{ rad/sec} \tag{5.26a}$$

and

$$\Delta\omega = (3.71\ 0.20)\times10^7 P_{He^4} + (8.59\ 0.20)\times10^7 \text{ rad/sec} \tag{5.26b}$$

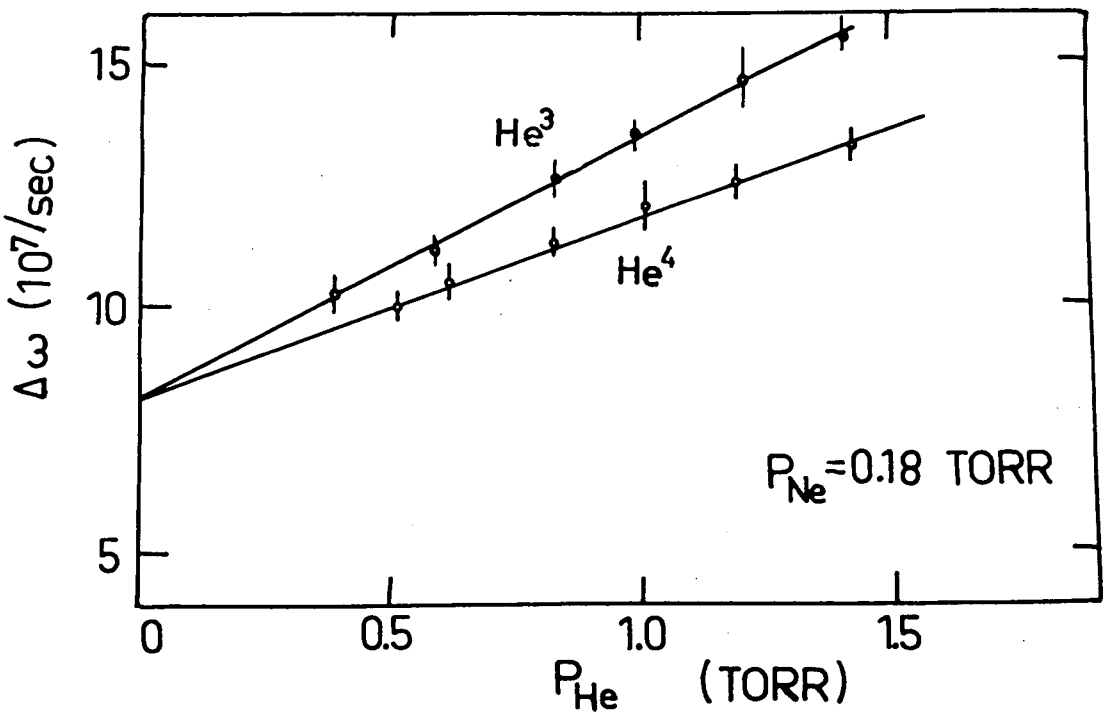

Fig. 5.7 Half-width at half-maximum of the magnetic resonance signal of the $2p_4$ state of neon as functions of partial pressures of He^3 and He^4, at the fixed partial pressure of 0.18 Torr of neon.

where P_{He^3} and P_{He^4} are partial pressures of He^3 and He^4, respectively, in units of Torr. The first terms in the right-hand sides of Eqs.(5.26) are the broadenings caused by collisions with helium, and correspond to $n_p\langle v\rangle\sigma^{(2)}$ in Eq.(5.12) where the relative velocity is defined as

$$\langle v\rangle = \sqrt{8kT/\pi M} \ , \tag{5.27}$$

and M is the reduced mass of the colliding atoms. Hence, we can obtain the alignment destroying cross sections for the $2p_4$ state of neon colliding with He^3 and He^4. When we assume that the gas temperature T was 400 K, we obtain

$$\sigma^{(2)}_{Ne^*-He^3} = (8.88 \pm 0.33) \times 10^{-15} \ cm^2, \tag{5.28a}$$

$$\sigma^{(2)}_{Ne^*-He^4} = (6.29 \pm 0.37) \times 10^{-15} \ cm^2. \tag{5.28b}$$

Here, it should be emphasized that the cross section for He^3 is about 30 percent larger than that for He^4. This seems to contradict the results of the theory using the van der Waals interaction. We will discuss on this anomalous difference between the cross sections for He^3 and He^4 in the next section.

Similar experiments were made by varying the partial pressure of neon while the partial pressure of He^4 was kept constant at 0.9 Torr. In Fig. 5.8, we show the experimental plots of the width $\Delta\omega$ as a function of the partial pressure of neon. The

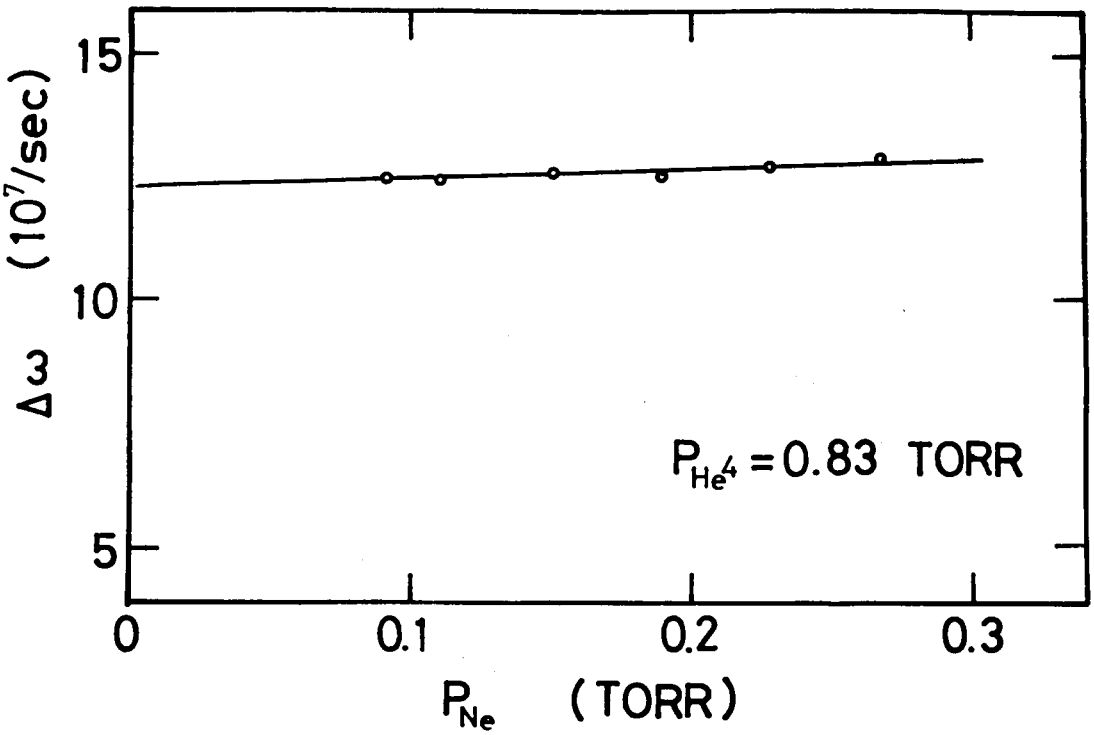

Fig. 5.8 Half-width at half-maximum of the magnetic resonance signal of the $2p_4$ state of neon as a function of the partial pressure of neon, at the fixed He^4 partial pressure of 0.83 Torr.

least-squares fit for these plots yields

$$\Delta\omega = (2.04\pm1.42)\times10^{7}P_{Ne} + (11.69\pm0.73)\times10^{7} \text{ rad/sec.} \tag{5.29}$$

We then obtain the alignment destroying cross section of neon in the $2p_4$ state colliding with neon in its ground state :

$$\sigma^{(2)}_{Ne^*-Ne} = (6.64 \pm 1.35) \times 10^{-15} \text{ cm}^2. \tag{5.30}$$

Furthermore, we investigated the alignment destructions of neon caused by collisions with heavier rare-gas atoms. In the present experiments, we used the He-Ne laser tube which was adulterated with a small amount of either argon or krypton. In Figs. 5.9 and 5.10, the resonance widths measured are shown as functions of the partial pressures of argon and krypton, respectively, while the partial pressures of helium and neon are kept constant at 0.83 and 0.18 Torr, respectively. In the case of the mixture of He-Ne-Ar, the discharge of argon prevented the He-Ne laser from oscillating when the partial pressure of argon P_{Ar} was increased, so that we could observe the double-resonance signal only when the partial pressure P_{Ar} was less than 0.04 Torr. Similarly, in the case of the mixture of He-Ne-Kr, we could observe the signal only for the partial pressure of krypton P_{Kr} less than 0.02 Torr. The least-squares fits for these experimental plots yield the following results :

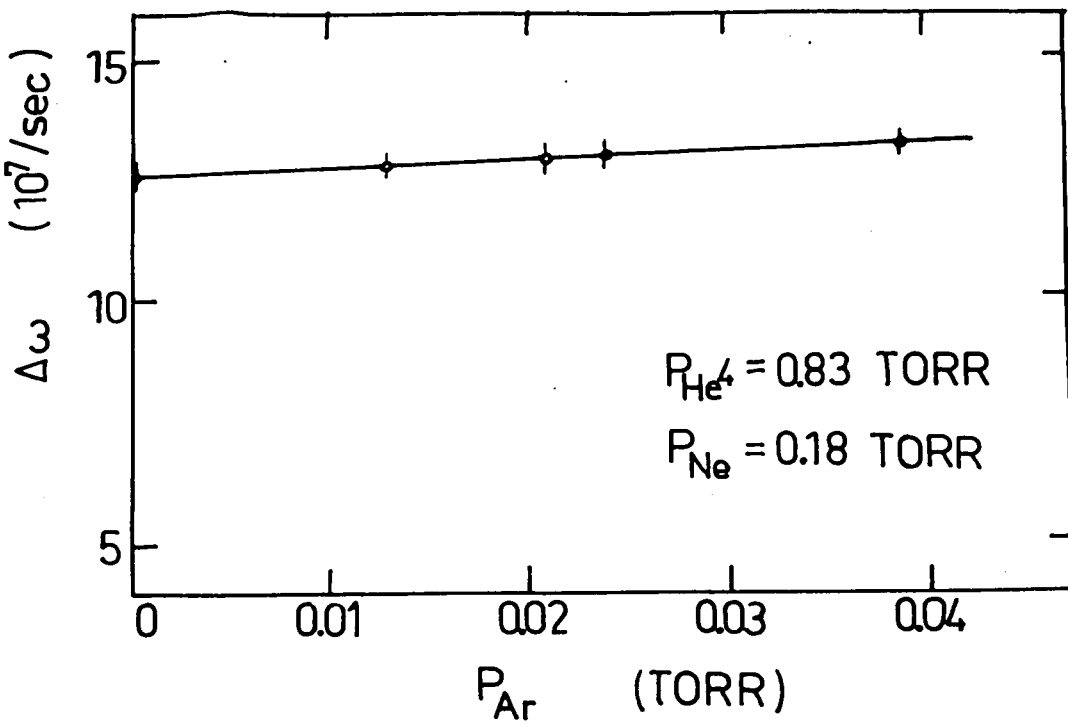

Fig. 5.9 Half-width at half-maximum of the magnetic resonance signal of the $2p_4$ state of neon as a function of the partial pressure of Ar, at the fixed partial pressures of He^4 and Ne, of 0.83 and 0.18 Torr, respectively.

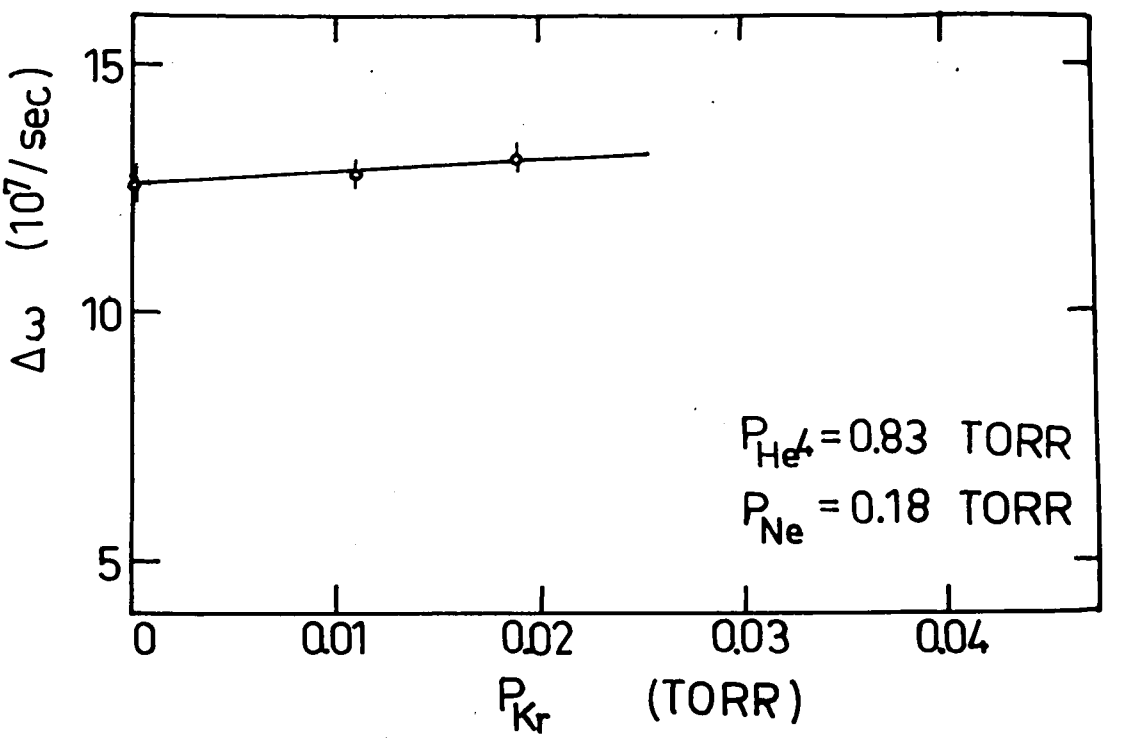

Fig. 5.10 As for Fig. 5.9, but as a function of the partial pressure of Kr.

$$\Delta\omega = (14.72\pm4.22)\times10^7 P_{Ar} + (12.60\pm0.08)\times10^7 \text{ rad/sec}, \tag{5.31}$$

$$\Delta\omega = (22.61\pm5.97)\times10^7 P_{Kr} + (12.60\pm0.07)\times10^7 \text{ rad/sec}, \tag{5.32}$$

where P_{Ar} and P_{Kr} are the partial pressures of argon and krypton, respectively, in units of Torr. We can calculate the cross sections from Eqs.(5.31) and (5.32). However, these least-squares fits are not so reliable compared with those for helium or neon because we could not vary the partial pressures so widely as in the case of helium or neon, Therefore, we can only estimate the possible ranges of the values of the cross sections from Figs. 5.9 and 5.10 :

$$\sigma^{(2)}_{Ne^*\text{-}Ar} = (15 \sim 55) \times 10^{-15} \text{ cm}^2, \tag{5.33}$$

$$\sigma^{(2)}_{Ne^*\text{-}Kr} = (15 \sim 90) \times 10^{-15} \text{ cm}^2. \tag{5.34}$$

The summary of the alignment destroying cross sections measured in the present experiments are presented in Table 5.1 together with the values measured previously and calculated theoretically by different authors[23),88),97)].

V.3.3 Discussions and Comparisons with Theory

In this section, we compare the experimental results described

Table 5.1 Alignment Destroying Cross Sections for Collisions of Neon in the $2p_4$ State with Rare Gases in Units of $10^{-15}cm^2$

PERTURBER	PREVIOUS WORKS	THEORETICAL WORKS	PRESENT WORK
He^3			8.88±0.33
He^4	5.4±0.4[a)] 6.3[b)] 8.54±0.29[c)]	3.0[a)] 4.84[b)]	6.89±0.37
Ne	8.2±0.4[a)] 15.7±1.2[b)] 9.29±0.35[c)]	7.7[a)] 9.93[b)]	6.64±1.35
Ar			15 ~ 55
Kr			15 ~ 90

a) Ref. 97.

b) Ref. 88.

c) Ref. 23.

in the previous section with the theory of isotropic collisions.

We use the theory of isotropic collisions applied to the case of emitters in the state with J=2 perturbed by the ground state atoms with J=0, on refering to the formalism given in Sec. III.3.1.

As mentioned in Chap. III, the relaxation rate of alignment, which is proportional to $\sigma^{(2)}$ when collisions are isotropic, is proportional to $B^{2/5}$ which is the only factor dependent on the characteristics of the virtual transitions, i.e., transition probabilities, energies of intermediate states, etc. In Chap. III, we have assumed that only one type of virtual transition occurs during a collision. However, as a matter of fact, virtual transitions to various intermadiate states with different angular momenta are possible. Therefore, we must generalize the theory to the actual case.

In the case of the $2p_4$ state, we consider three virtual transitions, that is, $2p_4$–$1s_5$, $2p_4$–$1s_4$, and $2p_4$–$1s_2$, while we neglect all other transitions, from the argument of energy conservation. These three transitions can be classified into two types: (b) $2p_4$–$1s_4$ and $2p_4$–$1s_5$ (j=2 – j'=1); (c) $2p_4$ –$1s_5$ (j=2 – j'=2). Taking account of these two types of virtual transitions, we can rewrite Eq.(3.27) as

$$\frac{dM}{d\theta} = i(\tilde{Y}_D + \tilde{Y}_E)M, \tag{5.35}$$

where $\tilde{Y}_D$ and $\tilde{Y}_E$ are defined by Eqs.(3.31) and (3.33), respectively.

From Table 3.2 and Eqs.(3.31) and (3.33), we can readily obtain the relation between the matrices $\tilde{Y}_D$ and $\tilde{Y}_E$:

$$\tilde{Y}_E = -\frac{B_E}{B_D}\tilde{Y}_D + q(\theta)I, \tag{5.36}$$

where

$$q(\theta) = \frac{192}{b^5 v_R}\cos^4\theta, \tag{5.37}$$

and I is the 5×5 unit matrix. Substituting Eq.(5.36) into Eq. (5.35), we obtain

$$\frac{dM}{d\theta} = i\left(1 - \frac{B_E}{B_D}\right)\tilde{Y}_D M + iq(\theta)M. \tag{5.38}$$

This differential equation can be transformed as

$$\frac{d\hat{M}}{d\theta} = i\left(1 - \frac{B_E}{B_D}\right)\tilde{Y}_D \hat{M}, \tag{5.39}$$

where

$$\hat{M} = M\exp\{i\int_{-\infty}^{\theta} q(\theta')d\theta'\}. \tag{5.40}$$

Because Eq.(5.40) is a scalar transformation, this transformation is trivial, so long as the relaxation among Zeeman substates is considered. Then, Eq.(3.27) is still valid for the present case if the factor B_D in Eq.(3.31) is replaced by

$$B = \sum(B_D - B_E), \tag{5.41}$$

Table 5.2 Transitions of Rare Gases and Their Wavelengths λ Together with the Oscillator Strengths f_{ik} and the Transition Probabilities γ_{ki}

	k	i	J_k	J_i	λ [nm]	f_{ik}	γ_{ki} [$10^7 sec^{-1}$]	
Ne (EMITTER)	$2p_4$	$1s_5$	2	2	594.5	0.0556	1.05	a
	$2p_4$	$1s_4$	2	1	609.6	0.157	1.69	a
	$2p_4$	$1s_2$	2	1	667.8	0.265	2.38	a
He	$^1P_1^\circ$	$^1S_0$	1	0	58.43	0.276	179.9	a
Ne (PERTURBER)	$1s_4$	$^1S_0$	1	0	74.37	0.0118	4.76	a
	$1s_2$	$^1S_0$	1	0	73.59	0.162	66.4	a
Ar	$1s_4$	S_0	1	0	106.7	0.059	11.6	b
	$1s_2$	S_0	1	0	104.8	0.228	46.5	b
Kr	$1s_4$	S_0	1	0	123.6	0.187	27.2	c
	$1s_2$	S_0	1	0	116.5	0.194	31.7	c

a) Ref. 134.

b) Ref. 135.

c) Ref. 136.

where the summation is taken over all possible virtual transitions. It should be noted that the cross section $\sigma^{(2)}$ is proportional to $B^{2/5}$:

$$\sigma^{(2)} \propto B^{2/5} \langle v^{3/5} \rangle / \langle v \rangle . \tag{5.42}$$

We then compare the ratio $\sigma^{(2)}_{Ne^*-X}/\sigma^{(2)}_{Ne^*-Ne}$ calculated from the experimental results with that estimated from this theory. Present theoretical estimations were made by assuming that perturbers undergo only the virtual transitions from the ground stat state $^1S_0$ to the first excited state $^1P^\circ_1$ for helium, and to 1s states for neon, argon, and krypton, while the emitter atoms of neon undergo the virtual transitions between the $2p_4$ state and the 1s states. The values of the transition probabilities necessary for the present calculations are tabulated in Table 5.2. The transition probability γ_{ki} for a transition from the state k to the state i is related to the reduced matrix element $\langle i \| d \| k \rangle$ of the electric dipole moment as follows :

$$|\langle i \| d \| k \rangle|^2 = \frac{9}{32\pi^2} \hbar \lambda^3 \gamma_{ki} , \tag{5.43}$$

where λ is the wavelength for the transition. Then, we can calculate the factor B for each pair of colliding atoms using Eqs.(3.32), (3.34), (5.41), and (5.43). The ratio of the alignment destroying cross section for collisions with rare gas X to that for the collisions with neon can be derived easily from

Eq.(5.42) as

$$\frac{\sigma^{(2)}_{Ne^*-X}}{\sigma^{(2)}_{Ne^*-Ne}} = \left[\frac{M_{Ne-X}\, B_{Ne^*-X}{}^2}{M_{Ne-Ne} B_{Ne^*-Ne}{}^2}\right]^{1/5}, \tag{5.44}$$

where M_{Ne-X} is the reduced mass for binary system of Ne and X.

In Table 5.3, the ratios calculated from Eq.(5.44) are shown together with the experimental results. Our theoretical calculations show that the cross section increases monotonically with the increase of the mass of perturber. On the other hand, the cross section obtained experimentally for He^3 is about 30% larger than that for He^4, and both of them are larger than that for neon, which cannot be explained by the above theory using the electrostatic dipole-dipole interaction of the van der Waals type.

This anomaly in the cross sections for helium has not been reported for the case of the $2p_4$ state of neon, until now. So far as we know, there has been only one series of measurements of the alignment destroying cross sections for Ne-He^3 collisions and Ne-He^4 collisions, which has been made for the $2s_2$ state (J=1) of neon by Wang et al.[73]. The reported cross section for He^3 is larger than that for He^4, namely

$$\sigma^{(2)}_{Ne^*_{2s_2}-He^3} = (2.99 \pm 0.32) \times 10^{-15}\ cm^2, \tag{5.45}$$

$$\sigma^{(2)}_{Ne^*_{2s_2}-He^4} = (2.78 \pm 0.37) \times 10^{-15}\ cm^2. \tag{5.46}$$

although they have taken no notice of this anomaly.

Table 5.3 Measured Cross Sections and Their Ratios to the Cross section for Collisions with Neon Together with Theoretically Calculated Ratios

PERTURBER	PRESENT EXPERIMENT		THEORETICAL RATIO
	$\sigma^{(2)}_{Ne^*-X}$ $[10^{-15}cm^2]$	$\sigma^{(2)}_{Ne^*-X}/\sigma^{(2)}_{Ne^*-Ne}$	$\sigma^{(2)}_{Ne^*-X}/\sigma^{(2)}_{Ne^*-Ne}$
He^3	8.88±0.33	1.34	0.854
He^4	6.89±0.37	1.04	0.897
Ne	6.64±1.35	1	1
Ar	15 ~ 55	2.2 ~ 8.3	1.77
Kr	15 ~ 90	2.2 ~ 15	2.30

It might be interesting to note that one may find a dip around neon if one plotts the measured cross sections against the atomic numbers of perturbers as was done in Ref. 25. Similar dip has been found in the elastic scattering cross sections for collisions between electrons and rare-gas atoms[137]. More recently, similar properties have been reported in cases of alkali atoms in the first excited P states perturbed by rare gas atoms, for instance, the depolarization cross sections of sodium[32], potassium[25], rubidium[26),27),28)], and cesium[26),27),29)], and the fine-structure mixings of sodium[30], potassium[31], rubidium[31], and cesium[31]. For the case of fine-structure mixing of sodium, Masnou-Seeuws has explained these anomalies for collisions with light perturbers by taking account of the repulsive exchange interaction whose effective range is much shorter than that of the van der Waals interaction[138]. The above-mentioned anomalous properties may be explained as follows. In the case of heavy perturbers such as argon or krypton, since the relative velocity is rather small, the short-range repulsive interaction is negligible compared with the van der Waals interaction, so that, as the mass of perturber is increased, the cross section becomes larger due to the increase in the polarizabilities of rare-gas atoms. On the other hand, for light perturbers such as helium, the polarizabilities are generally smaller and the relative velocities are relatively large, so that the short-range repulsive interaction originating in the overlap of electronic orbitals of emitter and perturber becomes important, and which results in the cross

sections larger than those expected from the van der Waals interaction. Especially, the difference between the cross sections for He^3 and He^4 should be attributed only to the difference in the relative velocity. Here, it may be noted that the nuclear spin of He^3, to which we have not given attention, gives no significant effect on the alignment destroying cross sections so long as the magnetic interaction, which is expected to be much smaller than the electric interaction, is neglected.

V.4 Conclusions

In this chapter, we have investigated the alignment destruction of neon in the $2p_4$ state colliding with helium, neon, argon, and krypton in their ground states, by means of the double-resonance techniques of the He-Ne laser. The alignment destroy ing cross sections have been measured from the pressure broadening of the double-resonance signal. We have compared these experimental results with the cross sections calculated by using the theory of isotropic collisions in which the van der Waals interaction is assumed.

Although there have been large errors in measurement of cross sections for argon and krypton, we have found the increase in the cross section with the increase of the atomic numbers of perturbing rare-gas atoms from neon to krypton, which is consistent qualitatively with the theory using the van der Waals

interaction. On the other hand, the cross section for He^3 was about 30% larger than that for He^4, and both were larger than that for neon, which cannot be explained by the above theory.

It must be concluded that, as is in the case of alkali atoms in the first excited P states colliding with helium, the short-range repulsive interaction is predominant in the Ne-He collisions rather than the long-range van der Waals interaction, which has been expected but has not been made clear. The relatively large difference of the measured cross sections for He^3 and He^4 may also indicate the possibility that the relative trajectory of colliding pair of atoms deviates from a straight-line path by the short-range repulsive interaction, as has been pointed out by Carrington and Corney[34].

CHAPTER VI

SUMMARY AND CONCLUDING REMARKS

In the present work, we have made the theoretical and experimental investigations on the effects of collisional relaxation and transfer on laser-induced multipole moments in the excited state of neon atoms. The first half of this thesis has been devoted to the study of anisotropic collisions (Chapter II – IV). In the latter half, we have investigated isotropic collisions with various rare-gas atoms (Chapter V).

In chapter I, we have presented a historical review of the theoretical and experimental studies on atomic collisions of our present interest, giving a special attention to collisional depolarizations of atoms in the excited states. The importance of anisotropic collisions for atoms excited by a laser has been emphasized. In this connection, we have briefly reviewed different types of anisotropic relaxations investigated heretofore. Furthermore, we have pointed out the importance of depolarizing collisions in understanding the polarization characteristics of the Zeeman laser and the anomalous circular polarization of interstellar masers.

In chapter II , we have introduced the density-matrix

formalism and its representation on the basis of irreducible tensorial sets as convenient mathematical foundations in dealing with phenomena of optical pumping and relaxation. We have shown that the irreducible representation provides a simple expression for a polarized state of a Zeeman multiplet in terms of multipole moments, for example, the orientation (the magnetic dipole moment), the alignment (the electric quadrupole moment), and so on. The behavior of these multipole moments under the influence of an external magnetic field and relaxation is well described by the master equation for the internal state of atoms with an arbitrary total angular momentum.

We have also studied some properties of multipole relaxations within a Zeemen multiplet from the point of view of the symmetry of the system regardless of particular origin of the relaxation. When the situation is isotropic (i.e. spherically symmetric), each multipole component relaxes independently without coupling with each other. On the other hand, when the system has lower symmetry, couplings between different multipole components become allowed. We have studied especially on the system with axial and plane-reflection symmetries, and derived a number of useful relations for relaxation matrix elements with respect to the multipole components.

In chapter III, we have theoretically investigated the depolarization of atoms in their excited state under the influence of collisions with atoms in their ground state. We have extended the conventional theory of depolarizing collisions to

the case of atoms excited by a single-mode laser.

Theoretical calculations have been made for emitters in the excited state with an arbitrary total angular momentum. At first, we have investigated the effect of anisotropic collisions on emitters moving with a definite velocity whose direction is fixed in the laboratory frame. In these calculations, perturber atoms considered are in the ground state and have a velocity distribution given by an isotropic Maxwellian function. The dependences of the relaxation matrix elements on the velocity of the emitter have been calculated. Such collisions can be considered to be important in the atomic beam experiments. Then the theory has been extended to collisions of emitters excited by a single-mode laser, which have a definite velocity along the laser beam but have a velocity distribution given by a two-dimentional Maxwellian perpendicular to the laser beam. Numerical calculations have been made for emitters in the excited state with J=1. The decay rates for each multipole component and the transfer rate between alignment and orientation have been calculated as functions of detuning of the laser frequency from the center of the absorption line and mass of the perturber. We have found that, even when the laser is tuned at the line center, the transfer rate is sufficiently large to be observed experimentally. Another important feature of such anisotropic collisions is the fact that the decay rate of each multipole component ρ_q^k increases as the detuning is increased, the amount being dependent not only on the order k but also on

the value of $|q|$.

We have also found that, as long as the system has both of axial and plane-reflection symmetries such that the axis of symmetry is contained in the planes of symmetries as in the present case, no shift of a magnetic resonance line is caused by anisotropy. On the other hand, the shift is induced in the system which has only an axial symmetry as shown by Happer[100]. In this connection, we have pointed out that the pressure-induced g_J-shifts observed by Yabuzaki et al.[36] are not caused by the anisotropic collisions studied in the present work.

In chapter IV, we have experimentally investigated the effects of anisotropic collisions on atoms excited by a single-mode laser. Magnetic depolarization signals have been observed in the fluorescence emitted from the $2p_4$ state (J=2) of natural neon which is excited by a single-mode dye laser tuned around the line center of the $1s_5$–$2p_4$ transition. We have made experiments to study mainly on three typical features of anisotropic collisions: (i) the dependence of the decay rate of alignment on the degree of anisotropy; (ii) the transfer from alignment to orientation; (iii) the transfer from orientation to alignment. The results of these experiments are summarized as follows :

i) We have measured the variation of the width of the Hanle signal by changing the detuning of the laser, and have found the fact that the width slightly increases with the increase of the detuning. This experimental result is in qualitative

agreement with the theoretical prediction.

ii) The transfer from alignment to orientation has been observed by detecting the circularly polarized fluorescence emitted by atoms excited by a linearly polarized laser light beam. The ratio of the amplitude of the orientation signal to that of the alignment signal has been measured by changing the laser frequency around the absorption line. By comparing the experimental results with the theory given in Chap. III, we have found that the ratio is strongly affected by the presence of Ne^{22} in spite of its small abundance. By taking the presence of Ne^{22} into account, we have found a fairly good agreement with the theoretical prediction. We have also found in these studies that the transfer rate does not largely depend on the value of total angular momentum J of emitters.

iii) The transfer from orientation to alignment has been observed by detecting the linearly polarized fluorescence emitted by atoms excited by a circularly polarized laser beam. We could obtain the signal of alignment having the shape just as predicted by our theory, but we could not make further quantitative discussions because of the low signal-to-noise ratio.

In these experiments, we could not vary the degree of anisotropy so widely, because the mass of the emitter was equal to that of the perturber. In order to make the anisotropy larger, it seems to be preferable to investigate the collisional effects

of heavy rare gas atoms on the first excited P state of alkali atoms pumped by a single-mode laser.

In chapter V, we have experimentally investigated the alignment destroying cross sections of neon atoms in the $2p_4$ state colliding with various rare-gas atoms, by means of the double-resonance techniques in the gaseous laser. In this experiment, we have used a multi-mode He-Ne laser operating at 632.8 nm, so that collisions can be considered to be approximately isotropic. By solving the rate equations for the laser transitions (J=1—2), we have shown that the resonant behavior appearing as the intensity change of the laser output is attributed to the magnetic resonance in the $2p_4$ state (J=2). We have measured the pressure broadenings of the magnetic-resonance signals by changing the partial pressures of various rare gases, and we have determined the alignment destroying cross sections of the $2p_4$ state of neon for collisions with He^3, He^4, Ne, Ar, and Kr. The experimental results have been compared with the theory in which the van der Waals interaction is assumed. We have found that the cross sections measured experimentally for He^3 is about 30% larger than that for He^4, and both are larger than that for Ne, which is contradictory with the theoretical prediction. For collisions with light perturbers such as helium, we have emphasized the importance of the short-range repulsive interaction rather than the van der Waals interaction.

REFERENCES

1) H. A. Lorentz, Proc. Amst. Acad. Sci. 8, 591 (1906).

2) V. Weisskopf, Z. Physik 75, 287 (1932).

3) H. M. Foley, Phys. Rev. 69, 616 (1946).

4) P. W. Anderson, Phys. Rev. 76, 647 (1949).

5) C. J. Tsao and B. Curnutte, J. Quant. Spectrosc. Radiat. Transfer 2, 41 (1962).

6) W. Hanle, Z. Physik 30, 93 (1924).

7) W. Happer and E. B. Salomon, Phys. Rev. 160, 23 (1967).

8) J. Brossel and A. Kastler, C. R. Acad. Sci. 229, B1213 (1949).

9) J. Brossel and A. Kastler, Phys. Rev. 86, 308 (1952).

10) A. Kastler, J. Phys. Radium 11, 255 (1950).

11) M. A. Bouchiat, J. Phys. (Paris) 24, 379 (1963).

12) M. A. Bouchiat, J. Phys. (Paris) 24, 611 (1963).

13) A. Omont, J. Phys. (Paris) 26, 576 (1965).

14) M. I. D'yakonov and V. I. Perel', Zh. Eksp. Teor. Fiz. 48, 1483 (1965) [Sov. Phys. -JETP 20, 997 (1965)].

15) F. Masnou-Seeuws and M. A. Bouchiat, J. Phys. (Paris) 28, 406 (1967).

16) F. W. Byron, Jr. and H. M. Foley, Phys. Rev. 134, 625 (1964).

17) M. I. D'yakonov and V. I. Perel', Zh. Eksp. Teor. Fiz. 48, 345 (1965) [Sov. Phys. -JETP 21, 227 (1966)].

18) M. I. D'yakonov, Zh. Eksp. Teor. Fiz. 47, 2213 (1964) [Sov. Phys. -JETP 20, 1484 (1965)].

19) A. Omont, J. Phys. (Paris) 26, 26 (1965).

20) A. Omont and J. Meunier, Phys. Rev. 169, 92 (1968).

21) C. H. Wang and W. L. Tomlinson, Phys. Rev. 181, 115 (1969).

22) P. R. Berman and W. E. Lamb, Jr., Phys. Rev. 187, 221 (1969).

23) C. G. Carrington and A. Corney, J. Phys. B: Atom. Molec. Phys. 4, 849 (1971).

24) C. G. Carrington, D. N. Stacey, and J. Cooper, J. Phys. B: Atom. Molec. Phys. 6, 417 (1973).

25) W. Berdowski and L. Krause, Phys. Rev. 165, 158 (1968).

26) A. Gallagher, Phys. Rev. 157, 68 (1967).

27) A. I. Okunevich and V. I. Perel', Zh. Eksp. Teor. Fiz. 58, 666 (1970) [Sov. Phys. -JETP 31, 356 (1970)].

28) R. A. Zhitnikov, P. P. Kuleshov, A. I. Okunevich, and B. N. Sevast'yanov, Zh. Eksp. Teor. Fiz. 58, 831 (1970) [Sov. Phys. -JETP 31, 445 (1970)].

29) J. Fricke, J. Haas, E. Lüscher, and F. A. Franz, Phys. Rev. 163, 45 (1967).

30) J. Pittre and L. Krause, Can. J. Phys. 45, 2671 (1967).

31) L. Krause, Appl. Opt. 5, 1375 (1966)

32) M. Elbel and E. Naumann, Z. Physik 204, 501 (1967).

33) J. P. Faroux and J. Brossel, C. R. Acad. Sci. 265, B1412 (1967).

34) C. G. Carrington and A. Corney, J. Phys. B: Atom. Molec. Phys. 4, 869 (1971).

35) C. G. Carrington, A. Corney, and A. V. Durrant, J. Phys. B: Atom. Molec. Phys. 5, 1001 (1972).

36) T. Yabuzaki, N. Mita, and T. Ogawa, Phys. Rev. Letters 29,

336 (1972).

37) G. Hermann, G. Lasnitschka, and A. Scharmann, Phys. Letters 61A, 99 (1977).

38) G. Hermann, G. Lasnitschka, and A. Scharmann, Z. Physik A 282, 253 (1977).

39) G. Hermann and A. Scharmann, Z. Physik 254, 46 (1972).

40) M. Dumont, J. Phys. (Paris) 33, 971 (1972).

41) R. M. Herman, Phys. Rev. 175, 10 (1968).

42) E. I. Dashevskaya and N. A. Mokhova, Chem. Phys. Letters 20, 454 (1973).

43) E. Roueff and A. Suzor, J. Phys. (Paris) 35, 727 (1974).

44) E. Roueff, J. Phys. B: Atom. Molec. Phys. 7, 185 (1974).

45) O. Nedelec, P. Baltayan, and A. Orizet, C. R. Acad. Sci. 265, B542 (1967).

46) M. Lombardi, J. Phys. (Paris) 30, 631 (1969).

47) V. N. Rebane, Opt. Spektrosk. 24, 309 (1968) [Opt. Spectrosc. 24, 163 (1968)].

48) M. Carré, M. L. Gaillard, and M. Lombardi, J. Phys. (Paris) 38, 553 (1977).

49) M. Carré and M. Lombardi, J. Phys. (Paris) 38, 571 (1977).

50) E. Chamoun, M. Lombardi, M. Carré, and M. I. Gaillard, J. Phys. (Paris) 38, 591 (1977).

51) J. Ward, J. Cooper, and E. W. Smith, J. Quant. Spectrosc. Radiat. Transfer 14, 555 (1974).

52) J. Cooper and D. N. Stacey, Phys. Rev. A12, 2438 (1975).

53) W. Gough, Opt. Commun. 9, 294 (1973).

54) W. Gough, Proc. Phys. Soc. (London) 90, 287 (1967).

55) W. E. Baylis, Phys. Rev. A7, 1190 (1973).

56) J. C. Gay and W. B. Schneider, J. Phys. Letters (Paris) 36, L185 (1975).

57) J. C. Gay, J. Phys. Letters (Paris) 36, L239 (1975).

58) J. C. Gay, J. Phys. (Paris) 37, 1135 (1976).

59) J. C. Gay, J. Phys. (Paris) 37, 1155 (1976).

60) V. N. Rebane and T. K. Rebane, Opt. Spektrosk. 30, 367 (1971) [Opt. Spectrosc. 30, 199 (1971)].

61) P. Goldreich, *Atomic and Molecular Physics and Interstellar Matter* (Les Houches Summer School XXVI, 1974) ed. by Balian et al. (North-Holland, Amsterdam, 1975) p. 413.

62) D. ter Haar and M. A. Pelling, Rep. Prog. Phys. 37, 481 (1974).

63) V. S. Strel'nitskii, Usp. Fiz. Nauk 113, 463 (1974) [Sov. Phys. -Usp. 17, 507 (1975)].

64) D. A. Varsharovich, Zh. Eksp. Teor. Fiz. 56, 614 (1974) [Sov. Phys. -JETP 29, 337 (1969)].

65) M. M. Litvak, Phys. Rev. A2, 937 (1970).

66) P. Goldreich, D. A. Keeley, and J. Y. Kwan, Astrophys. J. 179, 111 (1973).

67) L. M. Hall and D. ter Haar, Monthly Nat. Roy. Astron. Soc. 162, 97 (1973).

68) I. s. Shklovskii, Astron. Zh. 46, 3 (1969) [Sov. Astron. -AJ 13, 1 (1969)].

69) R. L. Fork, W. J. Tomlinson, and L. J. Heilos, Appl. Phys.

Letters 8, 162 (1966).

70) H. de Lang and G. Bouwhuis, Phys. Letters 20, 383 (1966).

71) W. L. Tomlinson and R. L. Fork, Phys. Rev. 164, 466 (1967).

72) A. I. Alekseev and V. M. Galitskii, Zh. Eksp. Teor. Fiz. 57, 1002 (1969) [Sov. Phys. -JETP 30, 548 (1970)].

73) C. H. Wang, W. J. Tomlinson, and R. T. George, Jr., Phys. Rev. 181, 125 (1969).

74) T. Manabe, T. Yabuzaki, and T. Ogawa, Phys. Rev. A20, 1946 (1979).

75) T. Yabuzaki, T. Manabe, T. Ogawa, Abstracts of the XIth ICPEAC (Kyoto, 1979).

76) T. Yabuzaki, T. Manabe, and T. Ogawa, J. Phys. Soc. Japan 47, 343 (1979).

77) U. Fano and G. Racah, *Irreducible Tensorial Sets* (Academic Press, New York, 1957).

78) A. Omont, *Progress in Quantum Electronics* vol. 5 (Pergamon Press, Oxford, 1977), p.69.

79) U. Fano, Rev. Mod. Phys. 29, 74 (1957).

80) A. Messiah, *Mécanique Quantique* (Dunod, Paris, 1959), chap. 13.

81) D. Smith and J. H. M. Thornley, Proc. Phys. Soc. (London) 89, 779 (1966).

82) F. Bloch, Phys. Rev. 70, 460 (1946).

83) J. P. Barrat and C. Cohen-Tannoudji, J. Phys. Radium 22, 329 (1961).

84) J. P. Barrat and C. Cohen-Tannoudji, J. Phys. Radium 22,

443 (1961).

85) M. Ducloy, M. P. Gorza, and B. Decomps, Opt. Commun. 8, 21 (1973).

86) M. E. Rose, *Elementary Theory of Angular Momentum* (Wiley & Sons, New York, 1957).

87) R. L. Fork and M. A. Pollack, Phys. Rev. 139, A1408 (1965).

88) T. Hänsch, R. Odenwald, and P. Toschek, Z. Physik 209, 478 (1968).

89) B. Decomps and M. Dumont, IEEE J. Quantum Electron. QE-4, 916 (1968).

90) M. Dumont and B. Decomps, J. Phys. (Paris) 29, 181 (1968).

91) B. Decomps and M. Dumont, J. Phys. (Paris) 29, 443 (1968).

92) M. Tsukakoshi and K. Shimoda, J. Phys. Soc. Japan 26, 758 (1968).

93) M. Ducloy, Ann. Phys. Paris 8, 403 (1973).

94) A. Ben-Reuven, Phys. Rev. 145, 7 (1966).

95) G. Nienhuis, J. Phys. B: Atom. Molec. Phys. 9, 167 (1976).

96) R. W. Davies, Phys. Rev. A12, 927 (1975).

97) B. Decomps, Thesis, Paris (1969).

98) F. Abramowitz and J. A. Stegun *Handbook of Mathematical Functions* (Dover, New York, 1968).

99) M. Lombardi, C. R. Acad. Sci. 265, B191 (1967).

100) W. Happer, Phys. Rev. B1, 2203 (1970).

101) A. Ricard, J. Phys. (Paris) 30, 556 (1969).

102) O. P. Bochkova, L. P. Razumovskaya, and S. E. Frish, Opt. Spektrosk. 11, 697 (1961) [Opt. Spectrosc. 11, 376 (1961)].

103) T. Yabuzaki, T. Endo, M. Kitano, and T. Ogawa, Opt. Commun. 22, 181 (1977).

104) T. Endo, T. Yabuzaki, M. Kitano, T. Sato, and T. Ogawa, IEEE J. Quantum Electron. QE-14, 977 (1978).

105) J. M. Hollander, I. Perlman, and G. T. Seaborg, Rev. Mod. Phys. 25, 469 (1953).

106) K. Levenberg, Quart. Appl. Math. 2, 164 (1944).

107) S. M. Roberts, D. H. Wilkinson, L. R. Walker, Anal. Chem. 42, 886 (1970).

108) E. Giacobino-Fournier, C. R. Acad. Sci. 276, B535 (1973).

109) M. Pavlovic and F. Laloë, J. Phys. (Paris) 31, 173 (1970).

110) V. I. Odintsov, Opt. Spektrosk. 18, 357 (1965) [Opt. Spectrosc. 18, 205 (1965)].

111) A. V. Phelps and J. P. Molner, Phys. Rev. 89, 1202 (1953).

112) P. W. Smith, J. Appl. Phys. 37, 2089 (1966).

113) C. V. Shank and S. E. Schwarz, Appl. Phys. Letters 13, 113 (1968).

114) R. H. Cordover and P. A. Bonczyk, Phys. Rev. 188, 696 (1969).

115) W. E. Bell and A. L. Bloom, Phys. Rev. 107, 1559 (1957).

116) J. N. Dodd and G. W. Series, Proc. Roy. Soc. (London) A263, 351 (1961).

117) W. Culshaw, Phys. Rev. 135, A316 (1964).

118) W. Culshaw, Phys. Rev. 142, 204 (1966).

119) W. Culshaw, IEEE J. Quantum Electron. QE-4, 979 (1968).

120) T. O. Carroll and G. J. Wolga, IEEE J. Quantum Electron. QE-2, 456 (1966).

121) T. O. Carroll,IEEE J. Quantum Electron. QE-6, 516 (1970).

122) T. O. Carroll and G. J. Wolga, Phys. Rev. Letters 21, 670 (1968).

123) T. Yabuzaki and T. Ogawa, J. Appl. Phys. 39, 4477 (1968).

124) T. Yabuzaki and T. Ogawa, J. Phys. Soc. Japan 34, 769 (1973).

125) E. U. Condon and G. H. Shortley, *The Theory of Atomic Spectra* (Cambridge Univ. Press, London, 1935).

126) C. P. Slichter, *Principles of Magnetic Resonance* (Harper and Raw, New York, 1963).

127) W. E. Lamb, Jr., Phys. Rev. 134, 1429 (1964).

128) M. Sargent III, M. O. Scully, and W. E. Lamb, Jr., *Laser Physics* (Addison-Wesley, Reading, 1974).

129) B. Decomps and M. Dumont, C. R. Acad, Sci. 265, B249 (1967).

130) W. Franzen, Rev. Sci. Instrum. 33, 933 (1962).

131) F. Bloch and A. Siegert, Phys. Rev. 57, 522 (1940).

132) A. Abragam, *Nuclear Magnetism* (Oxford Univ. Press, Oxford, 1961).

133) A. L. Bloom, Appl. Opt. 1, 61 (1962).

134) W. L. Wiese, M. W. Smith, and B. M. Glennon, *Atomic Transition Probabilities*, NBSDS-NBS4, vol. 1 (U. S. Government Printing Office, Woshington, D. C. , 1966).

135) G. M. Lawrence, Phys. Rev. 175, 40 (1968).

136) P. M. Griffin and H. M. Hutcheson, J. Opt. Soc. Am. 59, 1607 (1969).

137) H. S. W. Massey and E. H. S. Burhop, *Electronic and Ionic Impact Phenomena* (Oxford Univ. Press, London, 1952).

138) F. Masnou-Seeuws, J. Phys. B: Atom. Molec. Phys. 3, 1437 (1970).